

KOOTENAY LAKE GEOTHERMAL PROJECT, PHASE THREE

GEOLOGICAL, GEOCHEMICAL, GEOPHYSICAL AND GEOSPATIAL INVESTIGATIONS INTO THE GEOTHERMAL POTENTIAL OF THE EAST SHORE OF KOOTENAY LAKE – SUMMARY REPORT, JANUARY 2024

Geoscience BC Report # 2024-04

Prepared For:



Prepared By:

Gordon MacMahon (1), Daniel Gatto (2), Sonni Greene (3),
Leslie Harker (4), Stefan Humphries (5), Lucinda Leonard (6), Theron Finley (7), &
Robert McQuarrie (8)

On behalf of

South Kootenay Lake Community Services Society



BRITISH
COLUMBIA



KOOTENAY LAKE GEOTHERMAL PROJECT – PHASE THREE

Geological, Geochemical, Geophysical and Geospatial Investigations into the Geothermal Potential of the East Shore of Kootenay Lake – Summary Report, January 2024

TABLE OF CONTENTS

1. Project Introduction	Pg. 5
2. Geological Setting	Pg. 8
3. Summary of Phases One & Two	Pg. 15
4. Phase Three – Scope of Work and Methodology	Pg. 17
A. Field Geology	
B. Field Geochemistry	
C. Temperature Probe Survey	
D. Electrical Resistivity Tomography (ERT)	
E. Geospatial Evaluation - Drone-based Surveys	
5. Results and Preliminary Interpretation	Pg. 25
A. Field Geology	
B. Field Geochemistry	
C. Temperature Probe Survey	
D. Electrical Resistivity Tomography (ERT)	
E. Geospatial Evaluation – Drone-based Surveys	
F. Geological and Geothermal Modelling	
6. Recommendations for Further Work, Phase Four (2024)	Pg. 63
7. Conclusion	Pg. 65
8. Acknowledgments	Pg. 66
9. References	Pg. 68
10. Appendix	Pg. 73
a. SRK Consulting Report (provided separately)	

- b. Geotronics Consulting Report (provided separately)
- c. University of Calgary - Geochemical Analyses
- d. Laboratory analysis summary – CARO Labs (provided separately)
- e. Multiparameter Testing 2023 Results Summary (provided separately)
- f. Temperature Data Logger Deployment Locations
- g. Electrical Resistivity Tomography (ERT) Profiles

Contributors:

1. Gordon MacMahon, B.Sc., M.A., P.Geol., (retired), Volunteer Project Lead, South Kootenay Lake Community Services Society
2. Daniel Gatto, B.Sc., Retired Geologist, Volunteer
3. Sonni Greene, B.Sc., Retired Geologist, Volunteer
4. Leslie Harker, M.Sc. Geochemist, SRK Consulting
5. Stefan Humphries, M.Sc., Hydrogeologist, SRK Consulting
6. Lucinda Leonard, Ph.D., Assistant Professor, School of Earth and Ocean Science, University of Victoria
7. Theron Finley, MSc, Ph.D. Candidate, School of Earth and Ocean Science, University of Victoria
8. Robert McQuarrie, B.A., M.Sc., Instructor, Selkirk College

We wish to acknowledge that the activities carried out as part of this project were conducted on the unceded lands of the Ktunaxa Nation. We hold a deep respect for this land, and for the people who have historically resided here and continue to do so.

1) Project Introduction

Geothermal heat and power have been developed in many places around the globe. However, until recently, only modest levels of early-stage development have occurred in Canada. In British Columbia (BC), high temperature geothermal power projects have the potential to produce significant long-term, clean electricity. Six potential geothermal power projects are at various stages of development: South Meager, North Meager, Valemount, Mount Cayley, Lakelse, and Mount Edziza in northeast BC. According to Clean Energy BC, these projects collectively have the potential to deliver more than 1,000 MW of electricity. As one of the smaller potential power projects, Tu Deh-Kah project, owned by Fort Nelson First Nation, may become the first commercial scale geothermal power plant operating in BC.

<https://cleanenergybc.org/sector/geothermal/#:~:text=British%20Columbia's%20Potential,of%20over%201%2C000%20MW%20collectively>

These high temperature power projects are designed to utilize geothermal resources with temperatures in excess of 120°C. Lower temperature geothermal systems on the other hand, with geothermal fluid temperatures in the range of 40–120°C can create small scale sustainable economic projects across a spectrum of direct heat and commercial applications such as greenhouse agriculture. These direct heat projects require much less capital than the larger power plant developments and can deliver social and economic benefits straight to the local communities where they are situated. It is this 40–120°C range of geothermal temperatures and the potential direct heat benefits which are the focus of this project.

In the United States (US), there are currently 23 geothermal district heating (GDH) systems, with a capacity totaling more than 75 MW of thermal energy (MWth) (Robins et al., 2021). Most of these systems have been in operation for over 30 years; the oldest GDH installation in North America dates to 1892 in Boise, Idaho (Robins et al., 2021). Boise's system is now the largest municipally operated geothermal system in the US, providing direct heat to over 90 buildings in the downtown area. In a 2021 market report on geothermal energy in the US, the National Renewable Energy Laboratory (NREL) stated that the barrier to expansion of the geothermal direct heat sector was not technical, but rather political, social, or economic. In Canada, there is currently only one small, direct-heat geothermal project located in Moosejaw, Saskatchewan.

The Kootenay Lake project area (see Figure 1) is host to several hot/warm spring occurrences, specifically Ainsworth, Riondel and Crawford Creek (see Figure 2). Ktunaxa First Nation's Peoples have experienced the hot springs for millennia and currently own and operate the Ainsworth Hot Springs Resort. In the historic Bluebell Mine at Riondel, temperatures of 40°C and flow rates of 150 litres per second were

encountered during mining operations (Desrochers, 1992). The Crawford Creek warm spring (32°C) is located within the project area and is a focus of the work carried out in Phase Three. Geochemical analyses of several hot springs in the Kootenay Lake area indicate that at depths of 2–3 km, water temperatures may exceed 120°C (Grasby et al., 2000). Kootenay Lake is situated in a geographic area where several positive geothermal indicators, such as deep-seated faults and surface thermal expressions, are located, supporting the view that further investigations in the area are warranted.

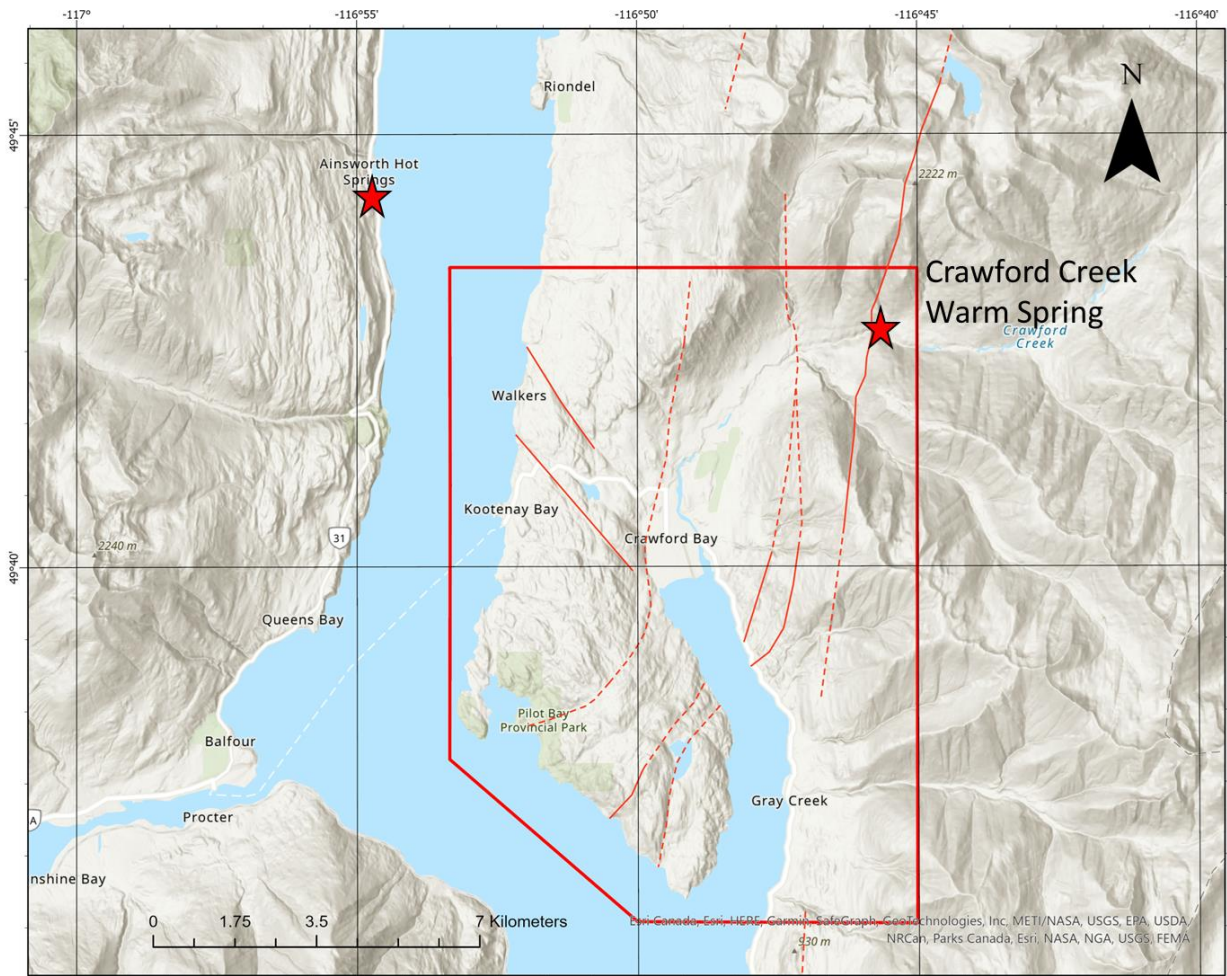


Figure 1 – Overview Map of Phase Three Study Area, (red outline is approximately 150 km²), red stars mark location of surface thermal waters; solid and dashed lines are mapped or inferred faults.

A preliminary evaluation of the Kootenay Lake area geology indicates that the East Shore of Kootenay Lake may be well suited to serve as a pilot project to test the feasibility of developing a geothermal direct heat source for renewable

district heating applications. A successful geothermal project in the Kootenays could create a template for similar developments within the Columbia Basin region. A confirmed geothermal direct heat source on the East Shore could bolster a local green economy, support local agri-business, and improve food security while increasing employment and augmenting economic resilience.

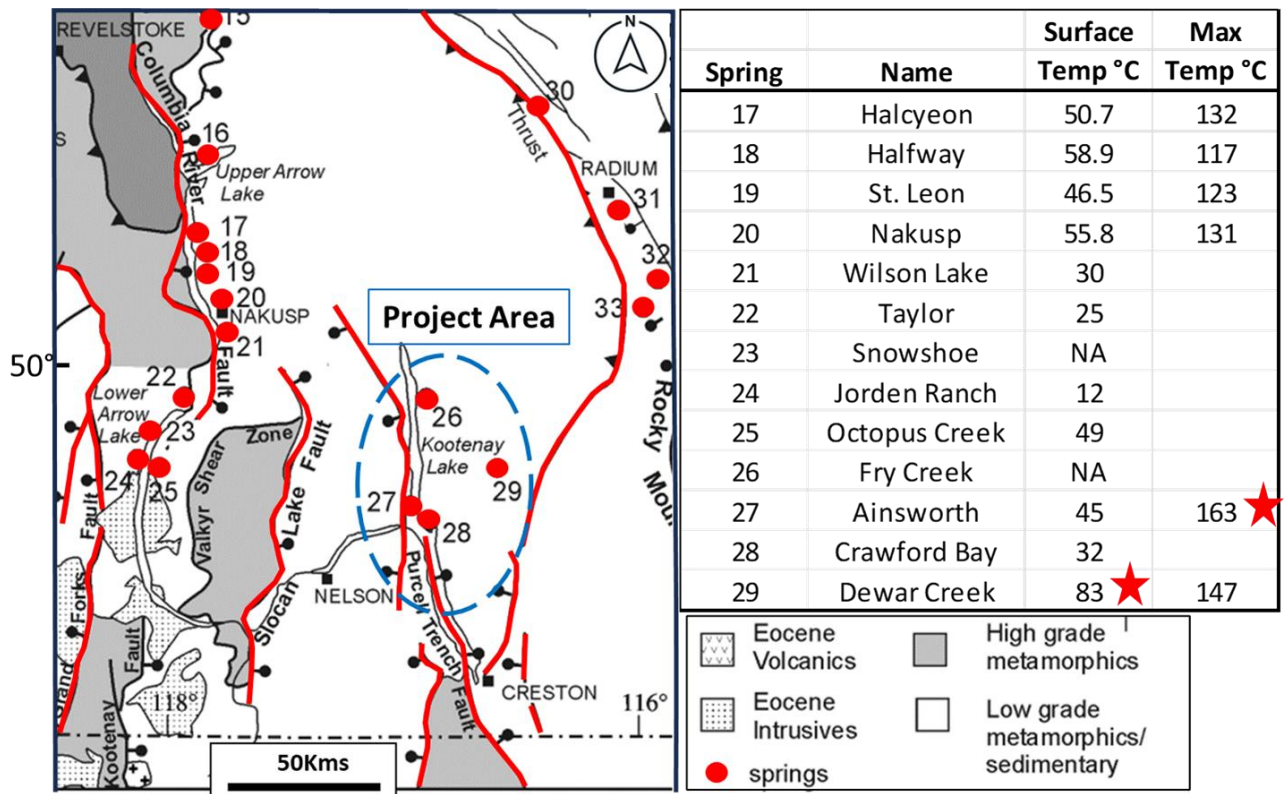


Figure 2 – Summary overview geological map of southeastern BC, showing major extension faults and main thrust faults. Locations of thermal springs (red dots) are shown, with a table of hot spring locations and hot springs data summarized from Grasby & Hutcheon (2001).

Rural areas and small population communities play an important role in the economy, culture, and social fabric of BC and were home to approximately 25% of the provincial population in 2016 (Statistics Canada). Demographic shifts, labour shortages, economic transition, and climate change are some of the major forces anticipated to drive changes in population demographics within BC in the coming decades. Formulating strategies to support adaptive capacity within rural areas is critical to their resilience. To be most effective, this support must emerge from the specific context of the communities. By employing geological, geochemical, geophysical and geospatial technologies in the Kootenay Lake area, this project will help advance the understanding of

geothermal resources in BC and Canada, laying the foundation for a potential commercial, geothermal, direct heat development.

2) Geological Setting

The Kootenay Lake area of Southeastern BC exhibits high heat flow (Majorowicz & Grasby, 2010). Deep, heat energy mapping illustrates that the modelled heat energy in the Kootenay Lake area is approximately 25–40% higher than the generalized background within BC (Figure 3; Majorowicz & Grasby, 2010).

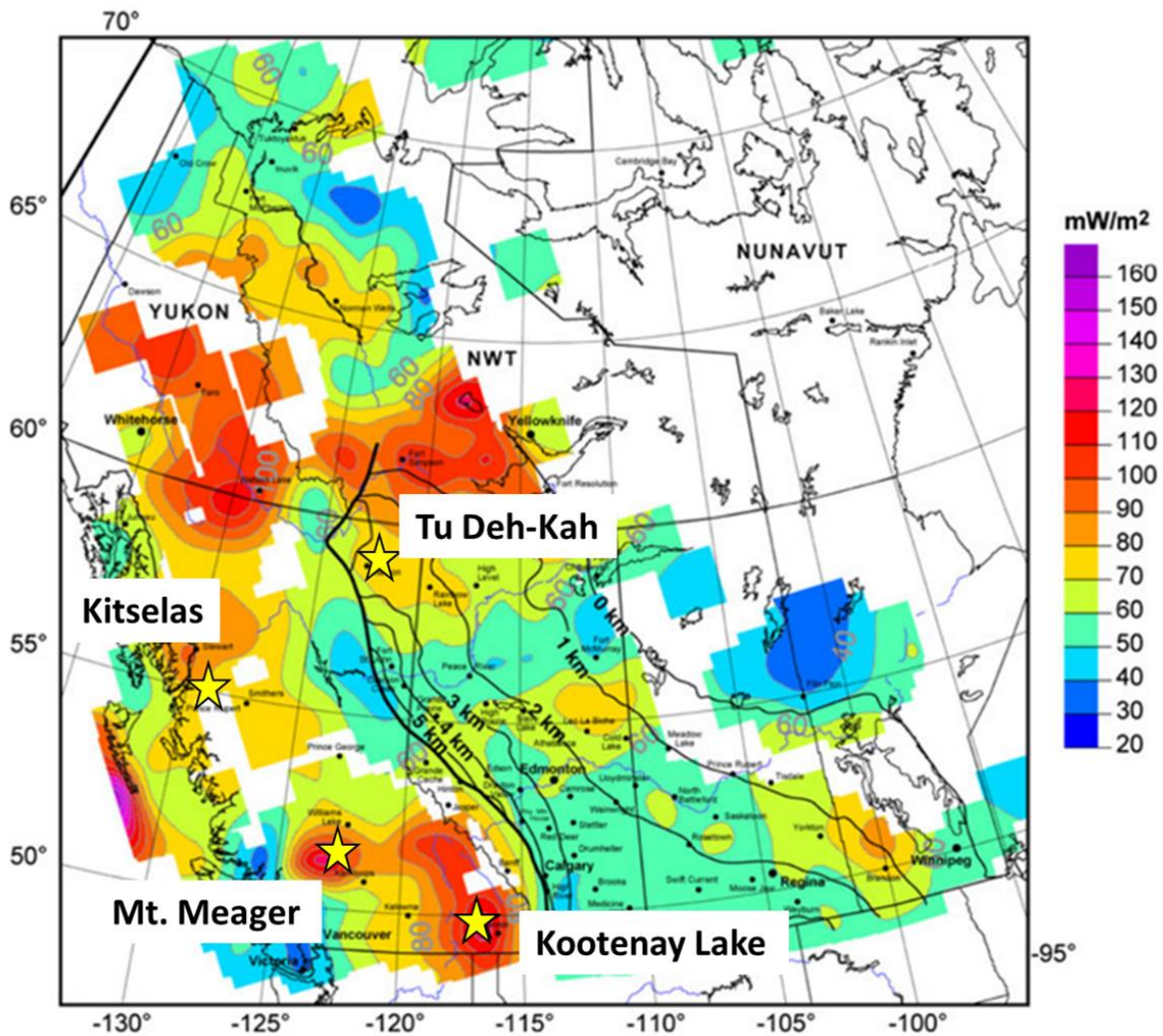


Figure 3 – Map showing averaged heat flow in western Canada. Approximate location of some key BC projects shown with a yellow star, including the location of the Kootenay Lake project. (Majorowicz & Grasby, 2010)

A major physiographic boundary within the Canadian Cordillera occurs at Kootenay Lake, with the Selkirk Mountains lying to the west and the Purcell Mountains to the east of the lake. The eastern portion is represented by the Purcell Anticlinorium, a Cordilleran structure with some of the oldest rock (Proterozoic) exposures of the Cordillera at its core. The Purcell Anticlinorium transitions to the west into the metamorphosed and deformed pericratonic / accreted island arc sequence of the Kootenay Arc (Rioseco & Pattison, 2018).

The area of anomalously high heat flow depicted in Figure 3 is essentially coincident with the location of the most highly metamorphosed rocks – proximal to Kootenay Lake. According to Moynihan & Pattison (2013), the area hosts rocks that were metamorphosed at approximately 25 km depth and at temperatures of $>650^{\circ}\text{C}$ and are now exposed at surface (Figure 4).

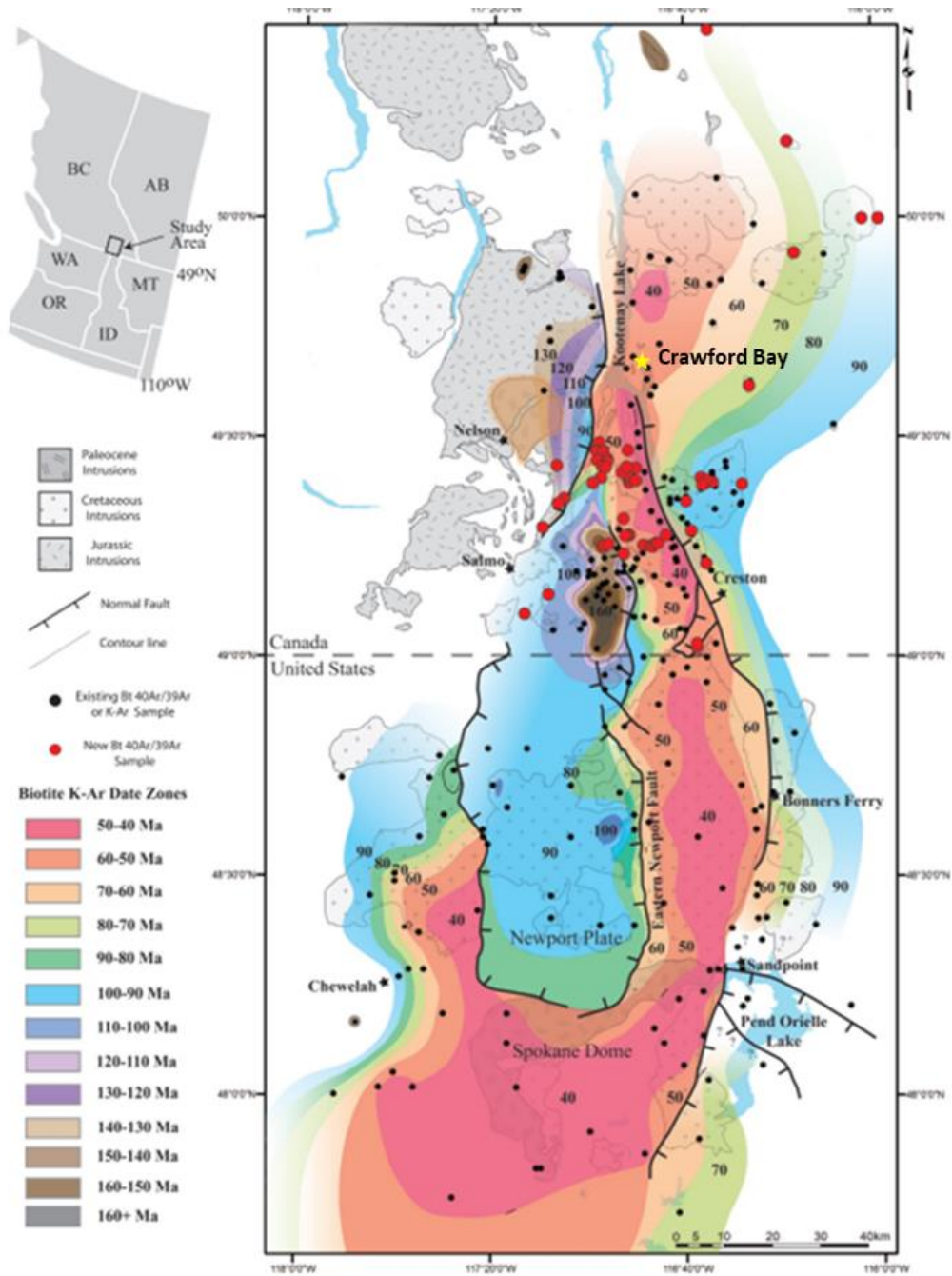


Figure 4 – Regional contours of K–Ar and $^{40}\text{Ar}/^{39}\text{Ar}$ dates in biotite (Bt) (Webster et al., 2020).

Webster et al. (2020) utilized Argon-Argon thermochronology to better understand the stages and timing of exhumation of this once deeply buried terrain, determining that final exhumation occurred during a period of regional extension along Eocene normal faults such as the Purcell Trench fault. Webster et al. (2020) believed that the exhumation of the highest-grade metamorphic rocks

in the Kootenay Lake area was a multi-stage process. The area experienced most of the exhumation during a period of regional contraction in the Late Cretaceous to Paleocene (76-61 Ma) with final exhumation in the footwall of Eocene (53-46 Ma) normal faults, when the area had transitioned to a period of regional extension. Figure 4 shows the main area of exhumation extending from Sandpoint, Idaho to Kootenay Lake near Crawford Bay, which occurred over the time period 90 to 40 Ma.

Geothermal activity occurs throughout the project area, in the form of hot/warm springs at Ainsworth, Crawford Creek and Riondel (see Figure 2). Most thermal springs in BC occur proximal to major faults, penetrate deeply into the crust (at least 5 km) and have a relatively recent (Eocene or younger) component of brittle deformation that is conducive to rapid fluid flow from great depths to the surface (Grasby & Hutcheon, 2001). Beaudoin et al. (1992) indicated that these Eocene faults were first-order controls on channeling deep-seated thermal and mineralizing fluids towards upper crustal levels. A subset of these Eocene or younger faults have been mapped through the Kootenay Lake valley. See a simplified summary map in Figure 2.

Finley et al. (2020) found that the stress fields in the Kootenays, as derived from earthquake focal mechanisms, reveal a transpressional stress regime that may well have persisted post Eocene to recent. The faulting and fracturing produced during this period likely maintain fault and fracture permeability.

The major fault known as the Purcell Trench Fault (PTF), which is a 'down to the east' normal fault, strikes south along the southern portion of Kootenay Lake and is mapped from Coeur D'Alene, Idaho, north, to Crawford Bay. Just west of the PTF is the Midge Creek / Gallagher Fault complex which extends from the Salmo area in the southwest to north of Kaslo on the west side of Kootenay Lake. Moynihan and Pattison (2013) interpreted the Midge Creek fault system, which dips down to the west, to be part of a larger Eocene fault complex that encompasses the Midge Creek, Gallagher, Lakeshore, and Josephine faults.

The bedrock sequence exposed in the study area was well defined by Höy (1980) during some of the earliest mapping in the region and is Neoproterozoic to Cambrian in age. Table 1 outlines a summary of Höy's geological divisions.

FORMATION	MAP UNIT	EST THICKNESS (M)	DESCRIPTION
INDEX	L4	Top not exposed	Micaceous schist and gneiss
	L3	400-450	Calc-silicate gneiss, amphibole, schist; impure marble; amphibolite layer and pure white quartzite layer near base
	L2	700	Biotite-hornblende gneiss, amphibolite; minor calc-silicate gneiss, marble and schist
	L1	150	Micaceous schist
BADSHOT	B	15-30	White crystalline calcite marble, dolomite
MOHICAN	M	~50	Interlayered quartzite, calcareous and micaceous schist, limestone and dolomite
HAMILL	H4	230	Dark quartzite, dark fine-grained quartz-rich schist
	H3	60-200	Massive white quartzite
	H2	2,000	Interbedded micaceous schist, quartzite and siltstone; minor amphibole
	H1	1,600	Massive white quartzite; gritty quartzite
THREE SISTERS	TS	900	Gritstone, quartzite and quartz-pebble conglomerate
WINDERMERE GP	WG	Base not exposed	Fine-grained light grey to green chlorite-muscovite schist and phyllite; rare white quartzite and marble

Table 1 - The primary geological divisions in the Riondel area (modified after Höy, 1980).

The project area is characterized by three geographic and geologic settings:

- **East side:** East of the West Bernard Fault and east of Crawford Bay lies the Neoproterozoic to Lower Cambrian Hamill Group quartzites and schists, which overlie the Three Sisters Formation and the Windermere Supergroup. This area is host to the Crawford Creek warm spring (32°C).
- **West side:** A broad region of mostly west-dipping Lardeau Group – Index Formation, composed of gneisses with interbeds of quartzite and higher degrees of metamorphism encountered closer to Kootenay Lake (Sillimanite/K-spar zone, Moynihan & Pattison, 2013). This area is also marked by a chain of Cretaceous intrusions known as the Lakeshore Intrusives. In the north of the project area is the former Bluebell Mine at Riondel, where geothermal fluids up to 40°C were encountered in underground mine workings.
- **Intervening area:** A band of tightly folded rocks comprised of Lardeau, Lower Cambrian Badshot marble and Hamill quartzite. This section is bounded on the west by the so-called Bluebell Mountain Fault (Crosby, 1968) and on the east by the West Bernard Fault. One or both faults

could be of a deep-seated nature capable of bringing geothermal fluids closer to the surface.

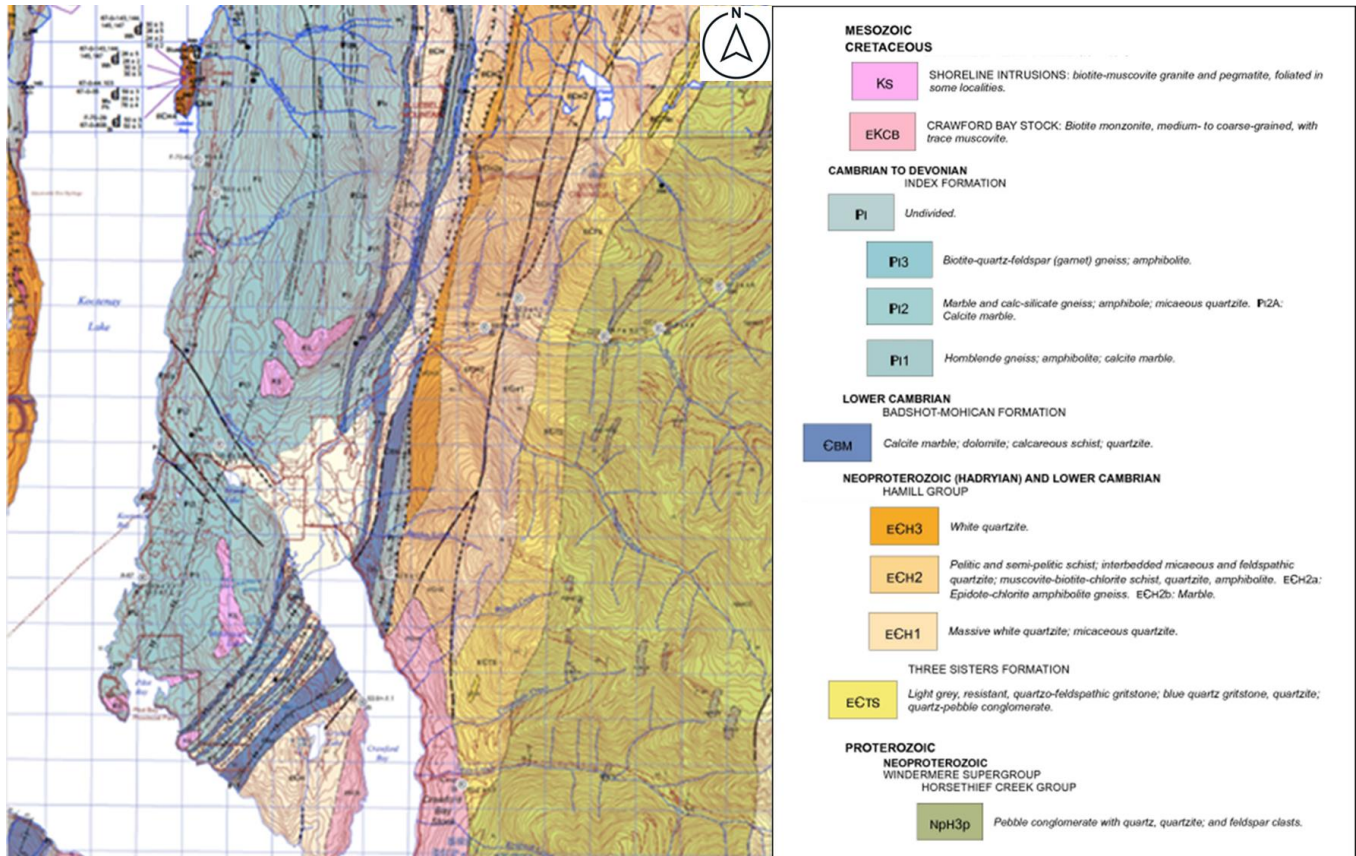


Figure 5 – Area geology map (merged Crawford Bay and Kaslo map sheets) Brown, D.A., et al. (2011).

Riondel, Bluebell Mine - Hot geothermal fluids have been encountered in two of the three regions described above; potentially deep-seated faults border all of these regions of interest. Detailed geological mapping for the project area is shown in Figure 5 where two map sheets have been merged to display the project area.

The occurrence of thermal fluids in the now-abandoned Bluebell Mine at Riondel has attracted interest in the geothermal potential of the east shore of Kootenay Lake, first assessed by Desrochers (1992). In mine workings at a depth of 300 m, miners encountered hot waters of up to 40°C flowing out of cracks and cavities. Flow rates ranged from 45–1,000 litres/sec, (Desrochers, 1992). To prevent the mine workings from flooding, pumps worked 24 hours a day, complicating mine development and eventually contributing to the mine closure in 1972. The depth

of the geothermal zone is approximately 200 m elevation (above sea level) or about 330 m below lake level (Desrochers, 1992). Figure 6 illustrates the relationship between WNW fractures and the location of mapped orebodies.

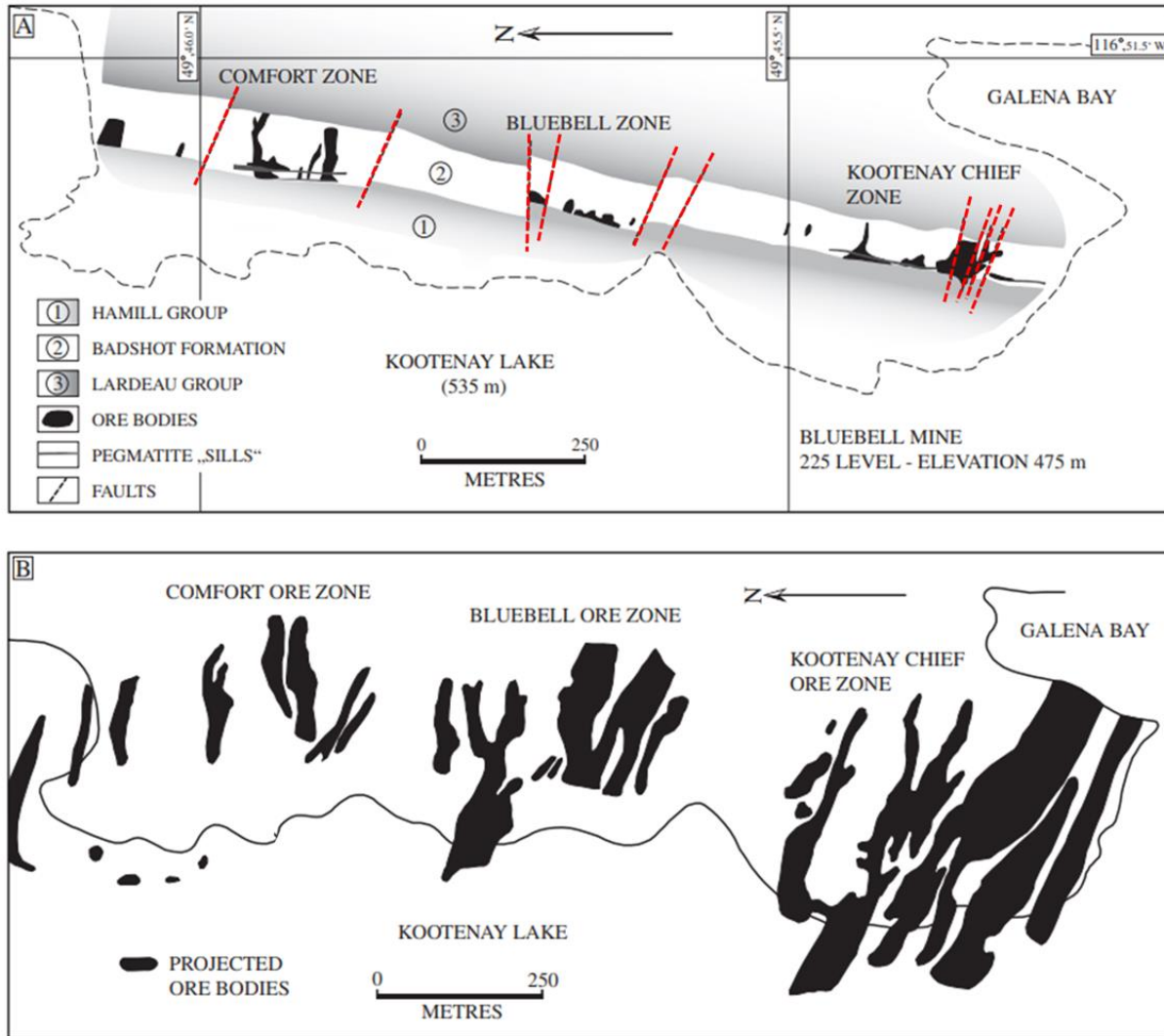


Figure 6 – A) Plan of the 225 level of the Bluebell Mine showing WNW fracturing in relation to orebodies. B) Plan of the Bluebell Mine showing the projection of orebodies onto the surface, the outline of the Riondel peninsula is also shown. Figure from Moynihan & Pattison (2011), adapted from Irvine (1957).

According to Moynihan & Pattison (2011), WNW faulting responsible for ore placement and the existence of hydrothermal fluid in the mine at Riondel occurred later than the WNW trending faults (red dashed lines in Figure 6). The Bluebell mine ore deposits are vein and replacement Ag-Pb-Zn-Au deposits found to occur around the Nelson batholith and adjacent areas. At Riondel, these ore

bodies were developed in the Badshot marble along steeply dipping fractures. These mineralized fractures strike west-northwest and dip steeply to the north (Moynihan & Pattison 2011).

The fieldwork conducted in the summers of 2022 and 2023 further highlighted the pervasive nature of WNW jointing throughout the study area. This will be discussed further in Section 4 – Results and Preliminary Interpretation.

3) Summary of Phases One & Two

Phase One - A Selkirk College Bachelor of GIS student sourced and compiled all available public domain, open-file, project-specific geothermal-related data in 2021 (MacMahon, 2021). The data collected included remote sensing data such as Light Detection and Ranging (LiDAR) and infrared imagery, as well as geological and geophysical data. The interpretation of this dataset was promising, helping to better frame the numerous hydrothermal mineral deposits and facilitated the beginning of a local geologic model for geothermal energy.

Phase Two - A fourth-year geology student from Simon Fraser University conducted geological and geochemical field investigations across the area of interest. The area of field study extended from just north of Riondel, south to Gray Creek on the east shore of Kootenay Lake, BC. This also includes Pilot Peninsula, in the west, and an area to the east up into the Crawford Creek drainage. The project study covers an area of between 250 and 300 km² on the east shore of Kootenay Lake and the area of interest for the GIS drone at Crawford Creek. (The Phase Two area of study extended farther north, south and east than the current Phase Three study area depicted in Figure 1.)

The Phase Two field program has provided a geological and geochemical framework, which has highlighted the geothermal potential of the local area and the Crawford Creek valley specifically. Crawford Creek is the site of an existing warm spring (30–32 °C), which is proximal to the Orebin Creek Fault (OCF), a south striking, steeply dipping fault. This fault may provide conditions favourable for the movement of geothermal fluids from depth.

The Crawford Creek warm spring has water chemistry with cation and anion concentrations similar to other area hot springs. Ainsworth and Dewar Creek hot springs are known to be slightly acidic (pH 6.3 - 6.4) and demonstrate elevated levels of sulphate, magnesium and sodium or potassium. While the Crawford Creek warm spring, with a pH of 6.4 does not exhibit the same concentration of sulphate, magnesium and sodium or potassium as Ainsworth and Dewar Creek, it does have levels which are different from the 'background levels' observed in

most of the water samples analyzed in the 2022 program. The bedrock near where the Crawford Creek warm spring is discharged is the Hamill H1, which is a massive, white quartzite. This quartzite is highly fractured in the immediate vicinity of the OCF with the persistent occurrence of WNW jointing (strike $\sim 119^\circ$ dip 70°). Steeply dipping bedding with frequent jointing within a brittle quartzite suggests the potential for elevated permeability and therefore conveyance of geothermal fluids from depth.

The drone-based Total Infrared (TIR) evaluation of the area surrounding the Crawford Creek warm spring and along the Orebin Creek Fault in 2022 has further assessed the area's potential. Preliminary thermal image mapping shows a surface expression suggesting higher relative temperatures, which extend beyond the primary warm spring, up and down the valley for a total of 400 m and upslope from the valley bottom over 55 m distance (Figure 7).

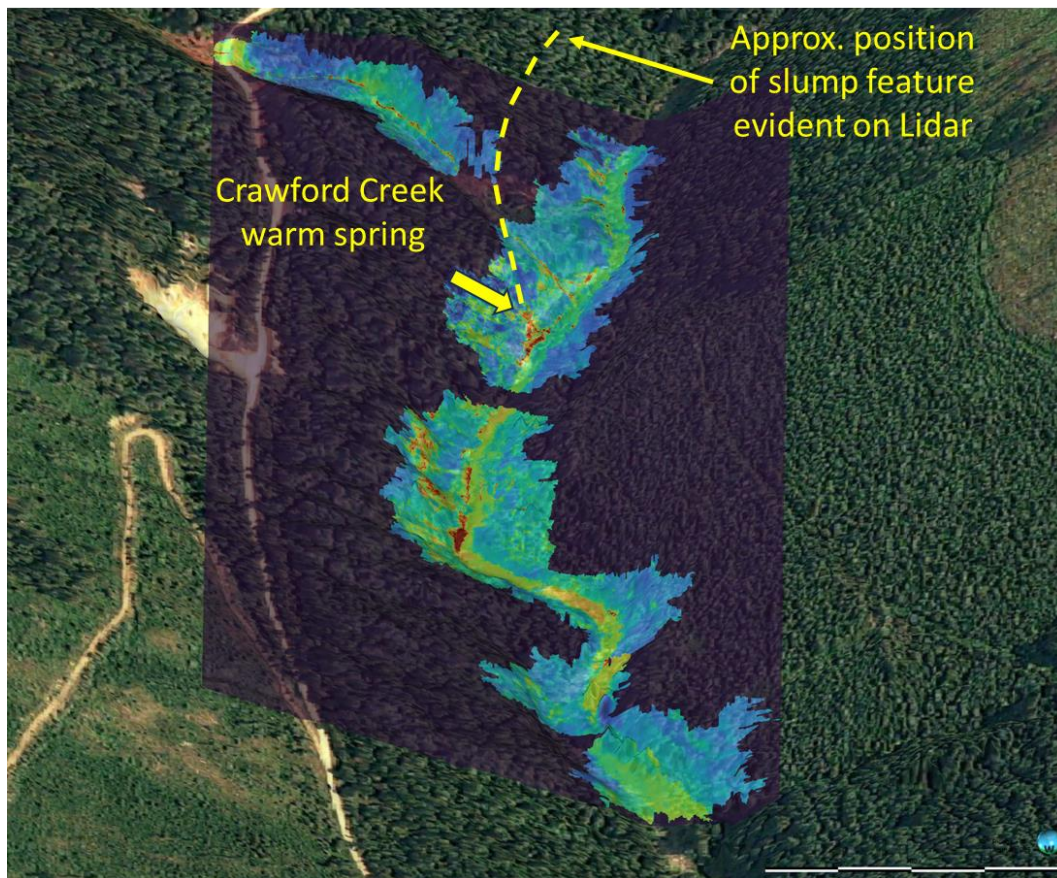


Figure 7 – 2022 (TIR) thermal mosaic showing relative surface temperature, looking east along Crawford Creek valley, (Aetna Geothermal, 2023).

The detailed LiDAR imagery acquired in this area, which filled a gap in the public domain data, shows a well-defined overburden slump feature extending east

from the warm spring. This slump of glaciofluvial till material appears to be responsible for masking and potentially suppressing a broader geothermal surface expression in the immediate vicinity (MacMahon et al, 2023).

4) **Phase Three – Scope of Work and Methodology**

Several key observations emerged during Phase One of this project regarding area fault orientation, the relative timing of faults and their potential relationship to both mineral deposition and geothermal activity. Phase Two furthered the understanding of these relationships particularly in the vicinity of the Crawford Creek warm spring, which is further highlighted on the drone-based TIR thermal imaging mosaic (Figure 7).

A. Field Geology

A University of Victoria geology student conducted fieldwork during the summer of 2023 collecting geological and geochemical data. The structure and fracture orientation data gathered was used to construct stereonet projections leading to the creation of a structural model for the areas of interest. Understanding the nature, orientation and distribution of distinct fracture sets, as well as their geological setting, is required to properly characterize subsurface geothermal reservoirs leading to the development of a hydrogeological model.

Structural data was collected using the application “Field Move Clino” downloaded onto an iPhone 8 Plus running IOS16.5. This app allowed for the collection of many data points during a relatively short field season. Structural measurements were taken for jointing, bedding or foliation planes, noting lithology and documenting any fault surfaces observed. Field Move Clino has a notes option, which allows for the documenting of joint density as the number of joints per metre. The density of joints was calculated by using a one-metre length string as reference and visually counting the joints with the same orientation within the metre.

The GPS location accuracy of the Field Move Clino app was at times low, plotting data points in locations known to be 10–20 m off from actual (i.e., plotting on the wrong side of a roadcut or creek). These inaccuracies are most likely due to dense tree cover and the steep nature of the Crawford Creek valley.

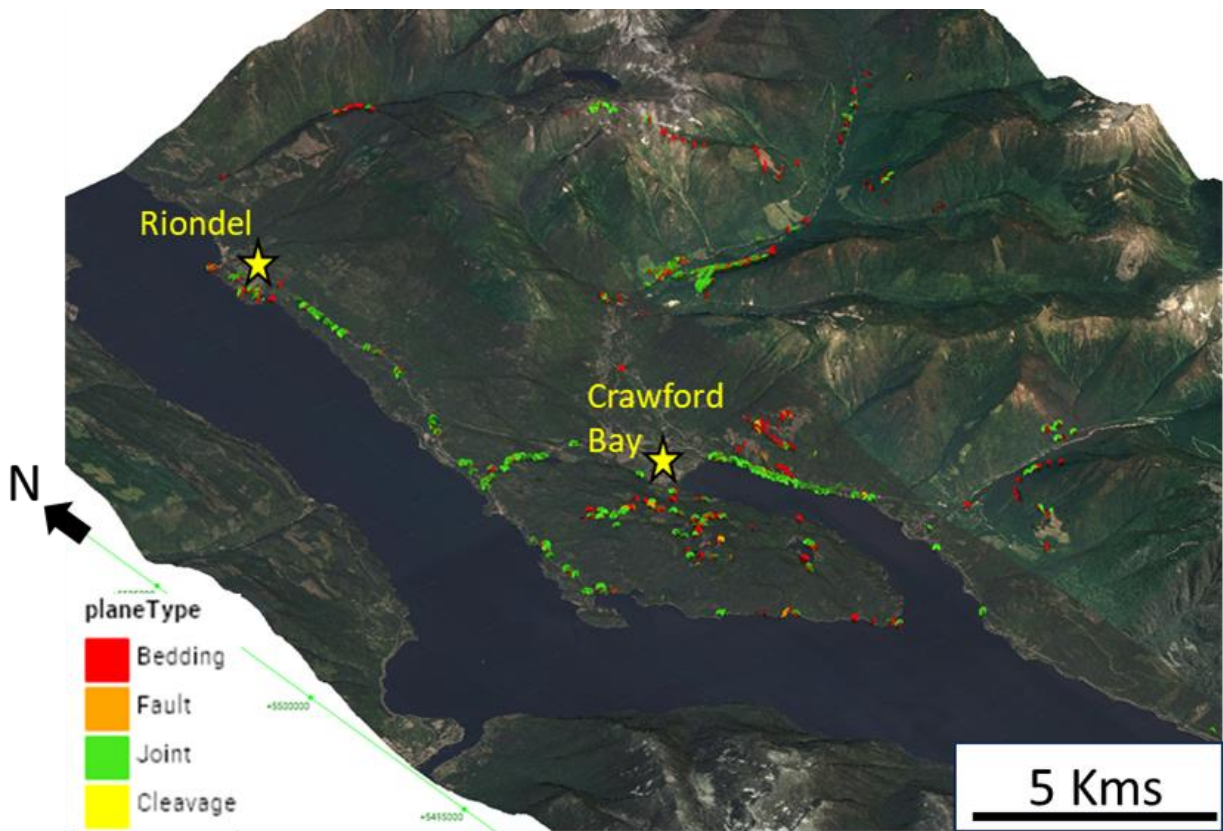


Figure 8 – 3-D overview of project area (looking northeast) showing bedrock measurements (2022-2023).

Over 1,378 surfaces (bedding, faults, and joints) were measured during the 2023 field program. This included over 1,025 measurements in the Crawford Creek area specifically, adding to the broad data base established in 2022 (see Figure 8). Mapping of geology and geochemistry for this report was performed using ArcGIS Pro Version 3.0 software (Esri Inc., 2022).

B. Field Geochemistry

The geochemical signatures from specific field samples collected in 2022 from the Crawford Creek area have highlighted similarities with known geothermal occurrences in the Central Kootenays. Phase Three geological fieldwork also included the verification of all thermal seeps and springs identified on the thermal photo mosaic in Phase Two at Crawford Creek, recording water hydrological properties and location. In 2023, warm springs were monitored through the summer field season, measuring hydrological properties and sampled for both major element anion/cation concentration and isotope composition (water ratios $^2\text{H}/^1\text{H}$ and $^{18}\text{O}/^{16}\text{O}$, dissolved inorganic carbon (DIC) ratios, $^{13}\text{C}/^{12}\text{C}$, sulphate

ratios $^{34}\text{S}/^{32}\text{S}$ and strontium ratios $^{87}\text{Sr}/^{86}\text{Sr}$). This work will improve the understanding of the Crawford Creek system and how it may be affected by shallow mixing with near surface fresh water.

The 2023 program also included some follow-up sampling on leads identified in 2022, which includes Lead #1 (Gray Creek) and Lead #3 (Beaver Creek). The analysis of these samples will assist in further evaluating these areas for additional sampling in a future sampling and/or additional geological / geospatial evaluations.

To further understand surface water properties, water samples from over 113 sites were tested in the field in 2023, complimenting data from over 100 sites tested in 2022. In both field seasons, water chemistry data were collected, with the aid of an Oakton PCTSTestr 50 multiparameter meter, which measures temperature, pH, conductivity, total dissolved solids (TDS), and salinity. The Oakton device was calibrated each day before going to the field to ensure reliable (more accurate) readings, improving on the less frequent calibration rate used in 2022.

Based on hydrological properties such as temperature (above 12°C) or pH (less than 7.0), several seeps, creeks, or springs encountered during fieldwork were flagged to be sampled for laboratory analysis, with all data integrated into the project data platform (ArcGIS) for interpretation.

The 2023 geochemistry program also allowed for select isotope composition analysis to quantify the amount of surface water that is mixing with potentially deeper-sourced geothermal fluids, in the Crawford Creek area specifically. This isotope work included carbon isotopes ($\delta^{13}\text{C-DIC}$), oxygen and hydrogen isotopes ($\delta^{18}\text{O}$ and δD), stable sulphur isotopes $\delta^{34}\text{S}$ in sulphide and sulphate and $\delta^{18}\text{O}_{\text{SO}_4}$ in sulphate and strontium ($^{87}\text{Sr}/^{86}\text{Sr}$) (via Thermal Ionization Mass Spectrometry, TIMS). Samples for specific isotope analyses were collected on August 31, 2023.

C. Temperature Probe Survey

Late in February 2022, a visit to the Crawford Creek warm spring revealed that the area immediately surrounding the warm spring had little to no snow coverage, while areas more distal to the warm spring had half to one metre of winter snowpack remaining (see photo, Figure 9). This suggested that there was significant radiant heat in the near surface area proximal to the warm spring outflow, despite the continued winter conditions in the area. Note that despite having a south facing aspect, the slope above the warm spring still has ample snowpack remaining, while the area around the warm spring remains in the shade through most of the day.



Figure 9 – Crawford Creek warm spring, February 26, 2022.

At Mount Meager, Chen et al (2022) utilized temperature data loggers to establish a ground surface temperature (GST) monitoring network. In 2023, temperature probes were provided by the Geological Survey of Canada (GSC) programmed and sent ready for deployment in the Crawford Creek region. These miniature temperature data loggers (HOBO Water Temp Pro-v2) are durable and waterproof with the ability to record temperatures between -40°C and $+70^{\circ}\text{C}$ in air and up to 50°C in water with an accuracy of $\pm 0.2^{\circ}\text{C}$. All the devices have an optical USB interface to offload data. The GSC provided data loggers are programmed to measure and record ground surface temperature every 30 min.

Chen et al. (2022) found that the most accurate ground surface temperatures are derived in the winter months as the snow cover or snow curtain removes impacts of sun and allows for an estimation of actual geothermal heat flow. To assist in establishing ambient temperature conditions at Crawford Creek, two additional probes were hung in trees approximately two metres above the ground to record air temperature – one in the valley bottom and one near the forest service road.

See example in Figure 10 below from the Mount Meager project.

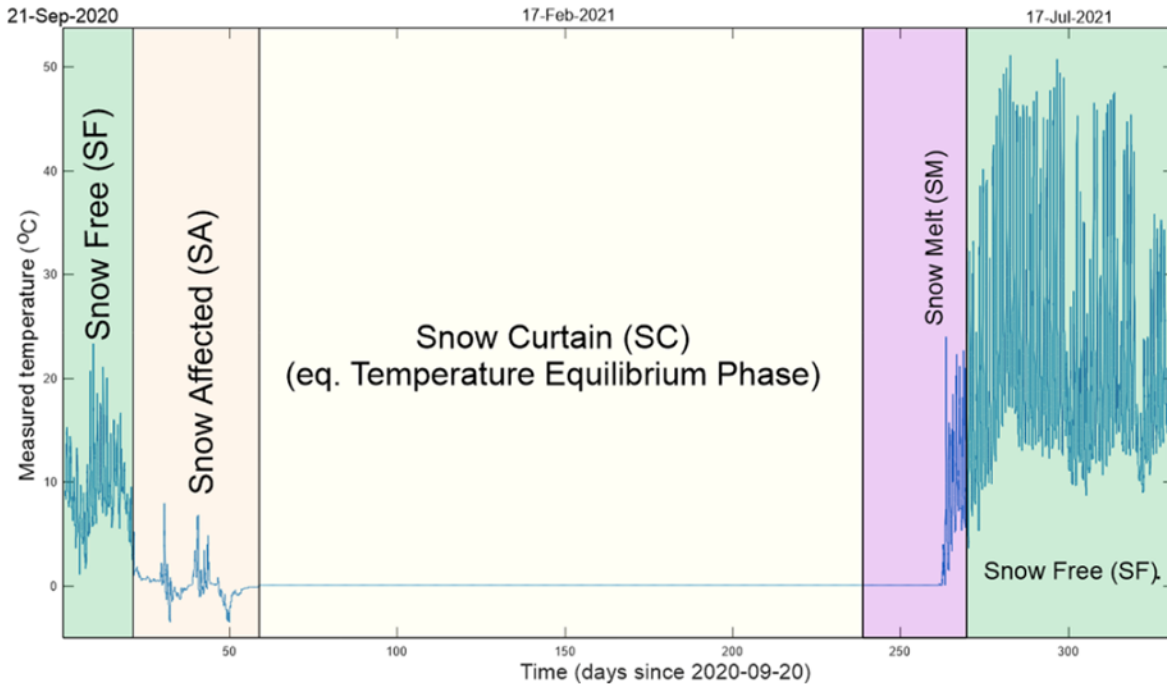


Figure 10 – Example of recorded ground surface temperature time series output display (from Chen et al., 2022).

Following the Mount Meager study, Chen et al. (2022) recognized that a multiple sensor configuration in the monitoring network may be capable of directly estimating heat flow. These heat flow estimates could then be used to characterize any observed temperature anomalies and their potential relationship to subsurface geothermal heat flow sources. As per communication with Zhuoheng Chen, it was decided to undertake a multiple sensor approach, deploying two data loggers per site in 2023.

D. Electrical Resistivity Tomography (ERT)

An Electrical Resistivity Tomography (ERT) survey facilitated through the University of Victoria was planned for the Crawford Creek area in 2023, to map overburden thickness and indirectly map underlying bedrock, identify any structures or contacts and how these features relate to the thermal anomalies identified thus far. Depending on the survey geometry, it is possible to image resistivity structure down to several hundred metres in depth, where resistivity is controlled largely by groundwater saturation levels and the permeability of bedrock and/or surficial sediments. This could assist in delineating spring flow pathways.

The eastern extent of the main glacial deposit in the valley bottom around the Crawford Creek warm spring is covering and likely masking the geothermal surface expression and represents an area where an alternative technology such

as ERT may provide further definition of overburden thickness, as well as variations in subsurface fluid saturation.

The ERT survey at Crawford Creek represents the first effort, as part of the Kootenay Lake Geothermal Project, to image subsurface geological conditions potentially related to the presence of saturated bedrock and potential geothermal fluid. This work will be instrumental in understanding the potential geothermal resource in the Crawford Creek area.

An AGI SuperSting electrical resistivity tomography (ERT) system was used to image the electrical properties of the subsurface in the vicinity of the Crawford Creek warm spring. The SuperSting system is equipped with 112 electrodes and over 1,000 m of cable, allowing for a maximum potential depth penetration of ~500 m. A dipole-dipole array configuration was selected to maximize resolution of lateral changes in the subsurface.

The dipole-dipole method works by inducing an electrical current between a pair of electrodes (a dipole) and measuring the voltage difference across a second pair of electrodes to estimate the apparent resistivity; this represents the average resistivity of the subsurface sampled by the current beneath both pairs. Thus, each measurement uses four electrodes at a time. The shallow subsurface is sampled using closely spaced dipoles; more widely spaced dipoles are selected to sample the deeper subsurface. The instrument is programmed to collect a sequence of measurements using many different dipole pairs, in order to sample a 2-D section of the subsurface.

E. Geospatial Evaluation – Drone-based Surveys

The 2023 drone-based remote sensing program targeted the area around Crawford Creek, where several compelling observations were made in 2022. The vicinity of the warm spring (32°C) near the valley bottom is also the location of three other warm springs with measured temperatures ranging from 17–32°C. This warm spring is proximal to a mapped regional fault known as the Orebin Creek Fault (OCF), a near-vertical fault striking south from Orebin Creek toward the Crawford Bay Stock which is located on the east shore of Crawford Bay (Kootenay Lake) (Brown et al., 2011).

Thermal Drone Video - Due to the limitations in collecting thermal images, a new methodology is being tested to improve thermal surface temperature assessment efficiency. In a standard thermal image survey there are many factors that can contribute to inconsistencies in data collection and temperature variation. These include but are not limited to:

- time of year;
- time of day;
- weather (cloud cover and precipitation); and
- flight plan overlap and drone speed.

For example, a thermal image survey flight over a highly forested area requires at least 90% flight line overlap to allow for orthorectification and stitching images together into a mosaic for mapping. The drone must also fly at slower speeds to allow for the same front lap between images on the same flight line. The thermal image sensor is also smaller than a typical RGB digital camera, meaning the resulting images will be smaller as well. Therefore, more images are required further reducing the speed of the survey.

This extra time to collect data increases the overall flight time and can lead to greater inconsistencies between images, such as an image taken early in the morning versus an image taken in the middle of the afternoon. Heat from the sun can greatly impact surface temperature results.

The original Crawford Creek study area is approximately 2 km² with high relief due to the mountains and creek valley nature of the topography. Long flight times and climbing in altitude depletes drone batteries and requires interruption to change batteries over. Through data collection in Phase Two of the project, it was discovered that most of the points of interest regarding surface temperature are near the hot springs at the bottom of the valley making a full survey of the area unnecessary. However, this would not be known unless thermal data had been collected.

A method needs to be developed to do a quick and preliminary assessment of a study area, allowing for a thermal image survey to be performed around those points of interest.

UAV Magnetometer Survey - A UAV Magnetometer survey, conducted in October 2023, focused on the Crawford Creek area to assist in the characterization of subsurface structures there (Figure 11). This will provide a better understanding of structural conditions likely to affect movement of geothermal fluids. This work will ultimately assist in determining the location of key structures and how they relate to the thermal springs observed at surface.

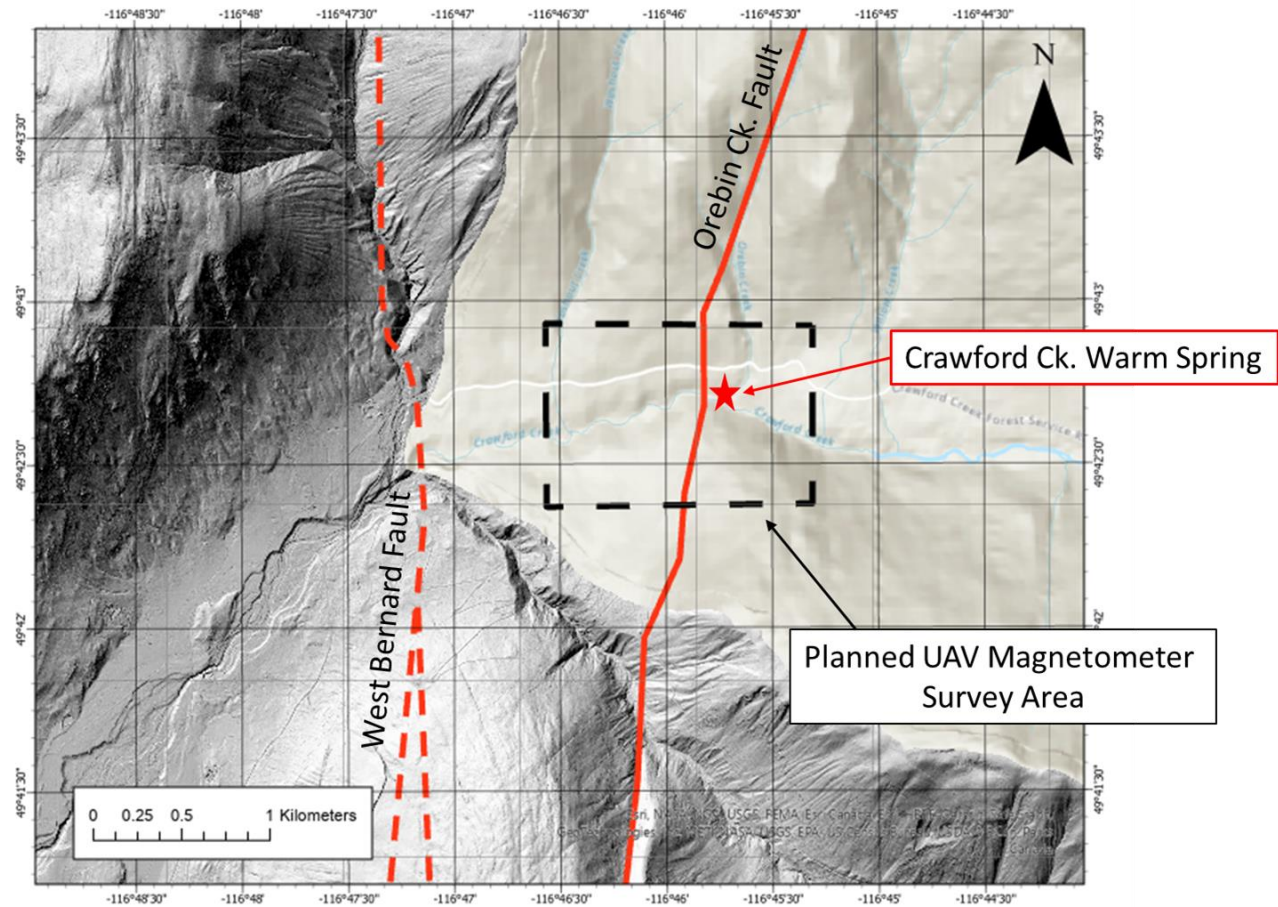


Figure 11 – Planned area of 2023 UAV Magnetometer Survey at Crawford Creek.

Magnetite and pyrrhotite are the two most commonly occurring, strongly magnetic minerals. Magnetic surveys detect the presence of these minerals occurring in varying concentrations. Since different rock types have different background amounts of magnetite, these surveys can be utilized to map lithology. Magnetic surveys can also be used in mapping of fault zones, which can alter magnetite into non-magnetic iron oxide and which therefore appear as linear magnetic lows.

5) Results and Preliminary Interpretation

A. Field Geology – Preliminary geological investigations focused on the Crawford Creek area with over 1,000 measurements being taken (joints, bedding and faults). The joint data suggests three different joint sets, each with unique orientations and dips (Figure 12). For example, Joint Set 1 were mostly steeply dipping (70–88°) compared to Joint Sets 2 and 3 which were dipping (0–55°). Joint Sets 2 and 3, though having non-distinct dips, have different observed orientations.

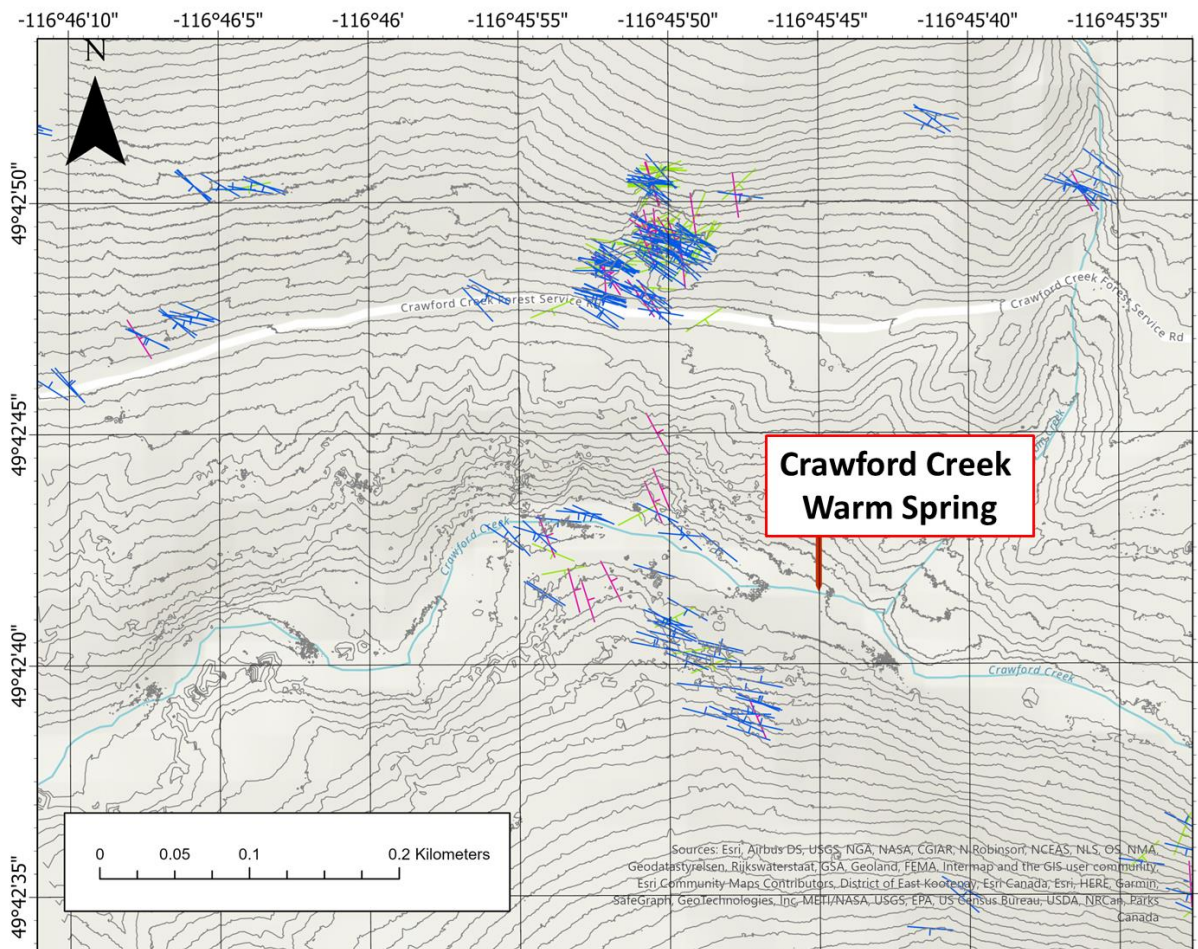


Figure 12 – Three joint sets measured at Crawford Creek: Joint Set 1 – blue, Joint Set 2 – magenta and Joint Set 3 – green.

A steep joint set, Joint Set 1, shown in blue in Figure 12, was the most prevalent, with an overall WNW–ESE strike and increasing joint density along the projected Orebin Creek Fault. These joints had a strike of 277–313° and a dip of 70–88° (Figure 13).

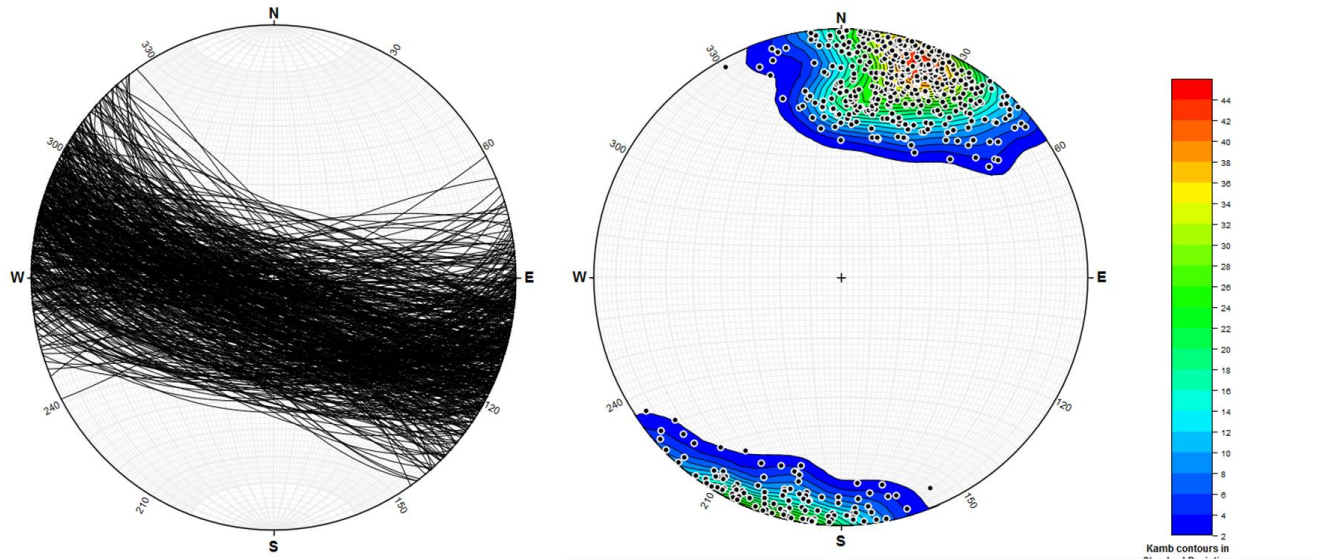


Figure 13 – Stereonet projection of Joint Set 1 (planes, left; poles to planes, right), measured at Crawford Creek.

A second joint set with a strike of 282–303° and a dip of 0–55° was also observed (magenta in Figure 12; Figure 14). Of the three joint sets measured, Joint Set 2 was the least common and was mostly observed on the north side of Crawford Creek. Joint Set 2 has a slight increase in density stretching east-west along the Crawford Creek valley and also where the projected Orebin Creek Fault appears in outcrop on the north side of Crawford Creek. Overall, the joint density of Joint Set 2 decreases on the south side.

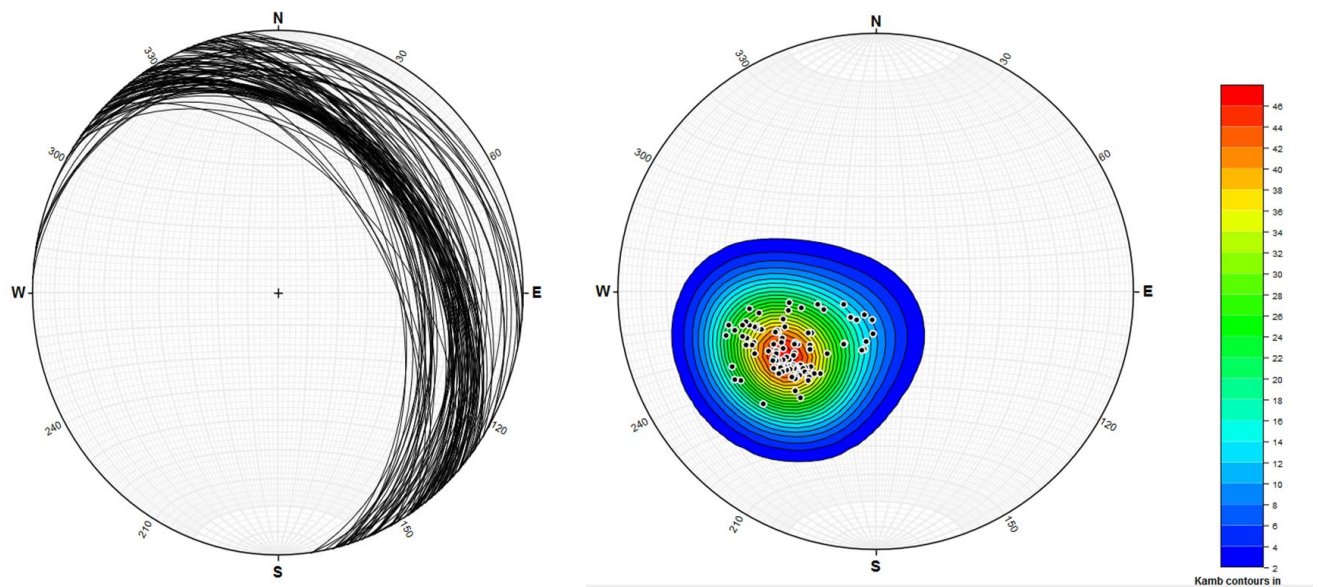


Figure 14 – Stereonet projection of Joint Set 2, (planes, left; poles to planes, right), measured at Crawford Creek.

The third joint set, Joint Set 3, (green in Figure 12; Figure 15) with a strike of 20–121° and dip of 45° was mostly observed on the north side of Crawford Creek, again with increased density proximal to the Orebin Creek Fault.

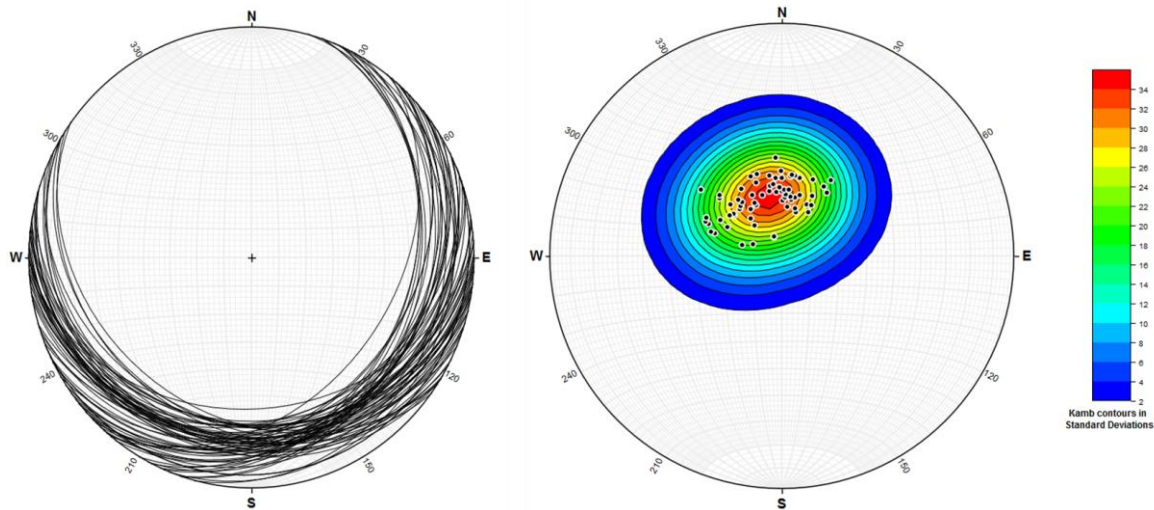


Figure 15 – Stereonet projection of Joint Set 3, (planes, left; poles to planes, right), measured at Crawford Creek.

Overall, there was significantly less fracturing and jointing observed on the south side of Crawford Creek.

In Figure 16, the joint density for Joint Set 1 is displayed. While there were several locations where an increase in joint density was observed closer to the Orebin Creek Fault, the overall joint density appears somewhat random, with no conclusion evident with respect to the reasons behind the observed patterns. Generally, joints were more prevalent north of Crawford Creek, however, vegetation covers much of the outcrop on the south side and, where exposed, it forms cliffs making measurements challenging.

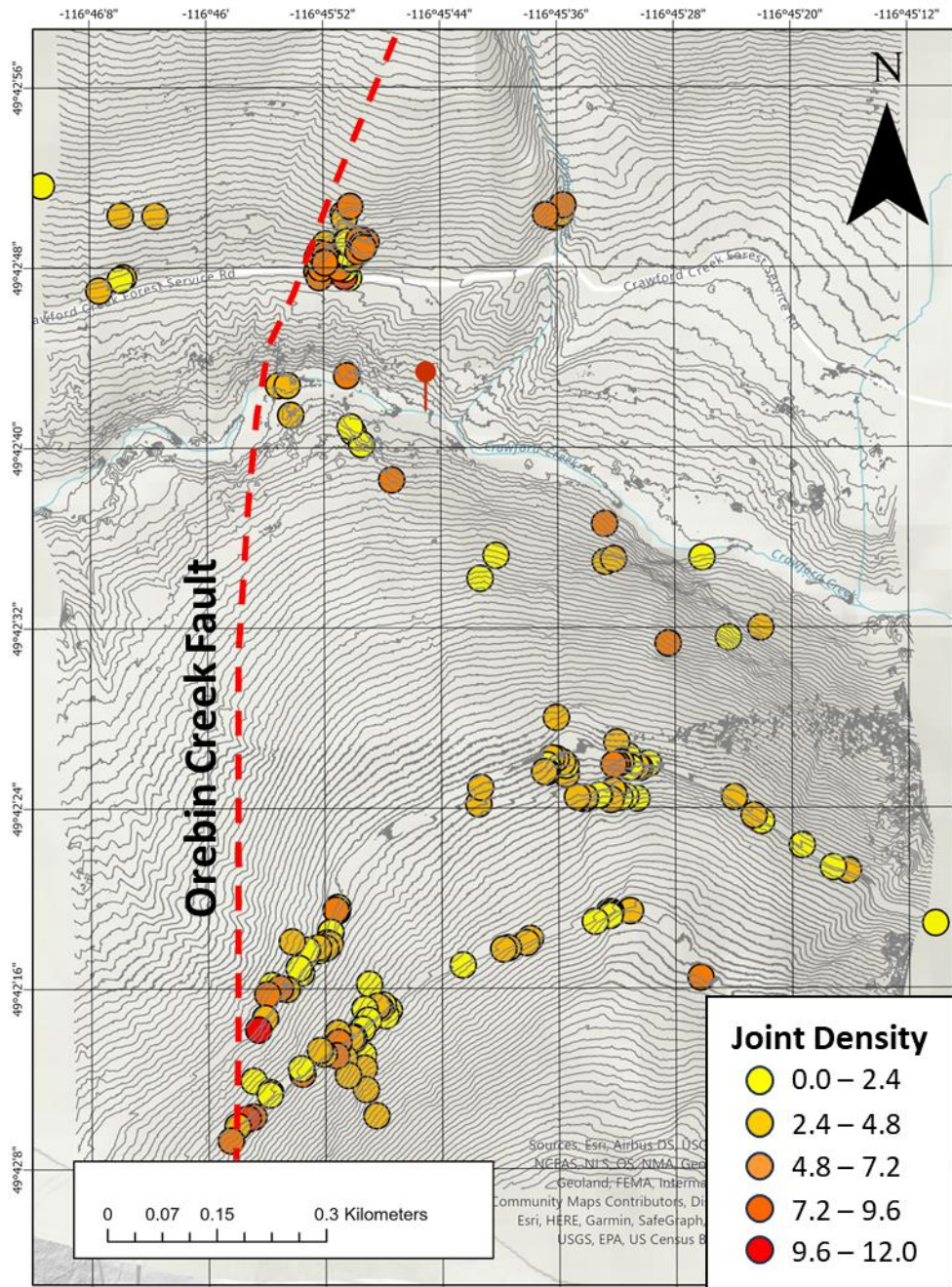


Figure 16 – Steep joints (Joint Set 1); joint density in joints per metre.

The orientation of Joint Set 1 is consistent with that of the Crawford Creek valley bottom in the vicinity of the observed warm springs. Of note, the mapped trend of the Orebin Creek Fault seems to change from NS (south of Crawford Creek) to more NNE–SSW north of Crawford Creek. In addition, joint occurrence and joint density increase going north from Crawford Creek suggesting there could be late-

stage structural movement related to these WNW trends. The WNW jointing at the Bluebell Mine seems to be related to the geothermal fluids encountered there. Comparing the brittle fractures measured near the Bluebell Mine (Moynihan & Pattison, 2011) to the steep Joint Set 1 fractures measured at Crawford Creek, a good correlation is evident, suggesting similar structural influences (Figure 17).

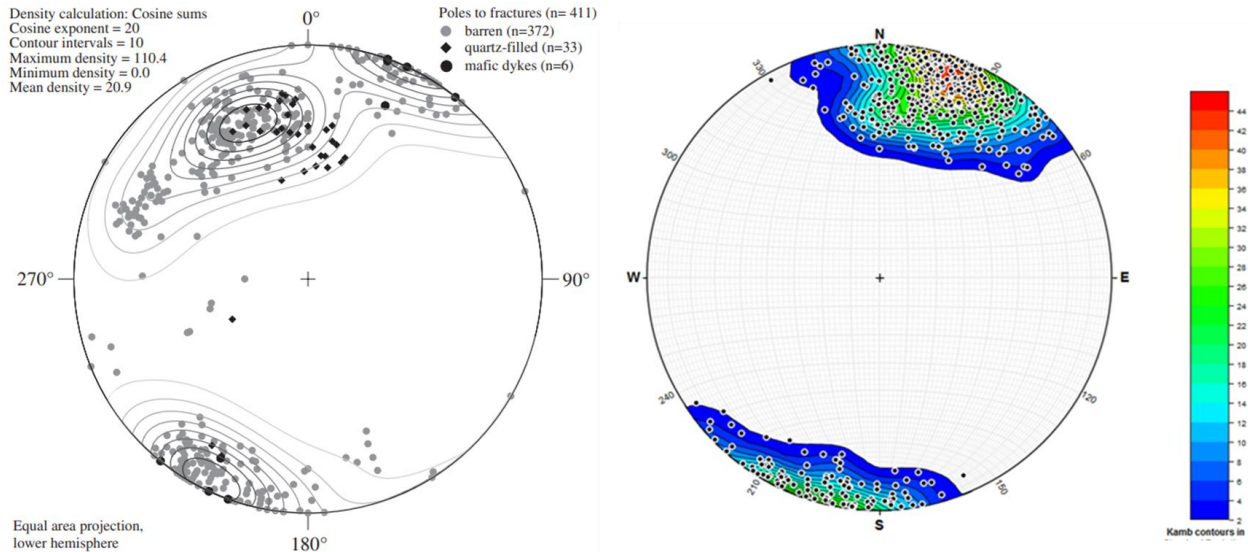


Figure 17 – Equal area lower hemisphere stereonet showing contoured poles to brittle fractures in the Hamill Group (hanging wall), directly to the west of the Comfort and Bluebell ore zones (Moynihan & Pattison, 2011), (left); compared to the WNW steep Joint Set 1 as measured in the Hamill H1 Fm. at Crawford Creek (right).

Areas of extreme fracturing and jointing were very difficult to quantify, in terms of the number of joints per metre; in sections where the density was too intense to quantify, they were identified as 'Fault Gouge'. In some locations the section of exposed outcrop was less than one metre or exposure was spotty, making joint density assessments more challenging and less consistent.

Verification of Thermal Anomalies - Another undertaking in 2023 fieldwork was ground truthing all thermal anomalies highlighted by the fall 2022 thermal drone survey (Figure 18). This survey area was focused on the vicinity of the Crawford Creek warm spring, where a number of compelling features were detected across 400 m, mostly in the valley bottom. Downstream from the main warm spring at Crawford Creek, a 19.7°C flow was observed emerging just below an outcrop of Hamill quartzite.

Further downstream, the westernmost thermal anomaly was completely submerged under early summer creek flow and no warm springs were noticed. By mid-July, however, a warm inflow was detected under a fallen tree with a measured temperature of 21.5°C. Although there were no prominent thermal anomalies on the south side of Crawford Creek, a warm spring was also detected during fieldwork later in the summer. This spring emerged from the hillside almost straight south of the west inflow and on trend with the projected Orebin Creek Fault. This spring was 17.4°C and maintained this temperature throughout the summer. Table 2 shows the sites that were retested through the summer and highlights the locations that were later sampled for geochemical analysis.

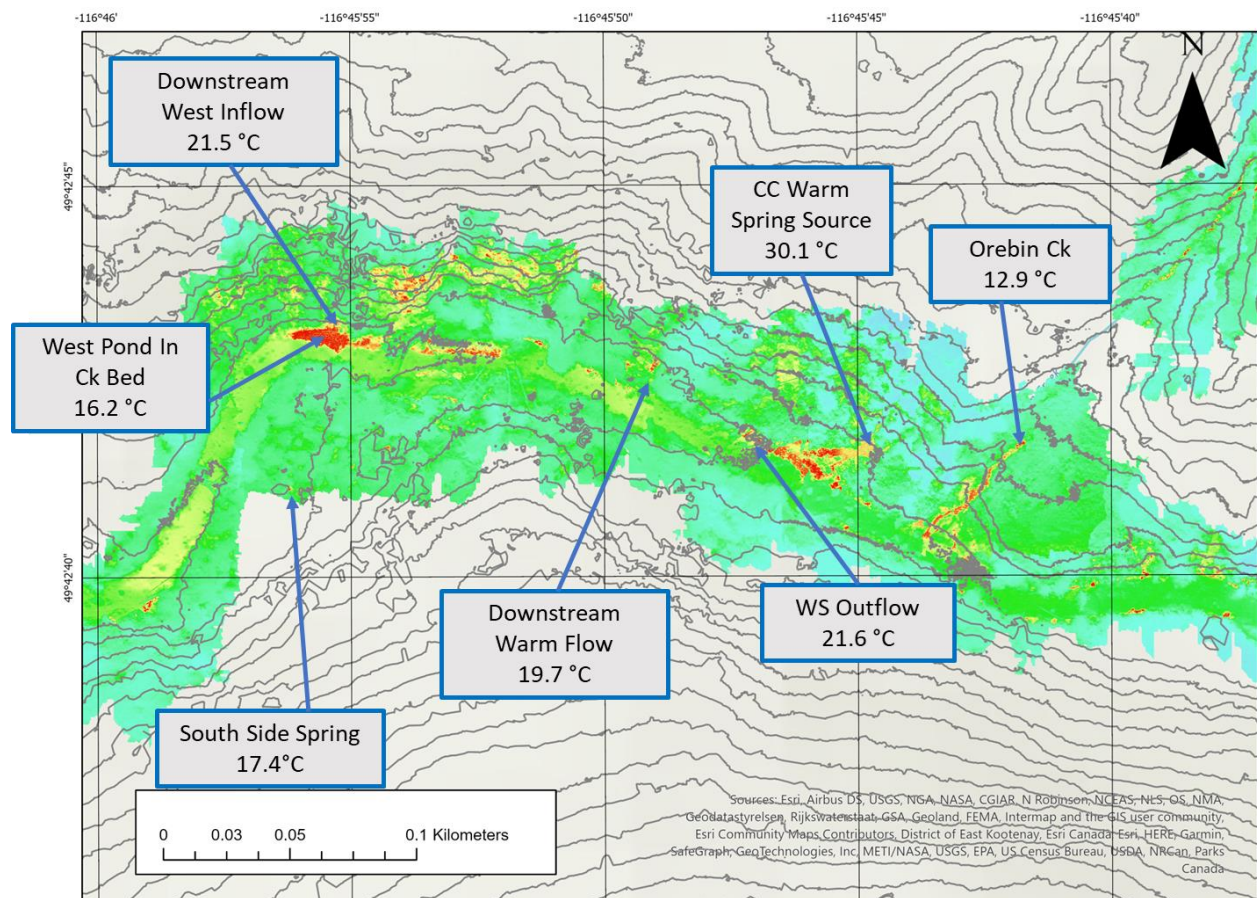


Figure 18 – Warm springs verified in the field, all targeted for geochemical sampling.

The one characteristic of all the warm springs in this area is a slightly lower pH (6.2-7.0) compared to springs outside the area of assumed thermal influence, where pH was as high as 7.9. Similarly, the warm springs have lower TDS (avg. 72 ppm)

and conductivity (avg. 74 $\mu\text{S}/\text{cm}$) compared to immediately outside the thermally influenced area where TDS was about 147 ppm with conductivity of 190 $\mu\text{S}/\text{cm}$.

Sample ID	Name/Location	Date	Water Temp	Air Temp	pH	Cond	TDS	Salinity
	Orebin Ck Anomaly	01-Aug	11.9	21	6.63	77	60.1	0
	Orebin Ck Anomaly	08-Aug	12.8	24	6.69	76.6	60.6	0
	Orebin Ck Anomaly	23-Aug	12.9	18	6.69	70.6	51.5	0
	West pond in ncreek bed	08-Aug	16.2	24	6.93	130.4	100	0
	West pond in ncreek bed	01-Aug	16.2	25	6.97	127.7	99.8	0
CC-23-02	Warm Flow	13-Jul	19.7	23	6.42	53.8	42.6	0
CC-23-02	Warm Flow	25-Jul	19.8	25	6.43	54.8	42.6	0
CC-23-02	Warm Flow	01-Aug	19.7	25	6.28	54.5	42.5	0
CC-23-02	Warm Flow	08-Aug	19.7	24	6.3	54.3	42.7	0
CC-23-02	Warm Flow	23-Aug	19.6	18	6.69	54.9	42.4	0
CC-23-02	Warm Flow	21-Jun	19.7	15	6.26	54.4	38.6	0
CC-23-01	Warm Spring	21-Jun	29.8	16	6.67	71.8	51.1	0
CC-23-01	Warm Spring	13-Jul	30	23	6.78	70.4	56.4	0
CC-23-01	Warm Spring	25-Jul	30.1	25	6.63	70.5	55.7	0
CC-23-01	Warm Spring	01-Aug	30.1	25	6.52	71.8	56.2	0
CC-23-01	Warm Spring	08-Aug	30.1	24	6.63	71.4	56.2	0
CC-23-01	Warm Spring	23-Aug	30.1	19	6.67	71.7	55.3	0
	warm spring outflow	21-Jun	21.6	16	6.96	72.1	50.2	0
	warm spring outflow	13-Jul	24.4	25	7.26	86.1	57.7	0
CC-23-03	West anomaly	13-Jul	21.4	26	6.99	95.3	75.7	0
CC-23-03	West anomaly	25-Jul	21.5	26	7.09	97.3	74.8	0
CC-23-03	West anomaly	20-Jul	21.5	29	7.07	98.2	75.8	0
CC-23-03	West anomaly	01-Aug	21.5	25	7.06	86.4	75.2	0
CC-23-03	West anomaly	23-Aug	21.4	19	7.07	96.3	74.7	0
CC-23-03	West anomaly	08-Aug	21.5	24	6.95	95.3	75.6	0

Table 2 – Crawford Creek warm springs re-test sites with recorded multiparameter readings.

The Crawford Creek warm spring was measured at 30.1°C where it emerged from the ground. After this spring water travelled some 50–60 m before it emptied into Crawford Creek, the temperature measured at that location was only 21.6°C; a temperature similar to what was actually measured at both the downstream ‘Warm Flow’ and the ‘West Inflow’ sites. The main Crawford Creek warm spring was flow tested in July 2023 using a five-gallon bucket and a stopwatch. The estimated flow rate was 10 gallons per minute.

Two other sites are worthy of mention. In the middle of the Crawford Creek bed about 10 m from the warm inflow (labelled West Anomaly in Table 2), there was a pond that continued to be filled (from below) with no apparent source but with fast outflow from the pool into the main creek nearby. The pond water measured 16.2°C while the active creek flow, 1–2 m away, had a temperature of 11°C. This

would suggest that part of the westernmost thermal anomaly, which lies within the creek bed, is being influenced by warm inflow from beneath. Figure 19 shows this small pond beside and slightly higher than the main flow of Crawford Creek.



Figure 19 – Small warm pond, yellow arrow (16.2°C) in Crawford Creek bed, flowing out into Crawford Creek right.

The other location of note lies within Orebin Creek itself. As part of the ground truthing process, the origin of the thermal anomaly within the creek was investigated. Within the creek, there was a temperature increase of 2-3°C. At the same location, a seep on the creek bank also indicated a temperature increase to 12.8°C compared to 11°C in the creek itself. However, there was a noticeable decrease in pH from 7.7 above to 6.7 in the seep. This site was flagged for geochemical sampling; however, by the end of August the flow from the seep had diminished, therefore it had insufficient clean flow for a sampling.

B. Field Geochemistry - Geochemical sampling was carried out in two batches. A total of 8 sample locations were selected for laboratory analysis in the first batch, early in August. A second batch of 17 samples was selected for sampling at the end of August. A map showing all 2022 and 2023 sample sites is presented in Figure 20 and the Crawford Creek sample sites are shown on the map in Figure 21. The goal to have preliminary results from Batch #1 was to allow for modifications to Batch #2 sample sites, however, these preliminary results were not received in time to make any program adjustments for the second batch.

Geochemical sampling was planned for late summer to minimize the impact of surface runoff and to provide access to sites within the Crawford Creek valley bottom which were covered by high water in the early summer period. For example, the western warm inflow was not even visible until creek levels dropped.

The water samples were collected according to suggested sampling methodologies (Nightingale, 2023), including sample filtration and rinsing of sampling equipment with deionized water (methodologies summarized in Table 3). Batch One samples were delivered to the lab at the University of Calgary on August 16. Batch Two samples were delivered to CARO Analytical Services in Kelowna (metals analysis) as well as the University of Calgary on September 10, 2023. The U of C Applied Geochemistry group – Chemistry (AGg-Chem) Lab analyzed for all anions and cations, including metals and silica (Si); and the Applied Geochemistry Group - Isotope Science Lab - AGg-ISL for isotope analyses.

The water samples collected were analyzed for concentrations of major ions, namely: alkalinity (carbonate/bicarbonate) sodium, calcium, potassium, magnesium, chloride, nitrate, and sulphate. In addition, the following analyzed parameters may also prove invaluable in interpreting the water chemistry and assessing its suitability for geothermal exchange: aluminum, boron, bromide, calcium, fluoride, silicon, iron, lithium, magnesium, manganese, and strontium. Silicon (Si) was collected separately with the filtered water sample diluted with deionized water (1:2 dilution) in the field, which prevents the precipitation of Si before the water is analyzed via ICP-OES (Inductively Coupled Plasma – Optical Emission Spectroscopy). Therefore, the U of C Geochemistry lab is not differentiating between total silica and dissolved silica. The primary metal analyses for arsenic, lead, sulphur, and zinc as well as sulphur and sulphide in water and a suite of other metals were conducted by CARO.

A water sampling device with a 0.45 µm filter was used to sample for both anions and cations as well as numerous isotopes. To use the water filtration device, a fresh filter was placed in between chambers and the top chamber was screwed on tightly. Water was taken from the source using a clean 500 ml Nalgene bottle and poured into the top of the filtering apparatus. The top lid was then screwed

on and the pump handle and tube were attached to the side of the lower chamber. The water was filtered as a vacuum was created in the lower chamber drawing water from the upper chamber through the filter.

Once sufficient water was filtered, the tube and handle were removed and filtered water was poured into the correct collection bottles. Excess water was discarded, and the filtration system was disassembled, disposing of the used filter. The top and bottom sections were rinsed once with deionized water. Deionized water was poured into one section at a time and then the section was turned clockwise as it was slowly tilted so the water could exit. If needed, multiple rinses were performed. The collection Nalgene bottle was also rinsed using the same method. Lastly, a new filter was placed in the apparatus and reassembled.

All samples were filtered and diluted in the field as per standard sampling procedures for surface waters and stored at cool temperatures until delivery at the respective laboratories (see Table 3 for summary of sampling procedures).

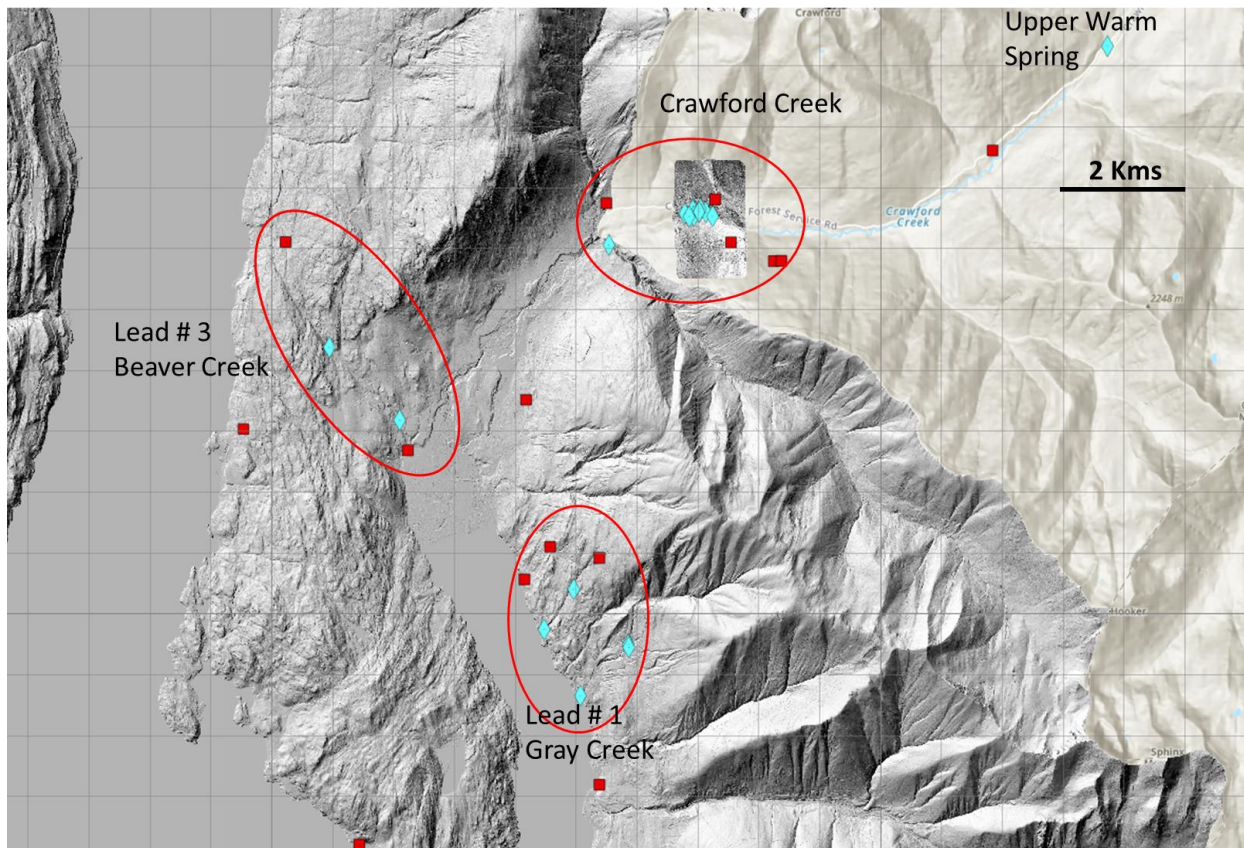


Figure 20 – Geochemical sampling sites (2022 – red, 2023 – blue). Red ovals to highlight areas of focus in 2023.

Note that Lead # 2 identified in Phase Two, is located at the south end of the Pilot Peninsula, just off the map in Figure 20. Given the remote location of this lead, the decision was made to not do any follow-up in Phase Three, but to defer it as a potential future consideration.

Instructions for the collection of isotope samples were very specific. Refer to Table 3 below, which outlines the sampling protocol as provided by the University of Calgary lab.

Isotope or Sample Type	Sample Bottle	Sampling Instructions
Sulfur Isotopes in Sulphide	125 mL Amber glass Bbottle	Dissolved sulphide is precipitated from a 60 125 mL filtered water sample as bright yellow cadmium sulphide by reaction with cadmium acetate. The bottle is then tightly capped and gently inverted a few times to mix.
Sulfur Isotopes in Sulphate	1000mL Nalgene bottle	Dissolved sulphate is precipitated from a 1000 mL of a filtered water sample as barium sulphate via reaction with barium chloride
Oxygen and Hydrogen Isotopes	30mL Nalgene bottle	Fill the 30 mL nalgene bottle with raw (unfiltered) water sample leaving no head-space and cap tightly.
Carbon Isotopes	10-mL Vacu-tainers, loaded with ammoniacal strontium chloride	The vacu-tainers are filled with approximately 1 mL of ammoniacal strontium chloride before going into the field. In the field, approximately 9 mL of a filtered water sample is injected into the vacu-tube using a needle and syringe. No atmospheric CO ₂ should ever be allowed in the vacu-tube, as this will be precipitated in addition to the dissolved carbonate species, skewing the subsequent analysis.
Strontium Isotopes	125mL Nalgene bottle	Fill the 125 mL nalgene bottle with filtered water
Alkalinity	125mL Flint glass Bottle	Fill the 125 mL glass bottle with raw (unfiltered) water sample leaving no head-space and cap tightly. If possible, cool to 4°C until delivered to the laboratory.
Anions	60mL Nalgene bottles	Fill the 60 mL nalgene bottle with filtered water. If possible, cool to 4°C until delivered to the laboratory.
Cations	125mL Nalgene bottle	Fill the 125 mL nalgene bottle with filtered water, leaving a little room for acid addition and mixing. Wearing gloves and eye protection, add approximately 5 drops of concentrated HNO ₃ to lower the pH of the water to around 1.5 or 2.0. The amount of HNO ₃ added will depend on alkalinity of the sample. After adding acid, cap the bottle tightly and invert several times to mix. Then test the pH with the pH paper. If the pH is not low enough, add a little more acid and repeat.

Table 3 – Geochemical Field Sampling Procedures, M. Nightingale, University of Calgary (2023).

	Sample ID	Location Description	Sample Type	Sampled August 14/15, 2023 ^c	Sampled August 28-31, 2023 ^{c, d, e}
Crawford Creek Watershed	CC-23-01 ^a	Crawford Creek Warm Spring, located on the northern side of Crawford Creek.	Spring	X	X
	CC-23-02	Warm Flow, located downgradient of the Crawford Creek Warm Spring (north side of Crawford Creek).	Spring	X	X
	CC-23-03	West Spring, located downgradient of the Crawford Creek Warm Spring (north side of Crawford Creek).	Spring	X	X
	CC-23-04	Toad Creek Spring, downgradient of the Crawford Creek Warm Spring (north side of Crawford Creek).	Spring	X	X
	CC-23-05	South side spring 1, downgradient of the Crawford Creek Warm Spring (south side of Crawford Creek).	Spring	X	X
	CC-23-06	South side spring 2, downgradient of the Crawford Creek Warm Spring (south side of Crawford Creek).	Spring	X	
	CC-23-07	East Spring, located upgradient of the Crawford Warm Spring (slope on north side of Crawford Creek).	Spring		X
	CC-23-08 ^b	Mossy Spring, downgradient of the Crawford Creek Warm Spring (south side of Crawford Creek).	Spring		X
	HC-23-01	Houghton Creek (tributary of Crawford)	SW		X
	US-23-01	Upper Warm Spring which flows from a cave.	Spring		X
Weasel Creek Watershed	GC-23-02	Weasel Creek downgradient of warm spring observed at intersection of Weasel Creek and Hwy 3A	SW	X	
	GC-23-03	Weasel Creek (upgradient)	SW		X
	GC-23-07	Spring on slope southeast of Weasel Creek	Spring		X
Wilmot Creek Watershed	GC-23-01	Wilmot Creek at Hwy 3A	SW	X	
	GC-23-04 ^b	Wilmot Creek	SW		X
	GC-23-06	Wilmot South Tributary	SW		X
Beaver Creek Watershed	BC-23-01	Beaver Creek Upper	SW		X
	BC-23-02	Beaver Creek by Hwy 3A	SW		X
Notes a) CC-23-01 (Crawford Creek warm spring) corresponds to location 72 from the 2022 sampling program. b) A duplicate sample (CC-23-09) was collected at location CC-23-08 (Mossy Spring). A duplicate sample (GC-23-05) was collected at location GC-23-04 (Toad Creek Spring). c) Submitted to the University of Calgary (UofC) Applied Geochemistry Lab (AGq) for analysis of major ions and select trace metals including silica. d) Submitted to CARO Analytical Services for analysis of major ions and trace metals. e) Samples from location CC-23-01 to 05 were submitted to the UofC Isotope Science Laboratory (ISL) for analysis of stable isotopic analysis of water ($\delta^{18}\text{O}$, $\delta^2\text{H}$), dissolved inorganic carbon ($\delta^{13}\text{C}_{\text{DIC}}$, sulphate ($\delta^{34}\text{S}$, $\delta^{16}\text{O}$), and strontium ($^{87}\text{Sr}/^{90}\text{Sr}$).					

Table 4 – 2023 Geochemical sample sites by watershed, SRK Report 2023

Major Ion Geochemistry - A review of all water quality samples collected in 2023 was carried out by SRK Consulting Inc.; see Appendix A for full SRK Report. Their analysis of results led to the identification of two distinct groups based on major ion chemistry.

- Group 1: Proportionally higher sulphate near the Crawford Warm Spring and select surrounding springs (CC-23-01, 02, 03, 05, 06 and 08).
- Group 2: Proportionally lower sulphate and higher bicarbonate at all other surface water and thermal spring samples (except for Sample 85, which is considered anomalously dilute). (SRK Report, 2023)

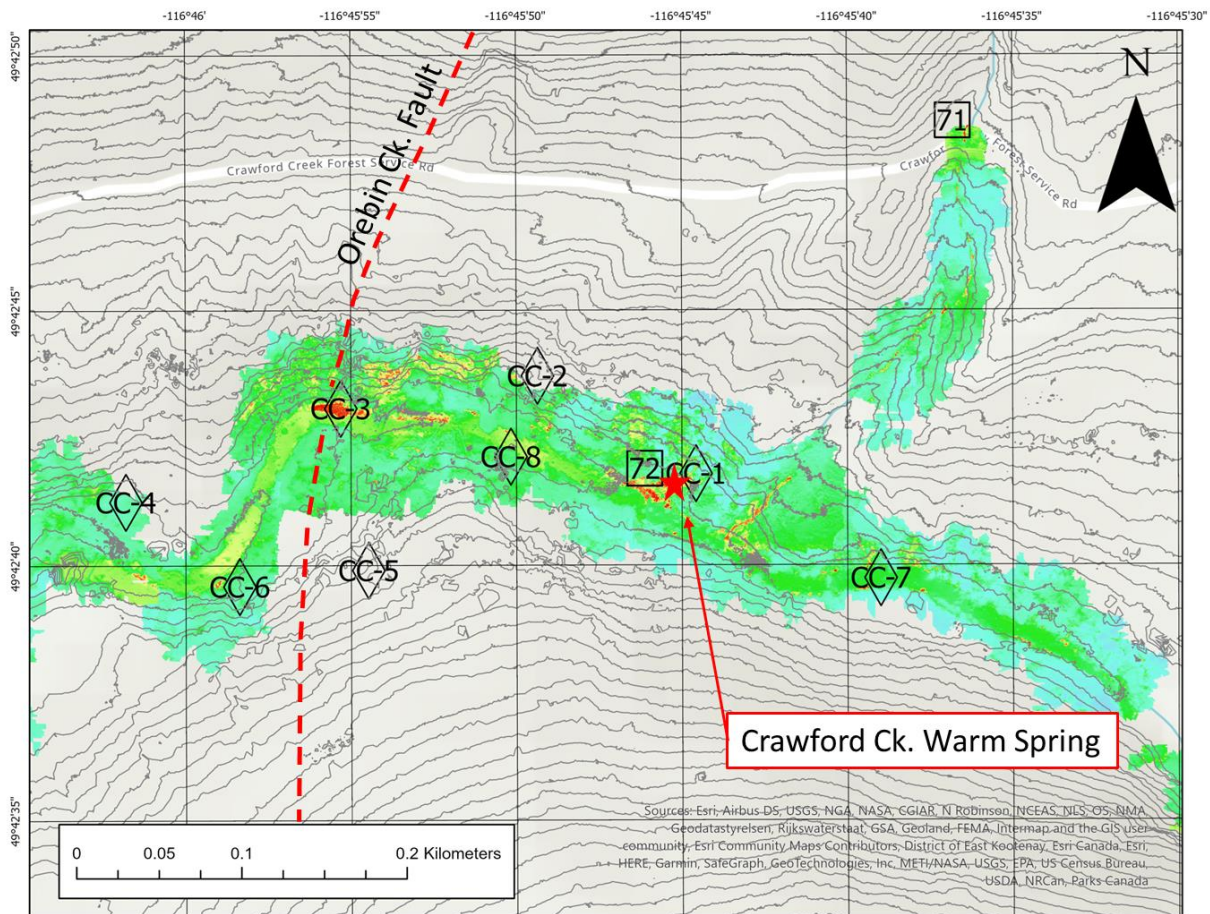


Figure 21 - Geochemical sampling sites at Crawford Creek (diamonds - 2023; squares - 2022), overlain on 2022 thermal mosaic and 5 m contours from Digital Elevation Model (DEM).

As discussed in the geology section and first introduced in Phase Two, the host formation of the Crawford Creek warm springs is the Hamill H1 quartzite, bound to the west by the Orebin Creek Fault and the Hamill H2 schist and phyllite. Figure 21 (above) shows the locations of the sample sites at Crawford Creek and also highlights the approximate position of the Orebin Creek Fault. Sample CC-23-04 was collected from a small creek within the H2 schist; Sample CC-23-06 is the outflow on the southside warm spring sampled downstream at CC-23-05. Therefore, all the sample sites shown in Figure 21 are sourced within the area underlain by the Hamill H1 quartzite, rock that is relatively resistant to weathering; except CC-23-04 to the west. As these sites were regularly tested through the summer field season, it was apparent that the thermally influenced waters within the H1 quartzite had low TDS and conductivity along with a pH between 6.26 and 7.09. Stepping outside the thermally influenced area, the TDS, pH and

conductivity were all observed to increase, while temperature decreased. This speaks to the local, unique nature of the thermal waters at Crawford Creek.

A comparison between samples from thermal waters on the north and south sides of Crawford Creek indicates that they have similar sources and have been subject to similar processes influencing major ion chemistry. These thermally influenced waters are present across a broad area, spanning 50 m on either side of the creek and 300 m along Crawford Creek. Crawford Warm Spring and surrounding spring samples suggest thermal water represented by samples CC-23-01, 02, 03, 05, 06 and 08 could be derived from a unique source (SRK Report, 2023).

Watershed	Number of Measurements	Water Temperature (°C)	Air Temperature (°C)	pH	Conductivity (µS/cm)
Crawford	30	9.7 – 30.1	15 - 29	6.3 – 8.3	9.9 - 896
Weasel	4	8.3 – 17.1	19 - 29	7.3 – 8.2	41 - 333
Wilmot	3	11.0 – 13.1	19 - 27	7.9 – 7.6	23.4 – 32.4
Beaver	3	12.7 – 14.4	16 - 17	7.4 – 8.0	113 - 185

Table 5 - Summary of field parameters measured (select 2022 locations and 2023 locations), SRK Report, 2023.

The Crawford Creek warm spring, CC-23-01 and Sample 72, as well as CC-23-02, 03, 05, 06 and 08, located near the Crawford Warm Spring all had proportionally higher sulphate, sodium and potassium, and lower calcium compared to surface water resulting in samples from the Crawford Warm Spring plotting in Group 1 on the Piper diagram (Figure 22).

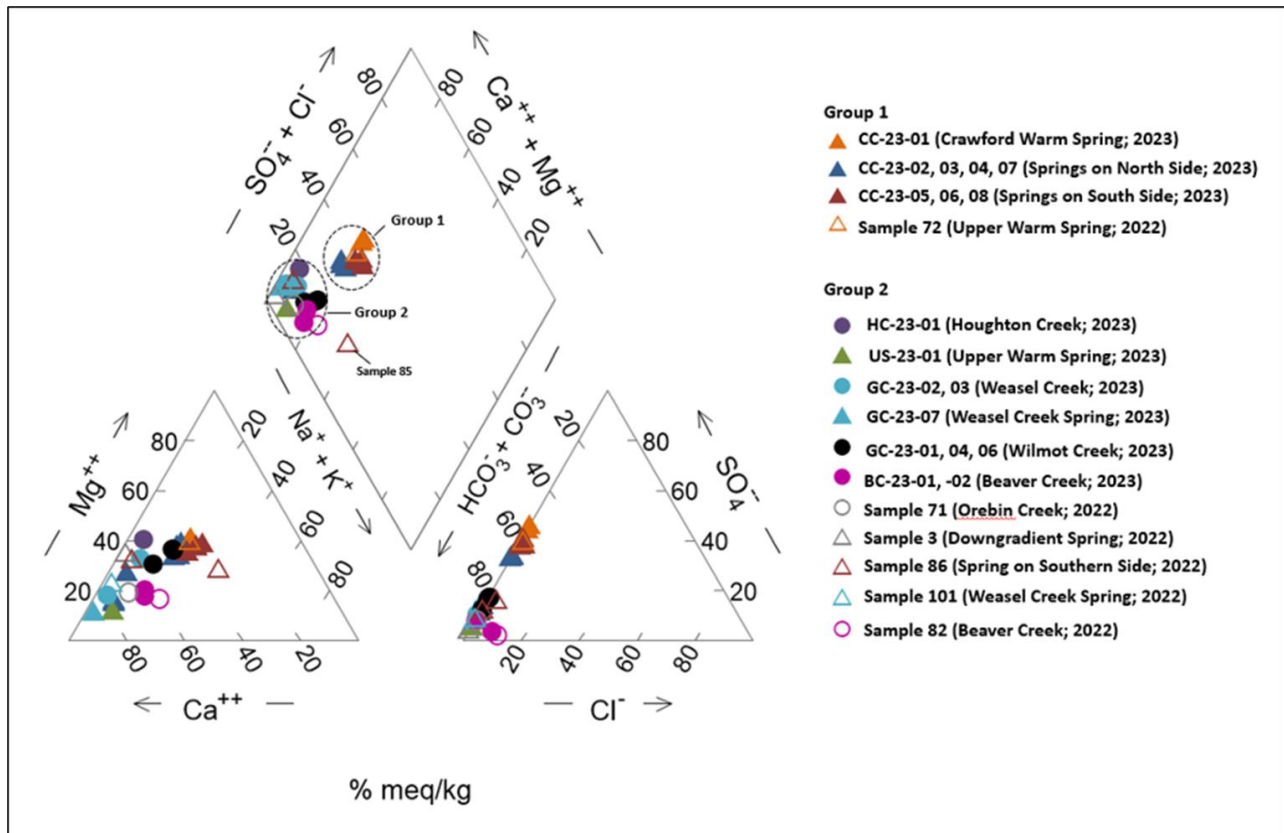


Figure 22 - Piper diagram of water samples collected from Crawford, Weasel, Wilmot and Beaver creek watersheds in 2022 and 2023. Samples collected from thermal springs are depicted with a triangle; the surface water samples are shown as a circle, SRK Report, 2023.

Sample 85, from the 2022 program, has a different proportion of major ions compared to the Crawford warm spring (Group 1), with proportionally higher sodium and potassium, and lower calcium compared to all other samples (SRK Report, 2023). In addition, it was observed to have a very low TDS of 7 ppm. The location where this sample was taken is at an elevation of approximately 990 m on the south side of Crawford Creek (some 250 m above the Crawford Creek warm spring). The sample location was in the Hamill H1 quartzite where water was flowing from a small fault. The temperature was 9.2°C, so no further sampling was initiated. However, water with a low TDS or very low concentration of ions in solution may be an indication that the sample is from precipitation and that has had limited water-rock interaction. The seeps and springs in the vicinity of sample 85 will be investigated further in 2024 to determine if it represents water along the pathway between recharge and discharge in the Crawford Creek warm spring area. Additional $\delta^2\text{H}\text{H}_2\text{O}$ and $\delta^{18}\text{O}\text{H}_2\text{O}$ isotope analysis of sample 85 and Group 2 could support the hypothesis that a mixing line appears between these groups and the Crawford Creek warm springs.

In addition, SRK completed the following geothermometers: quartz, chalcedony, amorphous silica, Na/K and Na-K-Ca. It was concluded that given the low cation concentrations (including silica) and relatively low temperatures of thermal springs in the study area, the underlying assumptions associated with use of geothermometers are not interpreted to be met (SRK Report, 2023). The geothermometers considered did not result in a reasonable estimation of reservoir temperatures and were therefore not included in this report. Details regarding the SRK work completed on geothermometers can be found in the SRK Report, included in the appendix.

Stable Isotope Ratios - During the 2023 field campaign, five sites at Crawford Creek were sampled for analysis of the following stable isotope ratios:

- Water (H₂O): ratios are ²H/¹H and ¹⁸O/¹⁶O
- Dissolved inorganic carbon (DIC): ratios are ¹³C/¹²C
- Sulphate (SO₄); ratios are ³⁴S/³²S and ¹⁸O/¹⁶O
- Strontium (Sr, ratios are ⁸⁷Sr/⁸⁶Sr)

The SRK Report (2023) made the following conclusions with respect to the isotopic analysis from select thermal springs from the Crawford Warm Spring area (CC-23-01 to CC-23-05).

- Review of limited $\delta^2\text{H}_{\text{H}_2\text{O}}$ and $\delta^{18}\text{O}_{\text{H}_2\text{O}}$ suggested the variation in values was correlated to temperature; samples most enriched in heavy isotopes (²H and ¹⁸O) had the highest temperatures, while the samples most depleted in heavy isotopes had the lowest temperatures.
- $\delta^2\text{H}_{\text{H}_2\text{O}}$ and $\delta^{18}\text{O}_{\text{H}_2\text{O}}$ values from Crawford Creek thermal springs do not allow for specific identification of sources or processes influencing waters, due to the limited dataset from the thermal springs and generally from surface water in the Crawford Creek Watershed.
- More enriched ¹³C_{HCO₃} values and higher calculated pCO₂(g) values from thermal springs compared to the atmosphere suggest that interaction between thermal springs and the atmosphere is limited and the dominant source of Dissolved Inorganic Carbon (DIC) is from soil CO₂(g).
- The $\delta^{34}\text{S}_{\text{SO}_4}$ values suggest the source of sulphate in thermal water originates from atmospheric deposition, however $\delta^{18}\text{O}_{\text{SO}_4}$ values plot within range of oxidation of sulphide minerals. These results suggest possible mixing of sulphate from atmospheric deposition and oxidation of sulphide minerals.

- Strontium isotope values ($^{87}\text{Sr}/^{86}\text{Sr}$) from thermal springs in Crawford Creek Watershed ranged from 0.739 to 0.740, suggesting water was in contact with silicate minerals.

For more detail on major ion geochemistry or stable isotope ratio results for Phase Three, refer to the 2023 SRK Report (Appendix A).

C. Temperature Probe Survey - The temperature data loggers provided by the Geological Survey of Canada (GSC) were turned on at the same time to record at 16:00, July 5, 2023. They are programmed to continuously record a temperature every 30 minutes. The battery life allows the recording to continue for up to 2.5 years; however, it was decided that one year of recorded temperatures would be sufficient for data interpretation. In this program, the probes were all deployed in July 2023 with a plan to recover them in July 2024.

To record sufficient data for a ground heat flow interpretation, it was recommended by the GSC (Z. Chen) to:

1. Bury two probes at each location, one near the surface and the other at a greater depth (minimum 30 cm).
2. Record both burial depths from the ground surface to the sensor with the sensor positioned horizontally.
3. Record environmental conditions (vegetation, type of ground surface and shadiness or sun exposure).
4. Record GIS coordinates and elevation.
5. Collect soil samples from the section between the probes for every site.
6. Record geological setting (near a fault, outcrop etc.)
7. Note the presence of any geothermal features, such as proximity to hot/warm springs, water seep, creek bank etc.
8. Position one or two loggers well above the ground (in a tree) to record the air temperature for comparison with the recorded ground surface temperatures.

(Z. Chen, pers comm., July 2023)

Twenty-two sites were selected along three traverses, one along the Forest Service Road (FSR), one along the north bank of Crawford Creek and one along the south side of Crawford Creek. Two probes were buried at each of these sites, one at a depth of 40–50 cm and a second shallow probe at a depth of just 3–5 cm. Two probes were hung in trees to record ambient air temperatures, one near Crawford Creek and one near the FSR. Figure 23 shows a map of the locations

where the temperature data loggers were deployed; Appendix F provides a brief description of locations.

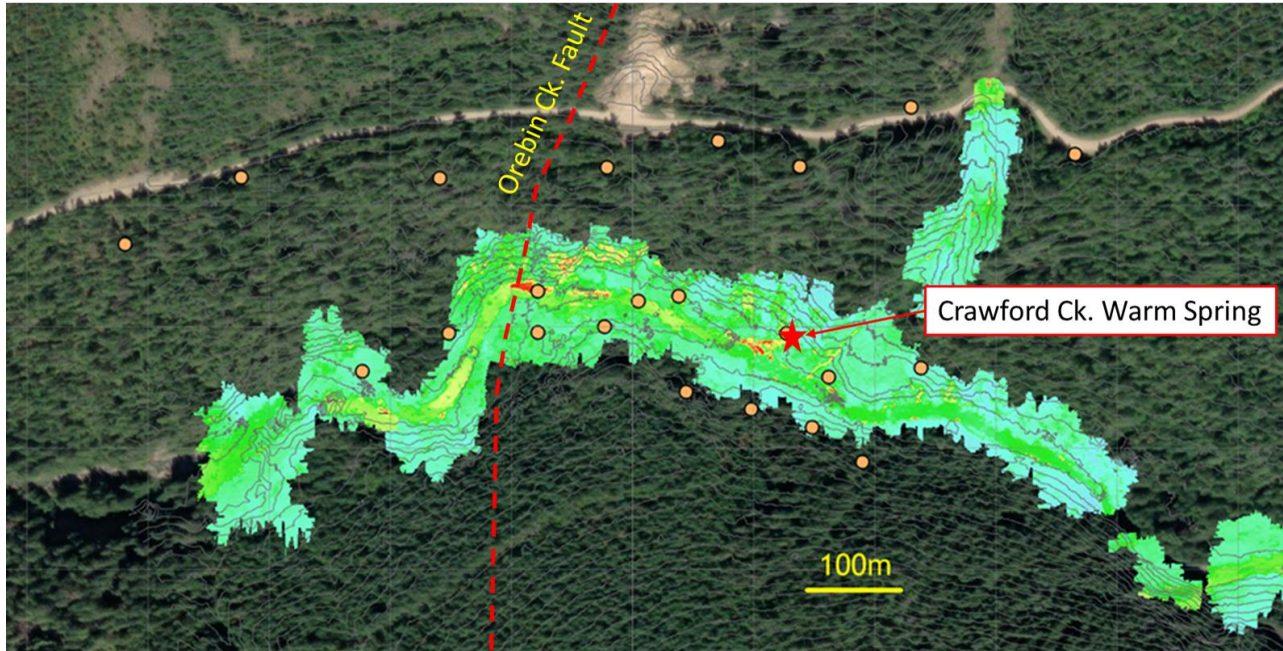


Figure 23 – Twenty-two sites (orange circles) where temperature data logger pairs were deployed at Crawford Creek (July 2023). Overlain on 2022 Thermal Mosaic.

When the data loggers are recovered, a soil sample will be collected in copper tubes of approximately 10 cm diameter, sampling a column of soil that is 15–20 cm in length. During soil and data logger recovery, a measurement of soil moisture will be documented for each site. With these data and soil samples, a lab can use a KD2 pro needle probe for soil thermal conductivity and diffusivity analysis. These measurements will then be used to estimate the heat flow at the sites in question.

D. Electrical Resistivity Tomography (ERT) - In August 2023, three ERT survey lines were conducted as follows: 1) a ~1,000 m long approximately W-E survey along the Crawford Creek Forest Service Road (FSR) with 10 m electrode spacing; 2) a 250 m long ~W-E survey on the north bank of Crawford Creek with 5 m electrode spacing; and 3) a 250 m long ~S-N survey perpendicular to profiles 1 and 2, with 5 m electrode spacing (see Figure 24). These survey lines were designed to cover all surface warm spring outlets and major geological features of interest (e.g., the Orebin Creek Fault). Access was made difficult by thick vegetation and steep terrain, and bearing deviations were required in some lines to avoid challenging terrain.

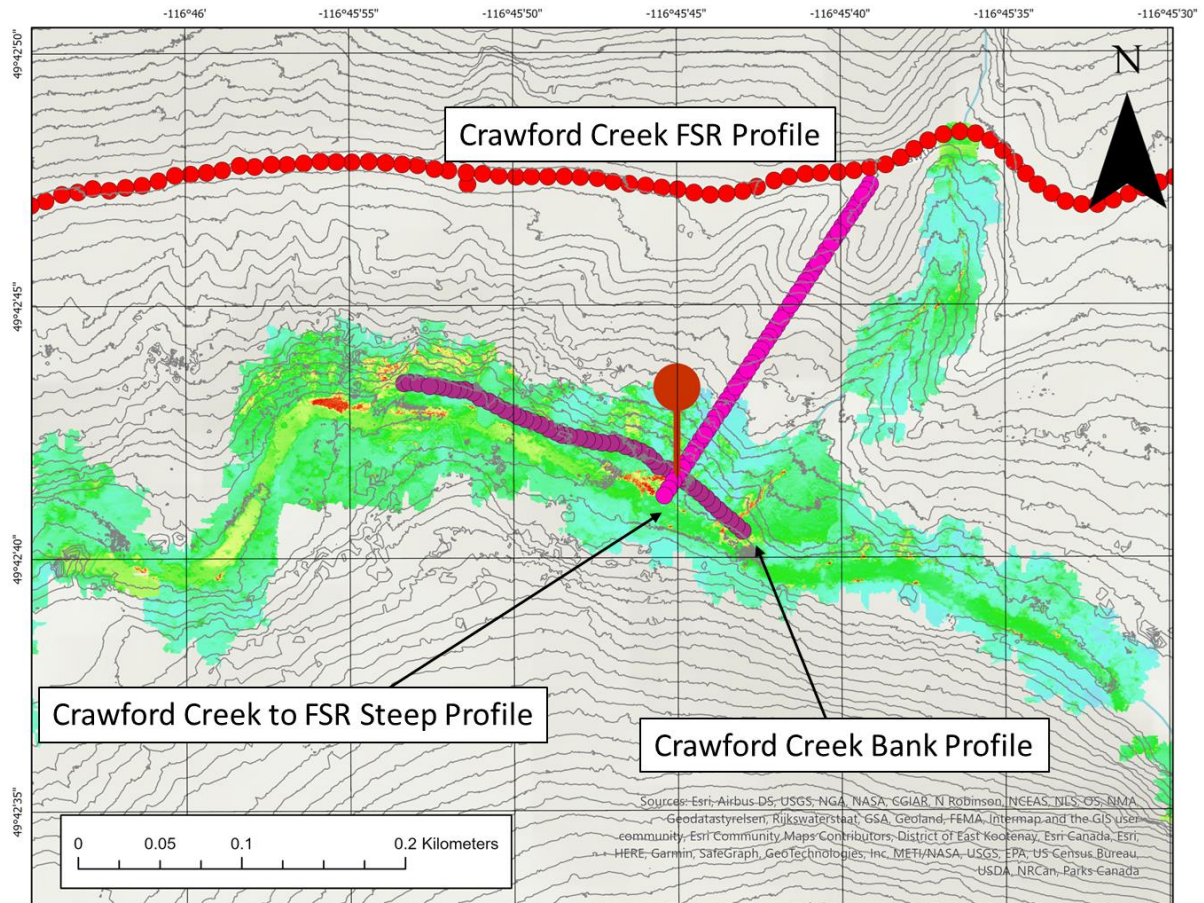


Figure 24 – Position of all electrodes for the three ERT profiles, Uvic August 2023.

Topographic profiles of each survey line were measured in the field using a Trimble R12 RTK GPS system and refined using LiDAR DEMs of the area, to correct for topographic variations along each profile. The apparent resistivity measurements from all combinations of electrode dipole pairs were plotted and contoured in pseudo-sections and then inverted using AGI EarthImager 2D software to solve for models of the true resistivity structure of the subsurface.

The electrical resistivity of rocks is quite variable, therefore, observed values ranged several orders of magnitude with considerable variability even within individual rock types (Figure 25). The rocks encountered in the Crawford Creek vicinity are composed of silicates predominantly, which suggests low conductivity or high resistivity. Pore space and fluid saturation, however, can lower the resistivity of bedrock significantly as reflected in the ranges shown for freshwater and saltwater below.

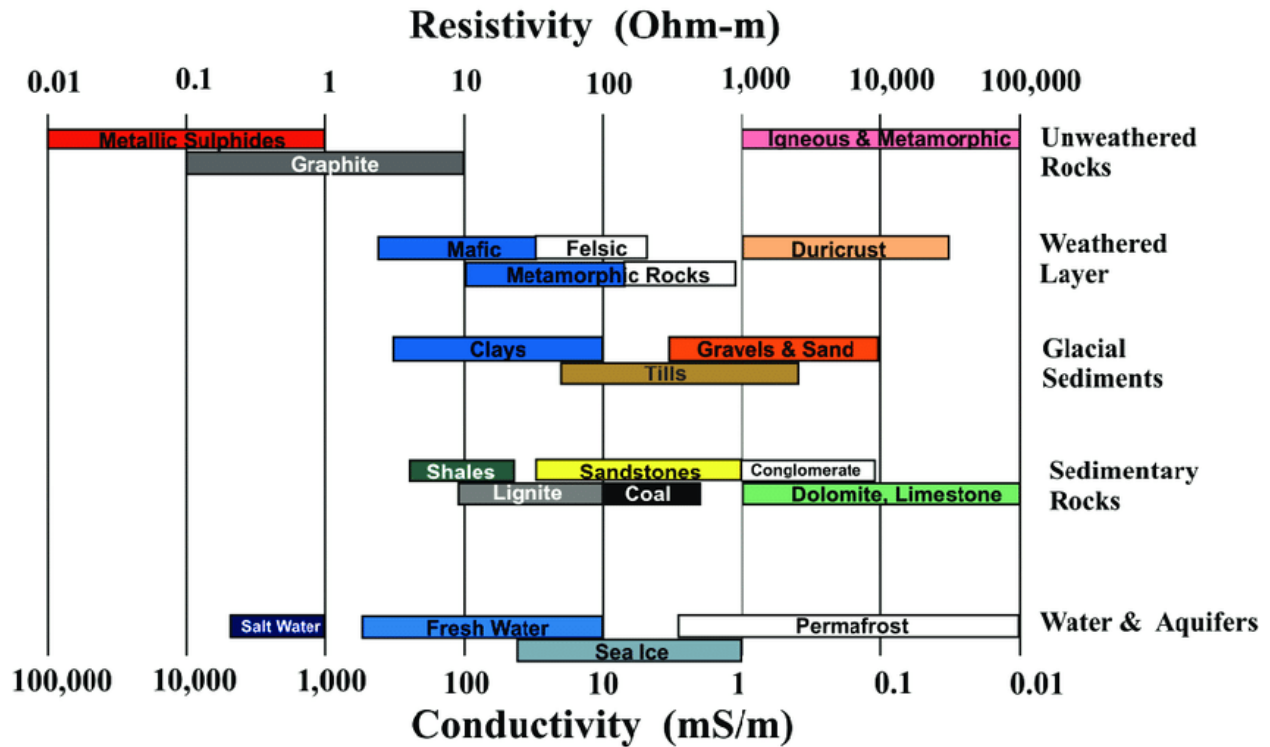


Figure 25 - Typical electrical resistivity and conductivity values found for Earth materials. Rosas-Carbajal (2014), adapted from Palacky (1988).

The first ERT section deployed was along the Crawford Creek Forest Service Road (FSR), with electrode spacing every 10 m. While the road itself was easy to access and lay out cable, the placement of electrodes in very compact, rocky substrate along the northern edge of the FSR was often challenging. Following layout of the cable and connection of the electrodes, the circuit was tested for contact resistance. The overall dry condition of the near road surface necessitated the addition of saline solution to improve soil to electrode contact on several of the electrodes. Upon re-test, all electrodes were determined to have good connectivity. There was one location at the west side of the quarry where near surface bedrock did not permit electrode placement, resulting in a gap.

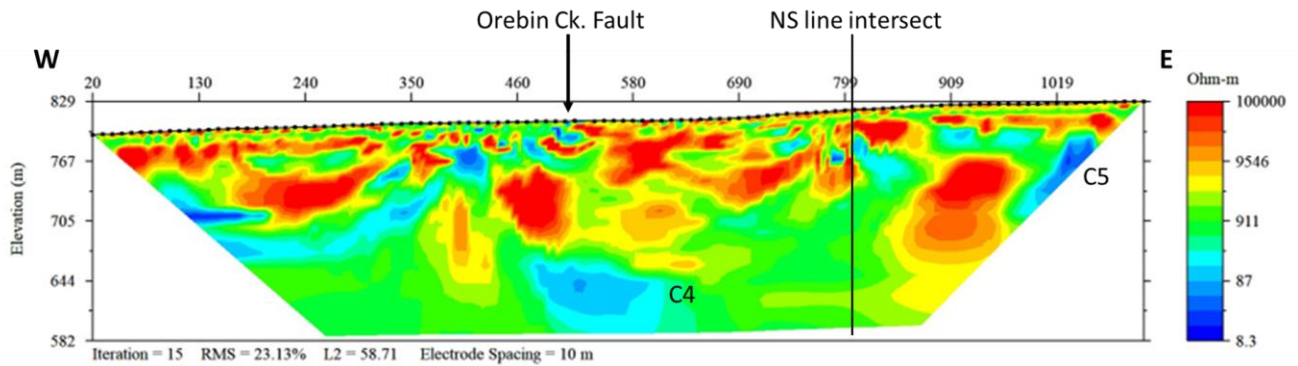


Figure 26 – Preliminary ERT inverted resistivity section – Crawford Creek FSR (electrode spacing 10 m, length ~ 1.2 km), B. Worsnop, UVic, November 2023 (elevation corrected).

A preliminary review of the near surface low resistivity features on the FSR section (Figure 26) west of the Orebin Creek Fault suggests that they correlate to the Hamill H2 micaceous schist, which hosts some localized occurrences of sulphides in surface outcrops and could account for these low resistivity features.

There is a significant low resistivity feature located near the middle of the FSR section, vertically beneath the surface expression of the Orebin Creek Fault. This feature (C4) occurs mostly between an elevation of 660 m and 580 m (about 160–220 m below the FSR). Another low resistivity feature (C5) is evident near the eastern end of the profile but considerably shallower, at 805–790 m. There is also a shallow feature (C5) on the CC to FSR profile near the top (800–795 m; Figure 28). For comparison, the elevation of the outflow of the Crawford Creek warm spring is approximately 743 m.

A second ERT profile (Figure 27) was laid out along the bank of Crawford Creek, extending from the Orebin Creek alluvial fan in the east to a Hamill H1 quartzite cliff band at the west end. This section passed below the Crawford Creek warm spring where there is a boggy surface saturated interval, crossing over an interval of slumped glacial till and past a warm outflow, which emerged under a quartzite cliff band just north of the creek. Immediately west of the surface bog below the warm spring, there is a small low resistivity feature (C2) at an elevation of approximately 726 m underlain by two more pronounced low resistivity features, C1 on the east end and C3 under the warm spring outflow (Warm Flow). Both features lie between 715 and 699 m elevation. It is interesting to note that the C1 low resistivity feature appears to be abruptly truncated to the east by a higher resistivity, near vertical feature.

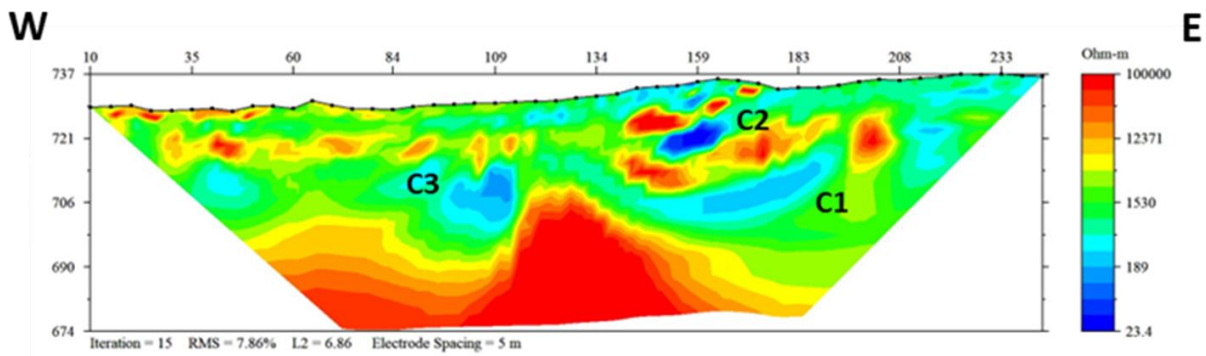


Figure 27 – Preliminary ERT inverted resistivity section – Crawford Creek Bank (electrode spacing 5 m, length ~ 255 m), B. Worsnop, UVic, November 2023 (elevation corrected).

The third ERT profile (Figure 28) extends from the FSR down to the north bank of Crawford Creek, running past the outflow of the Crawford Creek warm spring on route. The most obvious low resistivity feature emerges from the base of the section just north of the outflow of the Crawford Creek warm spring. The top of this near vertical feature (C1) sits at an elevation of 724 m compared to the top of the lower feature on the CC Bank profile which is at 722 m; we therefore interpret them to be the same feature.

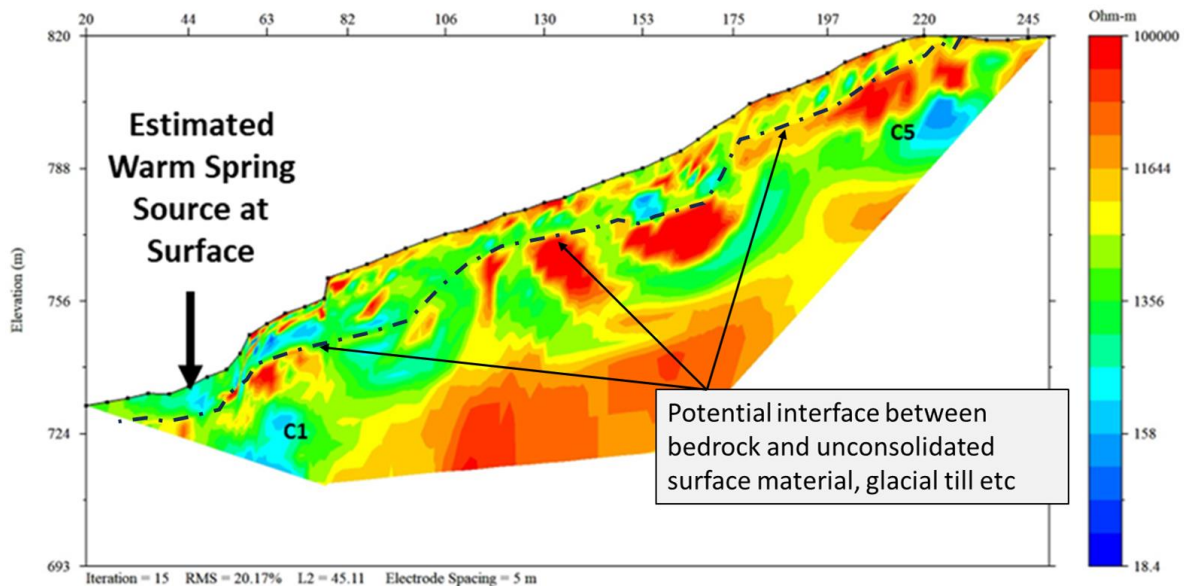


Figure 28 – Preliminary ERT inverted resistivity section – Crawford Creek to FSR Steep profile, above Warm Spring. (electrode spacing 5 m, length ~210 m) B. Worsnop, Uvic, November 2023 (elevation corrected). Interpreted potential bedrock surface shown in dashed black line.

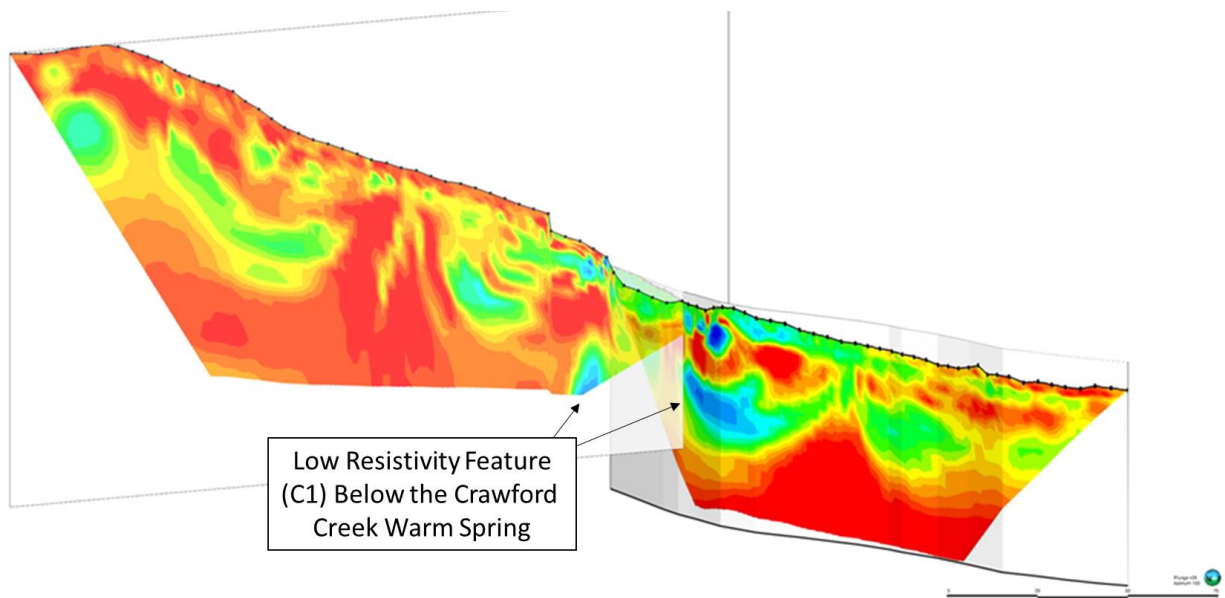


Figure 29 – Partial fence diagram using the Uvic preliminary ERT inverted resistivity sections – Crawford Creek to FSR steep profile (left) intersecting with the Crawford Creek Bank profile (right), Aetna Geothermal, 2023.

The fence diagram shown in Figure 29 highlights the low resistivity feature (C1) evident near the lower end of the FSR to Crawford Creek profile and how it is likely an extension of the low resistivity feature on the Crawford Creek Bank profile. Another similarity between profiles is also evident near the intersection between the FSR profile and the FSR-CC profile, reflecting the C5 feature on both lines. Following the acquisition of more ERT data in Phase Four it is anticipated that the areas of low resistivity or high fluid saturated bedrock can be mapped out with initial rock volumes estimated. The elevations of the various conductors observed are summarized in Table 6.

Electrical Resistivity Tomography (ERT) - Summary of Low Resistivity Features Identified			
Line	Conductor	Elevation Where Encountered (m)	Comment
FSR	C5	805-790	
	C4	660-580	Underlies surface expression of OCF
CC - FSR	C5	800-795	Evident on two lines
	C1	724 - ?	
CC Bank	C1	715-699	Evident on two lines
	C2	726- 715	
	C3	715-699	

Table 6 – Summary of occurrence of low resistivity features on three ERT profiles.

As previously stated, there appear to be low resistivity features present on all three lines which may be reflecting common intervals of fluid saturated bedrock.

E. Geospatial Evaluation – Drone-based Surveys

Thermal Drone Video – Phase Three of the geothermal project utilized a drone-based thermal video to collect and assess surface temperature far more quickly, with the goal to highlight where smaller areas of interest are located, for follow up detailed thermal image surveys. Thermal video capture can be flown at much higher speeds than an image survey. The video analysis is being performed through a frame-by-frame analysis of the thermal video using scripting tools and automation to establish a pixel threshold. Using the flight logs, the output will be geospatial points of interest where surface temperature spikes have been identified. The Crawford Creek warm springs are an ideal test case given the 2022 thermal (TIR) survey which has established the presence of thermal features. Currently, a Selkirk College Bachelor of GIS student is working on this process as a thesis project.

Thermal video was collected on October 19 between the hours of 8:30 a.m.–11:00 a.m. at Crawford Creek using a DJI Mavic 3T enterprise drone. The Mavic 3T's thermal camera has 640 × 512 resolution and supports point and area temperature measurement, high temperature alerts, colour palettes, and isotherms.

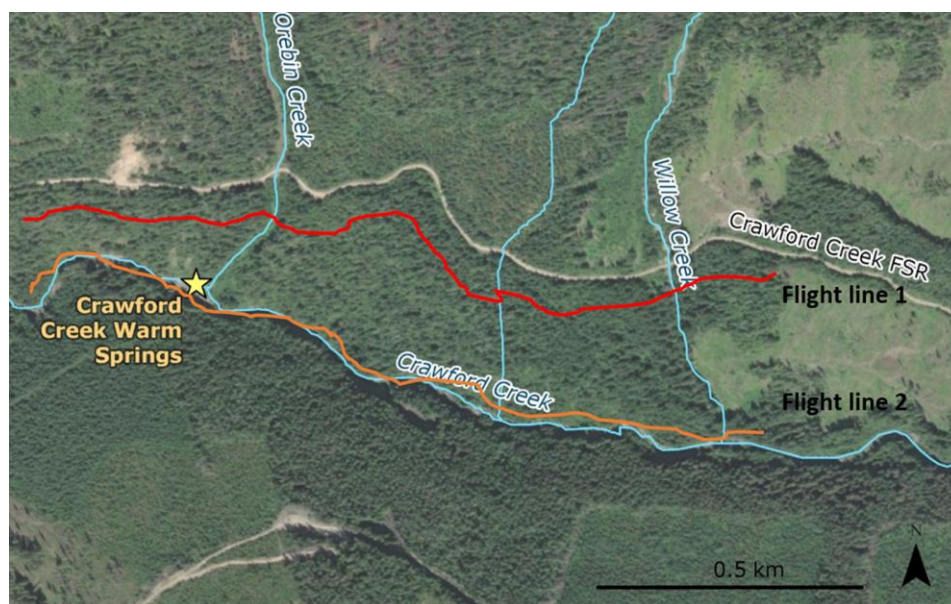
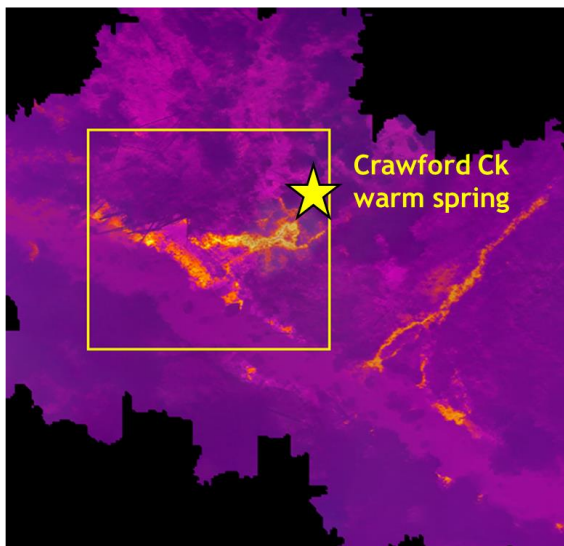


Figure 30 – Drone Thermal Video 2023 flight path, Selkirk 2023.

The thermal video collection was flown manually at an altitude of 120 m at varying speeds (flight path shown in Figure 30). The purpose is for a preliminary proof of concept tool to perform the frame-by-frame analysis and output locations of thermal interest. Upon testing the concept, automated flight planning at higher speeds can be conducted to further increase the efficiency of thermal video data collection. Then other locations can be assessed using this method.

Some preliminary video frame images have been processed over the area of the Crawford Creek warm spring (Figure 31) and when compared to the Thermal Infrared (TIR) mosaic from 2022 there appears to be a reasonably good comparison between the two different modes of thermal data acquisition. The angle of the video frame differs slightly from that of the TIR, however, it does suggest that the drone video approach was successful in the identification of anomalous surface temperatures.

2022 Total Infrared (TIR) Image



2023 Thermal Video Image

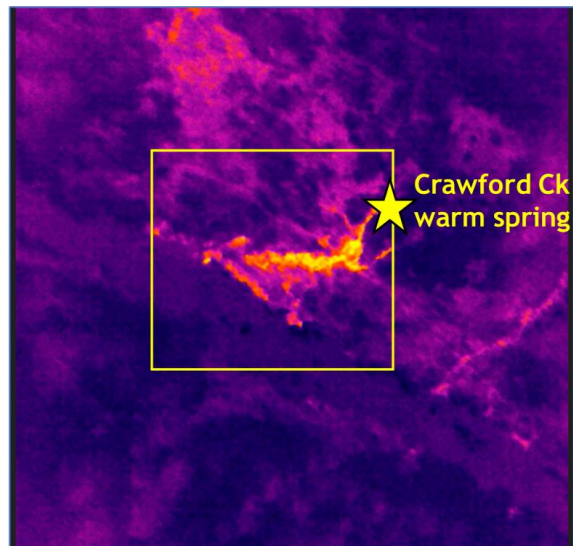


Figure 31 – Total Infrared (TIR) mosaic image (left) compared to drone thermal video frame (right) – location Crawford Creek warm spring (yellow box), Selkirk 2023.

This video methodology could be applied on certain reconnaissance missions, providing access into areas where thermal activity may be suspected or to determine if a thermal seep or spring is more persistent in areas of similar geology. This represents a very cost effective methodology, which could further highlight areas worthy of further detailed investigation.

UAV Magnetometer Survey – Geotronics Consulting Inc., based in Kaladen, BC, were on site on October 19, 2023, to conduct the planned UAV Magnetometer survey. Geotronics were assisted by a fourth year Selkirk College GIS student. Data were acquired over an area of about 1.5 km². The magnetometer used for the UAV (unmanned aerial vehicle) aeromagnetic survey was a GEM Systems potassium type, model GSMP-35U, which has the following specifications:

- sensitivity: 0.0002 nT @ 1 Hz
- resolution: 0.0001 nT
- absolute accuracy: +/- 0.05 nT
- dynamic range: 15,000 to 120,000 nT
- gradient tolerance: 50,000 nT/m
- sampling rate: 1, 2, 5, 10, or 20 readings/second
- operating temperature: -40°C to +55 °C

Mounted with the magnetometer was a laser altimeter for measuring terrain clearance and a GPS unit for measuring the UTM location to an accuracy of 0.7 m. This instrumentation was mounted on the DJI Matrice 300 (M300) RTK unmanned aerial vehicle (UAV) which is a quadcopter with a hovering accuracy of +/- 0.5 m vertical and 1.5 m horizontal. The M300 is controlled by a remote controller with a range of 15 km. The magnetic sensor, which is connected to the potassium magnetometer, was attached to the M300 via a single tow line maintaining a distance of 10 m from the UAV (Geotronics Report, 2023, Appendix B).

The UAV magnetic survey covered an area centred around the Crawford Creek warm springs, consisting of dimensions of 1,000 m in a N-S direction and 1,400 metres in an east-west direction, with a tie line flown in a northerly direction. The survey parameters were as follows:

- total number of kilometres flown: 56.3
- flight line direction: east-west
- flight line separation: 50 metres
- terrain clearance: 35 metres
- UAV speed: 10 m/s
- reading frequency: 20 readings/second
- reading interval: 0.5 metres

The diurnal variation of the magnetic field was monitored by a base station using a GEM Systems Overhauser magnetometer located within the northern part of the survey area as shown on the plan maps (Figures 32, 33 and 34). Its WGS 84 UTM coordinates are 517000 easting and 5506799 northing within zone 11. The magnetometer was set to take a magnetic reading every half second. The data from both the UAV and base station magnetometers were downloaded and the

UAV magnetic data was then corrected for diurnal variation (Geotronics Report, 2023). The Geotronics Report) includes a description of the following suite of maps along with a preliminary interpretation:

- total magnetic intensity (TMI), diurnally corrected
- reduce to the pole
- 1st vertical derivative
- 2nd vertical derivative
- horizontal X derivative
- horizontal Y derivative
- analytical signal
- gaussian regional TMI

The reduced to pole map (Figure 32) conveys a magnetic low centered around the Crawford Creek warm spring, with a very pronounced, linear magnetic high west of the Orebin Creek Fault. While this falls within the Hamill H2 outcrop, a section of massive black phyllite is observed in this area, which may have originally been a magnetic volcanic tuff that has since been metamorphosed.

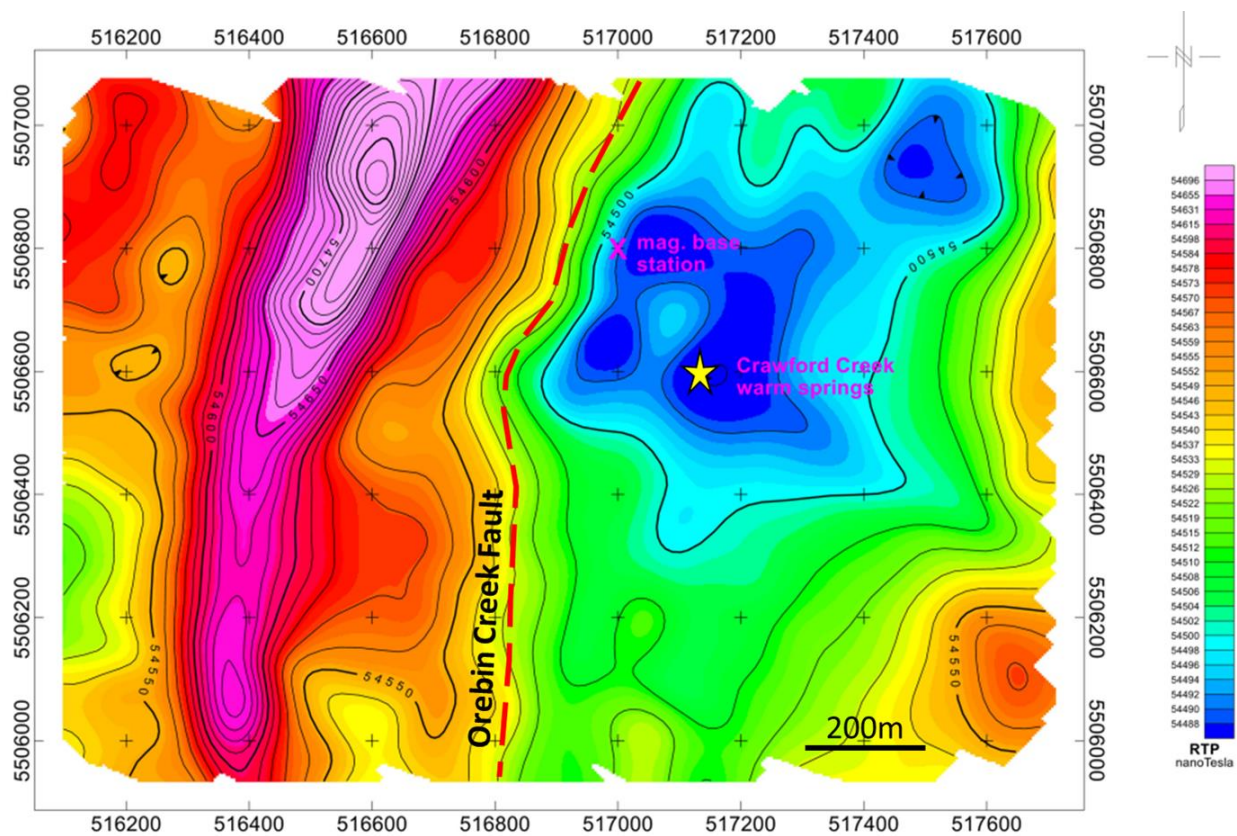


Figure 32 – Reduced to pole (RTP), Geotronics Consulting Inc., 2023

A review of the first and second vertical derivative maps (Figure 33) as well as the horizontal derivative maps (Figure 34) reveals a number of pronounced lineaments. The Orebin Creek Fault, for example, is expressed approximately at the transition from green to yellow (~54530 nano-Tesla) in Figure 31 above. Of note is how the fault essentially trends N-S until it approaches Crawford Creek when the fault then trends NNE-SSW (~21–23°). This orientation is similar to that of measured Joint Set Three (green in Figure 12).

Of particular interest are the strong features evident on the first vertical derivative. Feature A lies just east of the Orebin Creek Fault within the highly fractured Hamill H1 quartzite. The centre of this feature is also the approximate position of conductor C4, evident on the FSR – ERT profile. Feature B is coincident with the Crawford Creek valley as well as the strong lineament on the north horizontal derivative.

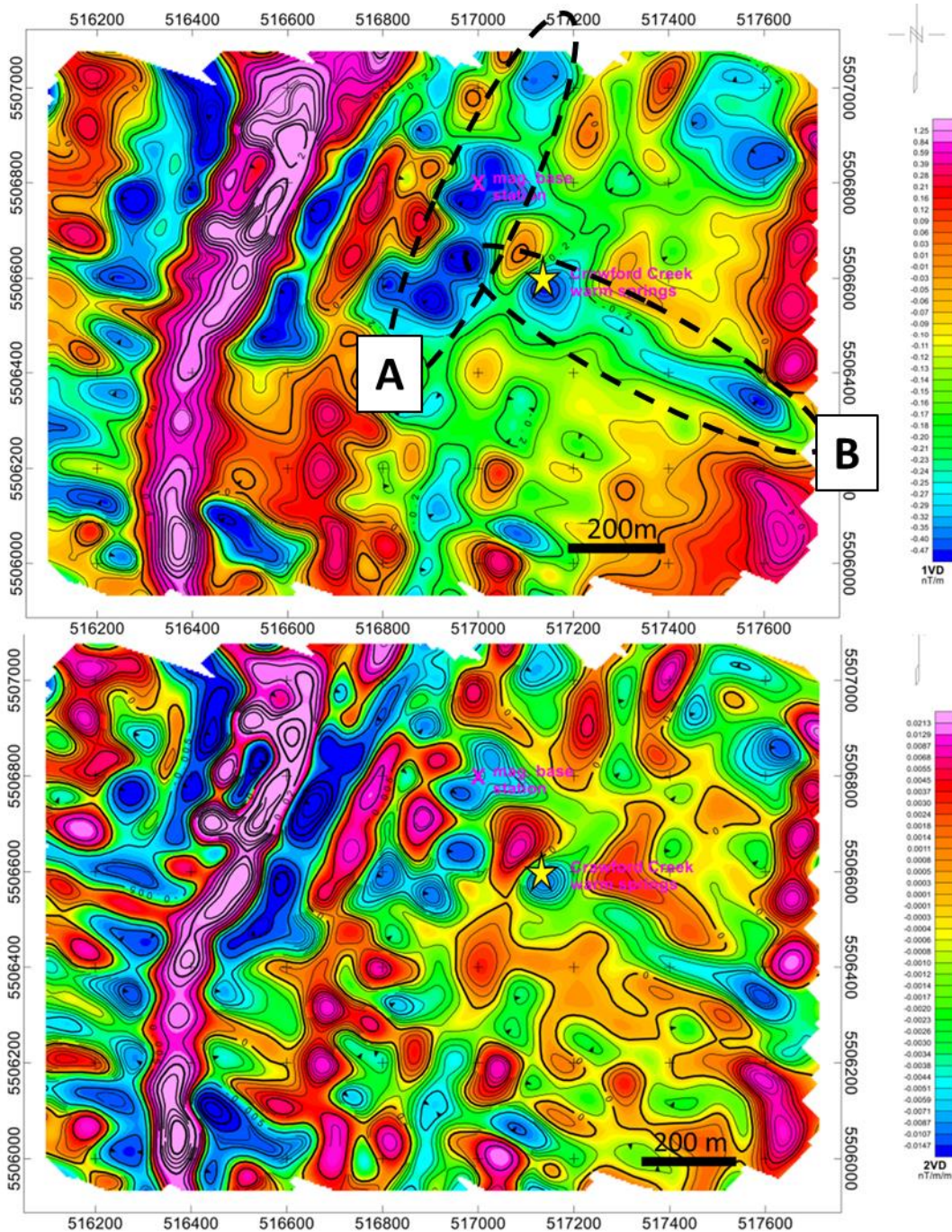


Figure 33 – First vertical derivative (top), second vertical derivative (bottom), Geotronics Consulting Inc. 2023 black dashed outlines (A and B) highlighting strong first vertical derivative features.

The horizontal derivative maps highlight the edges of features, (contacts or faults). Upon examination, another major lineament that is evident on several of the maps is a WNW-ESE trending feature (296–299°) right at the Crawford Creek valley where the warm springs are located. This is very evident on the first horizontal

derivative – North map, which is a measure of the rate of change in a horizontal direction, in this case, north/south (see Figure 34). This WNW-ESE orientation is the same orientation of the most prominent joint set in the area, Joint Set 1 (blue in Figure 12).

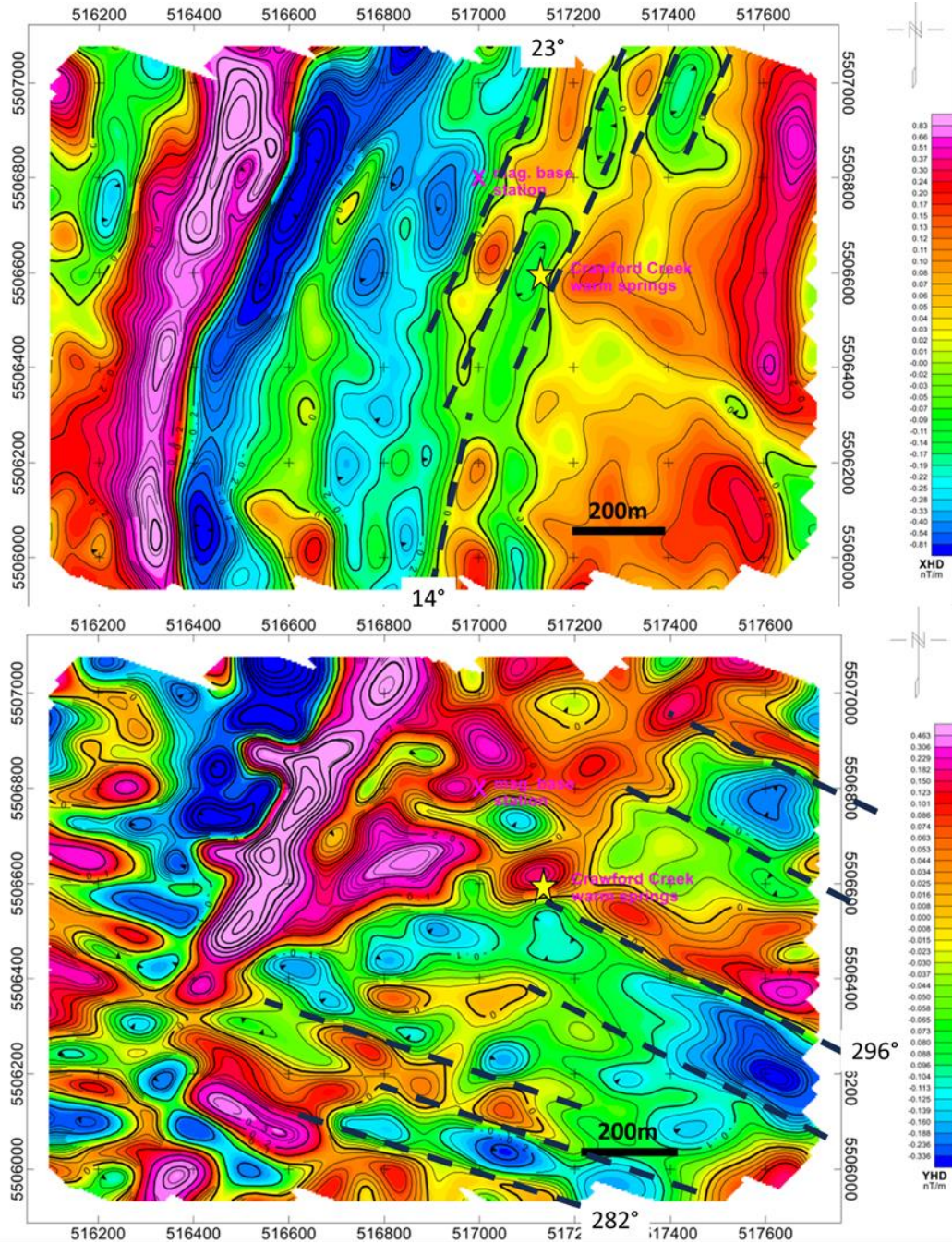


Figure 34 – First horizontal derivative – east map (top), north map (bottom), Geotronics Consulting Inc. 2023, black dashed lines are interpreted structural lineaments.

F. Geological and Geothermal Modelling – A key priority in Phase Three has been to commence the construction of a detailed and fully integrated 3-D model, showing bedrock lithology, bedding, jointing, and faulting, with geophysical results overlain and highlighting potential subsurface geological controls. Ultimately, the model could help provide an estimate of the flow rate for the entire system including observed seeps. This would constrain the hydrogeological model further, knowing the volume and heat content being emitted from the system. This 3-D model would be used to guide the drill planning process, as directional drilling to encounter enhanced fracturing/permeability could be considered.

The data integration completed thus far through Leapfrog Geo by Seequent, via Atena Geothermal, has directionally commenced the 3-D model objective highlighted above. However, additional data inputs will be required to meet the final goal of a fulsome hydrological model.

The geochemical analysis results from the Crawford Creek warm springs suggest that the thermal waters, although likely diluted by surface water flow, have likely not originated from great depths, but have evolved through a shallow geothermal or low enthalpy system. A low enthalpy geothermal system is defined as <90°C (Moeck, 2014). It is recognized that the Hamill H1 quartzite host formation is relatively benign and not prone to producing significant, dissolved mineral components. This was observed in field measurements with TDS values within the quartzite at less than 75 ppm, but most were under 50 ppm and as low as 7 ppm. A diagram from Moeck (2014) in Figure 35, depicts the fundamentals of this type of geothermal model, which may well be at play north and potentially south of Crawford Creek.

With this model in mind, it would seem logical that meteoric water entering near the top of a mountain peak, such as Mount Crawford, would move downward in a fractured, permeable quartzite, potentially penetrating thousands of metres within a quartzite host rock before returning to the surface within the same quartzite. This water will have effectively spent its entire life in the subsurface within a quartzite host; it is therefore reasonable to assume there would be fewer cations and anions associated with this host rock than a schist for example. The result is a relatively uncomplicated geochemistry in the thermal water emerging from the Crawford Creek warm springs.

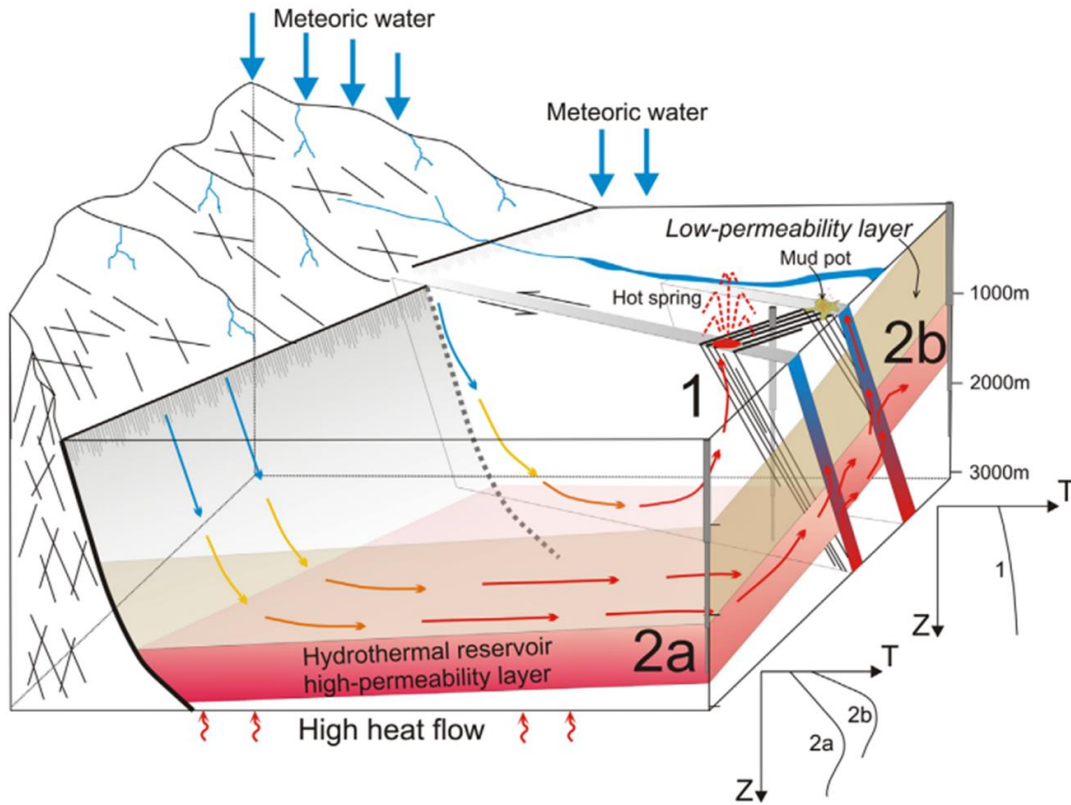


Figure 35 – 3-D schematic model of a non-magmatic active geothermal play system in active extensional terrains with different types of reservoirs (1, 2a & 2b).

Type 1 is a convection cell from infiltration to discharge along one fault. Temperature gradient is gradually increasing at well site 1. Type 2a and 2b are fault leakage-controlled plays. The temperature gradient of a well drilled into such an area rises up to the permeable layer and drops below the layer (well 2a and 2b) (Moeck, 2014).

A shallow or low enthalpy system in this area most likely has meteoric recharge in the region. The highly fractured and steeply dipping Hamill H1 quartzite represents a viable candidate for freshwater input at altitude due to the pervasive and extensive fracturing evident in outcrop. The Hamill H1 quartzite trends NNE from Crawford Creek, outcropping at Mount Crawford, pictured in Figure 35. From the summit of Mount Crawford (2,340 m), the white quartzite can be seen to stretch into the distance, past Plaid Lake (1,591 m) to the ridges in the distance, representing a potentially significant regional recharge area.



Figure 36 – Clockwise from the top left – Hamill H1 quartzite outcropping along the ridge that forms Mount Crawford, Peak of Mount Crawford (upper right), and view looking north from Mount Crawford (lower right) with approximate position of Hamill H1 quartzite outcrop shown above the distant ridgeline.

Photos courtesy of <https://westkootenayhiking.ca/mount-crawford-plaid-lake-trail/>

The 3-D geological section profiled in Figure 37 shows the Hamill H1 quartzite as it extends up to Mount Crawford, bound to the west by the Orebin Creek Fault and the relatively impermeable Hamill H2 schist to the west, with the Three Sisters Gritstone and the Windermere Group phyllite underlying the Hamill to the east. Regionally, this wedge of Hamill H1 quartzite is truncated against the Orebin Creek Fault prior to reaching the Crawford Bay Stock (granite) to the south and it continues north until it contacts the Fry Creek Batholith, some 14 km NNE of Crawford Creek.

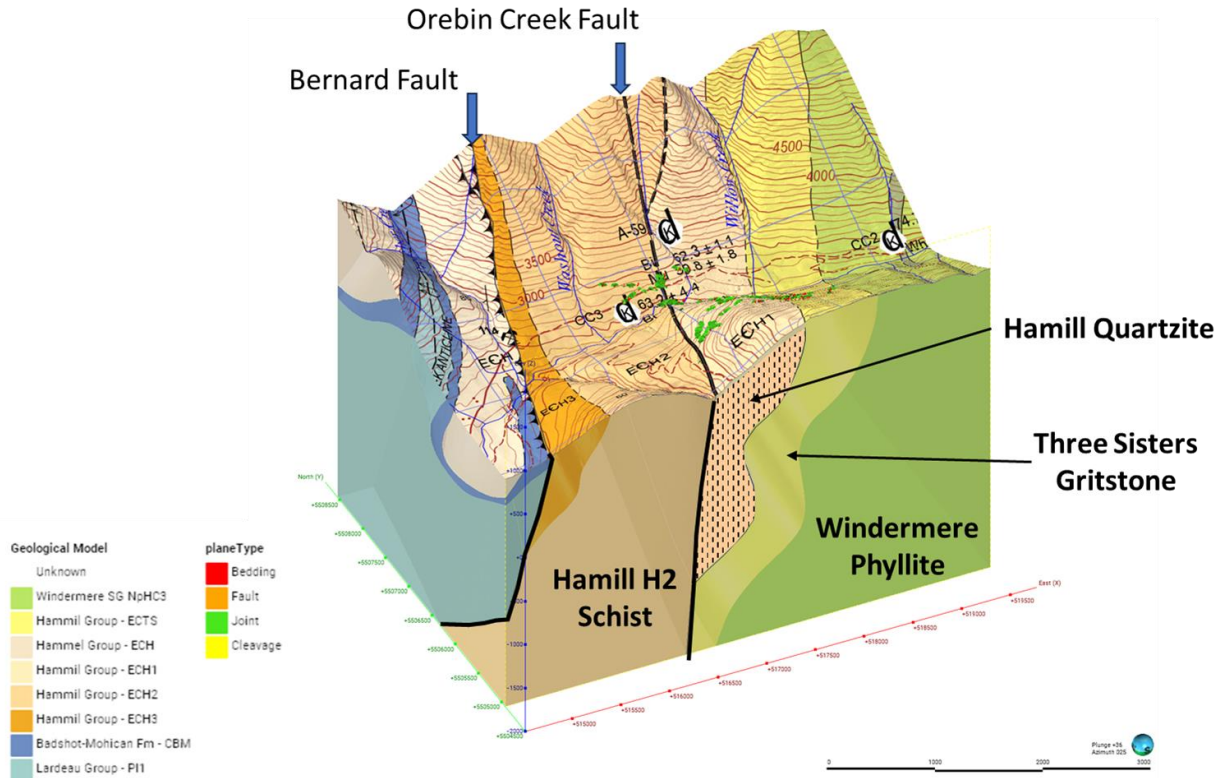


Figure 37 – EW cross section looking NNE towards Mount Crawford, Aetna Geothermal, 2023.

Figure 38 takes the Hamill H1 section and projects it along the Orebin Creek Fault in an NNE direction. This conceptual model shows the Hamill H1 quartzite unit only with the underlying Three Sisters and Windermere Group sections removed. While this is a conceptual model at this point, it demonstrates the potential scope of the low enthalpy geothermal system of which the Crawford Creek warm springs are a part. In addition, this model implies that the Hamill H1 quartzite could extend an additional 1,500 m below the Crawford Creek valley before the unit is truncated against the Orebin Creek Fault.

In Figure 38, the Orebin Creek Fault is shown as near vertical, however, some preliminary measurements in the field suggest that the fault dip may decrease at lower elevation. This implies that the Orebin Creek Fault could be arcuate in nature and more closely resemble the Bernard Fault as it is depicted in Figure 37. This would then imply greater potential depth for the Hamill H1 with a thicker section preserved.

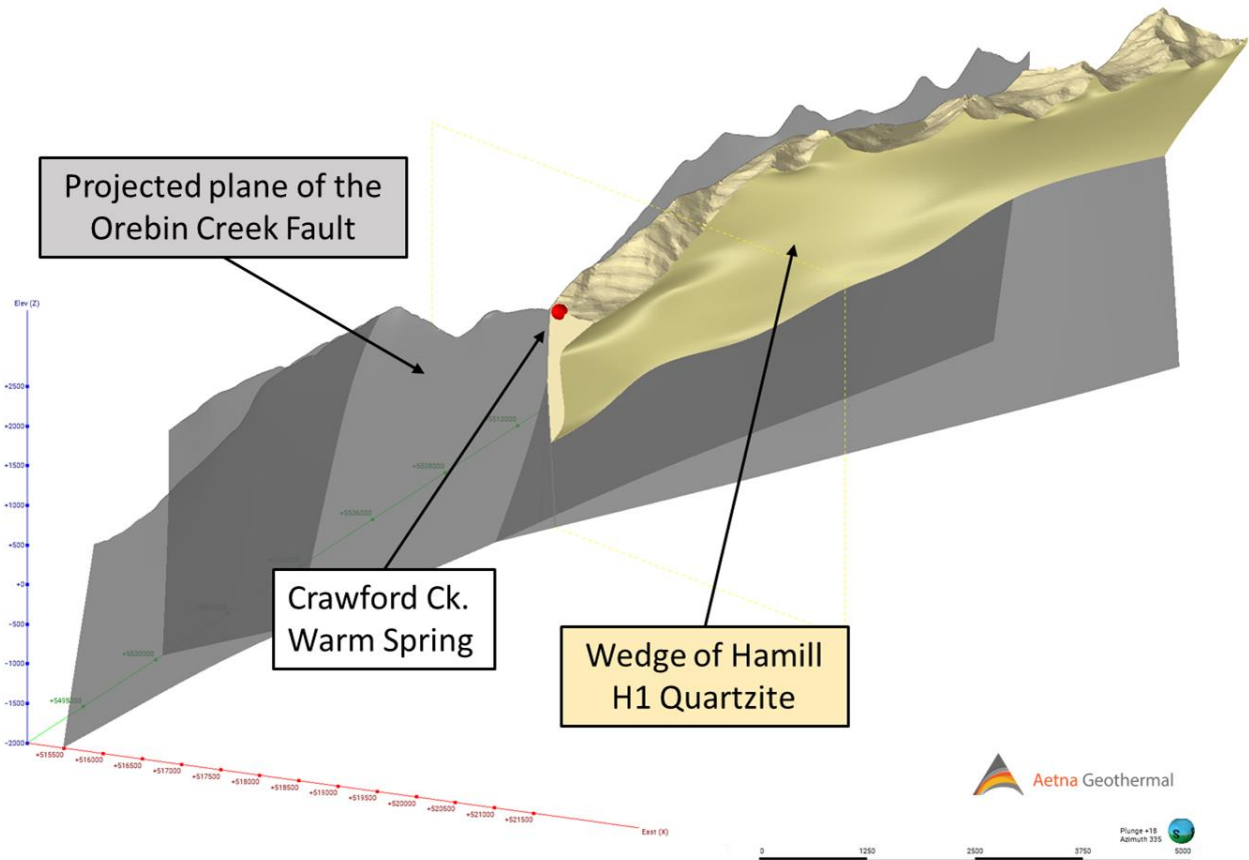


Figure 38 – Conceptual 3-D model showing the Hamill H1 quartzite wedge extending north from the Crawford Creek warm spring (red dot) up Mount Crawford and beyond. The plane of the Orebin Creek Fault is shown as grey, Aetna Geothermal, 2023.

From the Crawford Creek warm springs at an elevation of approximately 735 m, the topography rises to the summit of Mount Crawford at 2,340 m representing an elevation gain of just over 1,600 m. At a geothermal gradient of 3.5°C per 100 m, this represents a potential increase in temperature, for descending water of 56°C and at a gradient of 4°C per 100 m, the increase is potentially 64°C. The current conceptual model suggests that the Hamill H1 quartzite at Crawford Creek could extend down another 1,500 m, however, an additional 500 m of circulation at depth could represent potential additional heating of 17–20°C. Assuming an average water temperature of 0°C upon entry, indicates that the circulating fluids may potentially reach subsurface temperatures of 75°C to 85°C (or greater), within this system.

In terms of geothermal gradient, a review of the deep well data, acquired from the Canadian Geothermal Energy Association (CanGEA), highlights one key deep data point, the Moyie #1 well (located approximately 22 km south of

Cranbrook), which was drilled to a depth of 3,476 m in early 1987. A reliable downhole temperature reading of 108°C was acquired at a depth of 3,017 m (Moyie #1 Well Report, 1987), providing a geothermal gradient of 3.3°C per 100 m. The area where this Moyie #1 well was drilled is not recognized as having higher than normal geothermal heat flow. The geothermal gradient within the Kootenay Lake Geothermal Project area still needs to be verified.

Lead # 1, Gray Creek - In addition to the Crawford Creek warm spring focus area, several other areas of interest emerged in 2022 as field results were integrated into the project. Figure 39 highlights Lead #1, located on the east side of Crawford Bay. The area is host to Badshot marble and Lardeau gneiss, which are folded and faulted with two major faults identified and mapped; the two most likely being the West and East Bernard faults. In the outcrop, the Bernard fault zone was iron-stained brittle and highly chloritized.

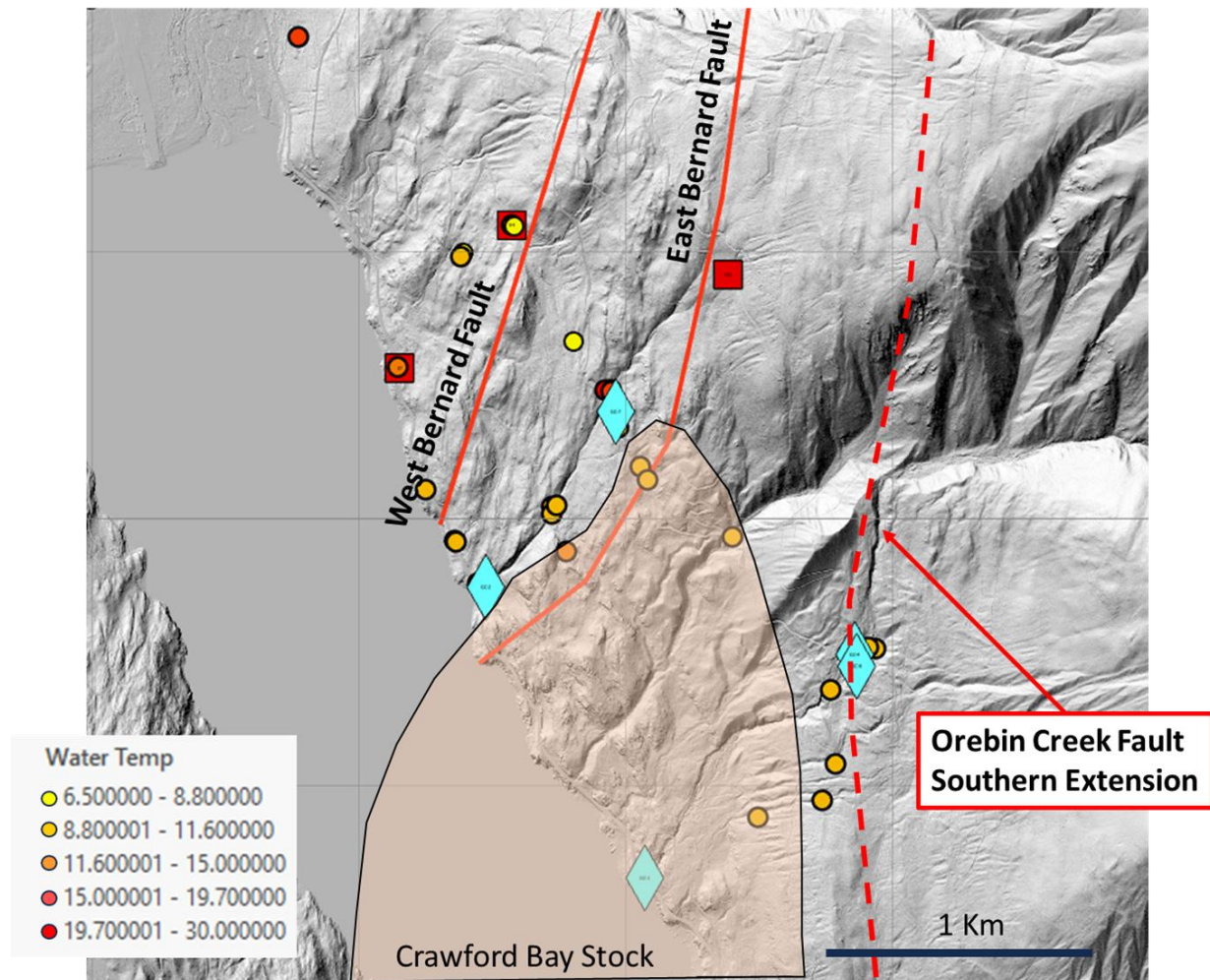


Figure 39 – Lead #1 Gray Creek, water sampling sites – (blue 2023, red 2022), 2023 water test sites – water temperature (ranges shown in °C).

To the east of the Bernard Fault and the deformed sequence of Badshot and Lardeau lies the southern extension of the Orebin Creek Fault. At Wilmot Creek, the Hamill H1 quartzite is found in outcrop, thinly bedded and quite heavily fractured (Figure 39). The Orebin Creek Fault was not located exactly but is believed to trend through the vicinity, close to the outcrop pictured in Figure 40. The rock fabric evident here is very similar to that of the Hamill H1 outcrop in the quarry on the Crawford Creek FSR, which is situated adjacent to the Orebin Creek Fault.



Figure 40 – Fractured Hamill quartzite exposed on Wilmot Creek near projected southern extension of the Orebin Creek Fault.

Surface waters tested in this area had elevated TDS (up to 490 ppm) and of the three sites sampled, one exhibited a surface temperature of 17°C. The site which had the highest temperature was proximal to Weasel Creek east of the Crawford Bay Stock. The higher temperature recorded in 2022 (23°C) was deemed to be

caused by solar heating due to low flow. This temperature could not be confirmed upon retest in 2023.

Springs with slightly elevated temperature and TDS were identified (Sample 101 and GC-23-07), however the measured field temperatures were less than 20°C and based on ion geochemistry no current reason was identified to further investigate this area.

One final option for this area would be to investigate the southern extension of the Hamill H1 in 2024. There is a small creek, called Haddon Creek, which has not been sampled and the source of Haddon Creek, which flows south, then west into Kootenay Lake, could lie near the southern end of Hamill H1 quartzite, as it is truncated by the Orebin Creek Fault.

Lead # 3, Beaver Creek - In 2022, a sample collected from Beaver Creek had some similarities to other samples of interest in 2022 and though the mineral content of Sample 82 is generally low, it was noted to have a high level of chloride (7.61 mg/L). This was the second highest level measured from all twenty samples analyzed in 2022. Chloride is generally considered an indicator of groundwater age with older groundwater having high levels of chloride (Humphries, pers. Comm.). Chloride measured at Ainsworth and Dewar Creek were in the range of 48–54 mg/L.

The analysis from sample BC-23-02 collected in Phase Three had a chloride level of 5.2 mg/L and was sampled upstream from sample 82. Another sample from the 2022 program, taken from a private water well, had the highest level of chloride measured in 2022 at 22 mg/L. Since this water well is located just on the other side of the Pilot Peninsula, some 2.5 km west of sample 82, a review of area water wells was conducted. The SRK report suggested that since both sites were close to roads there could have been contamination from road salt.

An advertisement was run in the local newspaper requesting area residents consider offering their water well analysis (on a confidential basis), however, only one water well analysis was received from a property north toward Riondel. If additional water well analysis comes forth, the area around Beaver Creek could attract future interest, however, since there has been no tangible geochemical evidence offering further encouragement for Lead #3, it is recommended that it be dropped from any further work plans at this time.

6) Recommendations for Further Work, Phase Four (2024)

Phase Three integrates detailed geologic mapping, geophysical surveys, geochemical sampling and geospatial analysis to gain a better understanding of surface and subsurface conditions, particularly in the Crawford Creek area. Structural mapping was conducted to determine the dominant orientation of fractures and the spatial variations in their occurrence. Geophysical surveys allowed the first look at subsurface structure and possible fluid flow paths in the shallow subsurface. Geochemical samples provide evidence of reservoir fluid characteristics. Thermal mapping using soil temperature loggers and drone-based thermal imaging is providing a detailed picture of the lateral extent of the geothermal system at the surface. The various methods being considered for Phase Four in 2024 are described in detail below.

Detailed Geology and Geochemistry

- Crawford Creek fracture and fault mapping with expanded scope up Mount Crawford and on south side
- More detailed geological mapping (lithofacies and structure)
- Expanded Crawford Creek geochemistry
- Temperature probe recovery and soil sampling at all sites

Drone Based Surveys

- Expanded UAV magnetometer survey, north of existing 2023 survey
- Depending on thermal drone video results from Phase Three, additional work will be considered for 2024

Electrical Resistivity Tomography, Second Survey - The compelling images which have emerged from the 2023 survey suggest that there is good reason to plan for a second ERT round in 2024. This survey would follow up on the 2023 survey by adding at least two additional N-S profiles parallel to the FSR-CC Steep profile and two or three longer E-W profiles parallel to the CC Bank profile, one which could be positioned on the south side of Crawford Creek (subject to access). A potential 2024 ERT survey is depicted on the map in Figure 41.

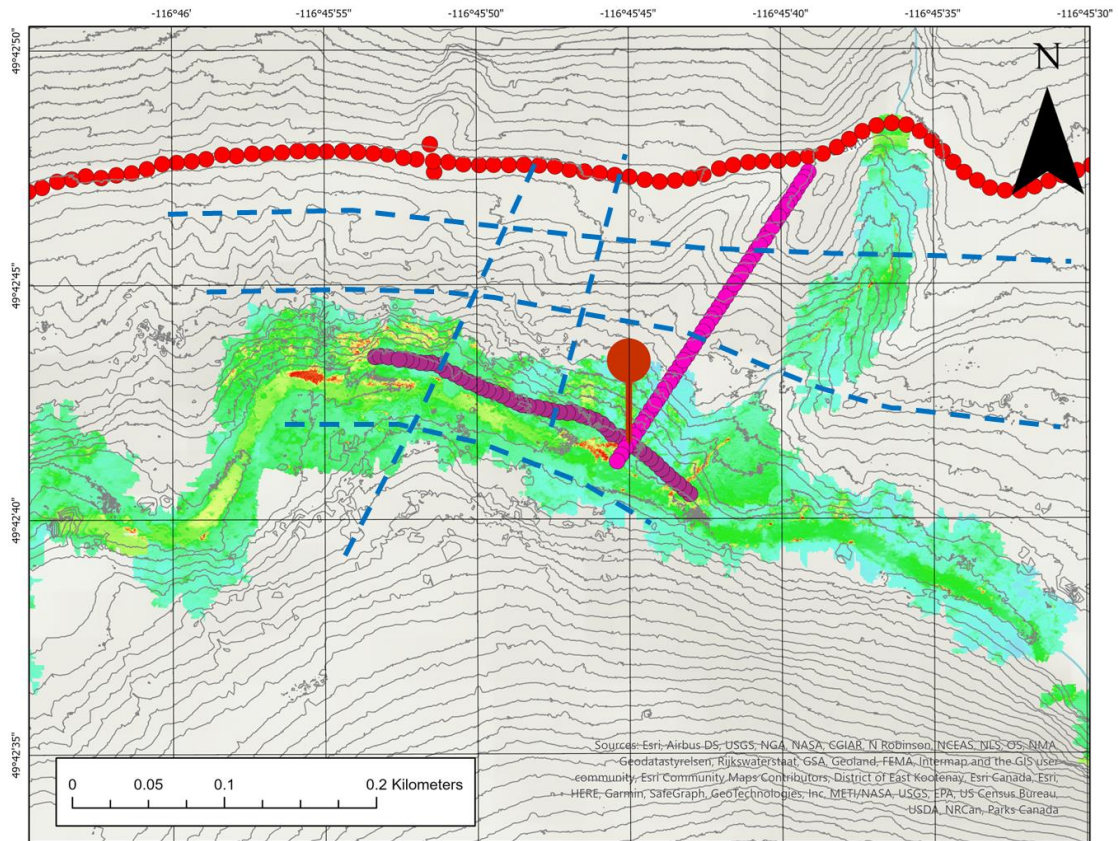


Figure 41 – Crawford Creek, proposed detailed ERT survey lines (2024 – blue dashed lines), compared to 2023 survey lines.

Further work is required to better understand the hydrology of the Crawford Creek geothermal system with additional ERT or alternatively a Versatile Time Domain Electromagnetic (VTEM) survey. A VTEM survey is a helicopter-based program that surveys electrical properties (conductivity) while collecting magnetic data in one program. Given the demonstrated merits of both magnetic and electrical surveys in 2023, a VTEM could be considered for 2024.

7) Conclusion

Joints with a WNW orientation have been observed all through the project area. Fracturing and faulting with a WNW orientation also exist in the Riondel Mine and are related to thermal waters evident there. The WNW joints (Joint Set 1) are the most pervasive in the Hamill H1 quartzite within the quarry exposure on the FSR at Crawford Creek. There is now strong evidence from the magnetometer survey that a WNW contact or fracture zone may well be present, in the Crawford Creek valley bottom, through the section where all the warm springs are located. In fact, where this WNW lineament intersects the NNE lineaments on the magnetometer 1st and 2nd order derivatives, is where the warm spring is situated.

The Crawford Creek valley, and an apparent WNW fracture zone located there, appear to represent a pivot point where the Orebin Creek Fault (OCF) goes from trending N-S (south of the creek) to trending NNE-SSW (north of the creek). The structural fabric evident on the 1st and 2nd order derivative maps also changes direction in a similar fashion. The orientations of these evident lineaments highlight that there are compelling, mappable changes in structural fabric occurring right at Crawford Creek where the warm springs are located.

Geochemical results and early geological modelling point towards a low enthalpy, shallow circulation (2–3 km) geothermal system that has been constrained within steeply dipping, fractured quartzites. These Hamill quartzites extend some 12.4 km to the north from the Crawford Creek valley, before intersecting the Fry Creek Batholith, and some 7 km to the south where the Hamill is mapped to truncate against the Orebin Creek Fault, before intersecting the Crawford Bay Stock. The model estimates that the Hamill H1 quartzite could extend another 1,500 m below Crawford Creek. The position and rock volume represented by steeply dipping, fractured Hamill H1 quartzite represent a very significant recharge area within a low enthalpy geothermal system; a system estimated to have the potential to generate subsurface geothermal fluid temperatures of up to 75–85°C or greater.

Preliminary resistivity inversions from the three ERT sections surveyed in 2023 show numerous low resistivity features, which could represent fluid saturated bedrock. These features occur at three different elevations from as shallow as 805–795 m to as deep as 660–580 m. The deepest low resistivity anomaly is situated some 150 m below the base of the Crawford Creek valley. This deep conductor (C4) is situated within fractured Hamill H1 quartzite immediately east of the Orebin Creek Fault. There is a strong NNE-SSW trending feature evident on first vertical derivative at the location of this (C4) conductor on the ERT data. The spatial relationship between these resistivity anomalies at depth and the warm surface outlets, suggests they may represent thermal fluid reservoirs and could be suitable targets

for drilling. Further, ERT surveys would be critical to defining the scale of subsurface targets.

The 2023 program has continued to provide evidence of a low enthalpy geothermal system at Crawford Creek, north of Crawford Bay, BC. This system, depending on the depth of circulation, could access thermal fluids with a temperature of up to 75 or 85°C. The verification of this potential resource could feed a range of direct heat applications for regional economic and social benefit.

The next phase, Phase Four, of this project will aim to understand and map the subsurface hydrology of the Crawford Creek system through an ongoing multi-disciplinary, geoscience-based investigation. Upon completion of this work, a drilling and testing plan for Crawford Creek geothermal system can be initiated.

8) Acknowledgments

Phase Three of this project was made possible through the preliminary funding support from The Regional District of Central Kootenay – Economic Development Commission (EDC). Additional funds were later made available through Geoscience BC, CiCan – The Colleges and Institutes Canada, the Province of BC's Rural Economic Diversification and Infrastructure Program (REDIP) and Mitacs through their Accelerate program.

Phase Two of this project was made possible through the initial funding support of Regional District of Central Kootenay – Community Sustainable Living Advisory Committee (CSLAC), Economic Development Commission (EDC) and a Community Development grant. Additional funds were later made available through CiCan – The Colleges and Institutes Canada, Geoscience BC and The Natural Sciences and Engineering Research Council of Canada (NSERC)

The CiCAN funding for this initiative has been provided in part by the Government of Canada through Natural Resources Canada's Green Jobs – Science and Technology Internship Program, as part of the Youth Employment and Skills Strategy. (*Le financement de cette initiative est fourni par le gouvernement du Canada par l'entremise du Programme de stages en sciences et technologie - Emplois verts*).

This project would not have been possible without the support of these groups.

Fourth-year geology student, Bethany Worsnop from the University of Victoria supported the project through her direct studies program, working in the field throughout the summer of 2023 and supporting the ERT operation. She has since conducted a literature review and completed an assessment of recent work utilizing ERT in geothermal exploration while integrating ERT results from the summer fieldwork. Bethany's technical advisors at the School of Earth and Ocean Science, University of Victoria are Dr. Lucinda Leonard and Theron Finley.

Stefan Humphries, hydrogeologist and Leslie Harker, geochemist both work for SRK Consulting Inc. and are based in Nelson, BC. Leslie and Stefan have greatly assisted in the integration, review and interpretation of geochemistry results from the 2023 field season. Leslie's background particularly in isotope geochemistry has been quite valuable in understanding the complexities of fluid mixing at Crawford Creek.

Thanks to the University of Calgary Department of Geosciences and Department of Physics for their support and guidance through the analyses process as well as with field sample collection protocols and storage. Dr. Bernard Mayer (Applied Geochemistry), his team Steve Taylor, Manager - Isotope Science Lab (Agg-ISL), Michael Nightingale, Manager - Applied Geochemistry Lab and Dr. Michael Weser (Thermal Ionization Mass Spectrometry, Physics) for the Sr isotope analysis. Special thanks to Ian Hutcheon for his guidance and assistance in helping our project navigate the geochemistry process.

The fall drone fieldwork was supported by Jamie Albino and Chenoa McLean (fourth-year Selkirk College students) and the ongoing mentorship provided by GIS instructor, Robert McQuarrie. The UAV Magnetometer survey was conducted by Geotronics Consulting Inc, out of Kaleden BC with field support from Selkirk College. Geotronics also provided a report on the survey which has been included in the appendix.

Overall data integration and preliminary modelling work was carried out by Bastien Poux of Aetna Geothermal Limited. Bastien's proficiency working with Seequent's Leapfrog Geo 3D modelling software was immensely helpful in combining various data inputs and bringing them into a 3-D space.

Finally, special thanks go to Rochelle Longval, PGeo. of Kaslo, BC and Dan Alonso Torres, G.I.T. of Nanaimo, BC who have kindly provided their time, insightful inquiry and overarching support for the project.

9) References

Allmendinger R. (2022) Stereonet Mobile App

<http://www.geo.cornell.edu/geology/faculty/RWA/programs/stereonet.html>

Andrews, G.D.M. and Russell, J.K., (2007) Cover Thickness across the Southern Interior Plateau, British Columbia (NTS 092O, P; 093A, B, C, F): Constraints from Water-Well Records. in Geoscience BC Summary of Activities 2007, Geoscience BC Report 2008-1, p.11-20.

BC Ministry of the Environment, (1980), Soil Resources of the Nelson Map Area, RAB Bulletin 20.

Beaudoin, G. Roddick, J.C., and Sangster, D.F., (1992), Eocene age for Ag-Pb-Zn-Au vein and replacement deposits of the Kokanee Range, southeastern British Columbia Can. J. Earth Sci.

Blewitt, G., Coolbaugh, M., Holt, W., Kreemer, C., Davis, J., & Bennett, R., (2002), Targeting of potential geothermal resources in the Great Basin from regional relationships between geodetic strain and geological structures: Geothermal Resources Council Transactions, v. 26, p. 523–526.

Brown, D.A., MacLeod, R.F., and Wagner, C.L., (comp.), 2011. Geology, Kaslo, British Columbia; Geological Survey of Canada, Open File 6306

Brown, D.A., Wagner, C.L., and Chow, W., (2011). Geology, Crawford Bay, British Columbia; Geological Survey of Canada, Open File 6307

Canadian Geothermal Energy Association, (2013) Geothermal Technology Roadmap: Global Best Practices Summary, Exploration through Generation, Calgary, Alberta.

Chen, Y. et al. (2019) Seismic evidence for a mantle suture and implications for the origin of the Canadian Cordillera, Nature Communications.

Chen, Z., Grasby, S., Yuan, W., and Liu, X. (2022) Ground surface temperature monitoring data analysis and applications to geothermal exploration in volcanic areas, Mount Meager, western Canada, Geothermics 108 (2023) 102610, <https://doi.org/10.1016/j.geothermics.2022.102610>

Clean Energy BC Website, (2023) Geothermal, BC's Potential

<https://cleanenergybc.org/sector/geothermal/#:~:text=British%20Columbia's%20OPotential,of%20over%201%2C000%20MW%20collectively>

Colpron, M. and Price, P.A. (1995) Tectonic Significance of the Kootenay Terrane, Southeastern Canadian Cordillera: An Alternative Model, *Geology*; January 1995; v. 23; no. 1.

Cook, F.A., (2016) Merging Geological, Seismic Reflection and Magnetotelluric Data in the Purcell Anticlinorium, Southeastern British Columbia, *Geoscience BC Report 2016-001*.

Crosby P., (1968), Tectonic, Plutonic, and Metamorphic History of the Central Kootenay Arc, British Columbia, Canada: Geological Society of America, Special paper 99, 94p.

Desrochers, D.T., (1992) Geothermal Feasibility Study for the Use of Hot Water Near Riondel, British Columbia, Geological Survey of Canada Open File 2502.

Doughty, P.T., and Price, R.A., (2000) Geology of the Purcell Trench Rift Valley and Sandpoint Conglomerate: Eocene En-echelon Normal Faulting and Synrift Sedimentation Along the Eastern Flank of the Priest River Metamorphic Complex, northern Idaho, *GSA Bulletin*; September 2000; v. 112; no. 9; p. 1356–1374.

Erkan, K., Holdman, G., Blackwell, D. and Benoit, W., (2007) Thermal Characteristics of the Chena Hot Springs, Alaska Geothermal System, Proceedings, Thirty-Second Workshop on Geothermal Reservoir Engineering Stanford University, Stanford, California.

Faulds, J., Coolbaugh, M., Bouchot, V., Moeck, I., and Oğuz, K., (2010) Characterizing Structural Controls of Geothermal Reservoirs in the Great Basin, USA, and Western Turkey: Developing Successful Exploration Strategies in Extended Terranes, Proceedings World Geothermal Congress 2010 Bali, Indonesia.

Faulds, J. E. and Hinz, N.H., (2015) Favorable Tectonic and Structural Settings of Geothermal Systems in the Great Basin Region, Western USA: Proxies for Discovering Blind Geothermal Systems, Proceedings World Geothermal Congress, Melbourne, Australia, 19-25 April 2015.

Finley, T. (2020) Fault-hosted geothermal systems in southeastern British Columbia, MSc Thesis, University of Alberta

Finley T., Johnston S, Unsworth, M., Banks J, and Dinu-Ion, P. (2022) Modern Dextral Strain Controls Active Hydrothermal Systems in the Southeastern Canadian Cordillera, to be published.

Fyles, J.T., (1967) Geology of the Ainsworth-Kaslo Area, British Columbia, BC Department of Mines and Petroleum Resources, Bulletin No. 53, Victoria BC.

Georgsson, L. S., (2009) Geophysical Methods Used in Geothermal Exploration, United Nations University Geothermal Training Programme, Reykjavik, Iceland.

Geoscience BC, (2016) An Assessment of the Economic Viability of Selected Geothermal Resources in British Columbia BC Hydro Updates and Sensitivities Revised Final (R1) Report March 31, 2016

Geotronics Consulting Inc. (2023) Geophysical Report on a UAV Magnetometer Survey Over the Kootenay Lake Geothermal Project Area, Crawford Bay BC., Geotronics Consulting Inc., 130 Saddlehorn Drive, Kaleden, BC

Ghomshei, M. (2010). "A presentation at the Canadian Geothermal Energy Association Annual Conference 2010". New Frontiers in Geothermal Energy. Vancouver: CanGEA.

Grasby, S.E., I. Hutcheon and H.R. Krouse, (2000) The Influence of Water-Rock Interaction on the Chemistry of Thermal Springs in Western Canada. Applied Geochemistry, Vol. 15, p. 439-454.

Grasby, S.E. and I. Hutcheon, (2001) Controls on the Distribution of Thermal Springs in the Southern Canadian Cordillera. Canadian Journal of Earth Sciences, Vol. 38, p. 427-440.

Grasby, S.E., et al. (2012) Geothermal Energy Resource Potential of Canada, Geological Survey of Canada Open File 6914.

Greene, S. A., (1981) Geological Report Jackass Claims, Barefoot Groups, Prepared for Springpoint Resources Ltd., Calgary Alberta.

Høy, Trygve, (1980) Geology of the Riondel Area Central Kootenay Arc Southeastern British Columbia, Bulletin 73 – Ministry of Energy Mines and Petroleum Resources, Victoria, BC.

Jessop, A.M., (1986) Catalogue of Boreholes 2 – Geothermal Energy Holes. Report for British Columbia Hydro and Power Authority, Internal Report No. 86-2, January 1986, 58 pages.

Leclair, A.D. (1988) Polyphase Structural and Metamorphic Histories of the Midge Creek Area, Southeast British Columbia: Implications for Tectonic Processes in the Central Kootenay Arc. Ph.D. thesis, Queen's University, 264 p.

Kerr Wood Leidal, Consulting Engineers, (2015) An Assessment of the Economic Viability of Selected Geothermal Resources in British Columbia, Geoscience BC Report 2015-11, Victoria BC.

Kimball, Sarah, (2010) Favourability Map of British Columbia Geothermal Resources, Masters of Applied Science Thesis, Faculty of Graduate Studies, UBC, Vancouver.

MacMahon, G. (2021) Kootenay Lake Community Geothermal Project, Phase One – GIS Project Set Up and Data Integration, Summary Interpretation Report, December 2021 https://cdn.geosciencebc.com/project_data/GBCReport2022-004/Phase%20One%20Geothermal%20Interpretation%20Report%20FINAL.pdf

MacMahon, G., McQuarrie, R., Gatto, D. & Humphries, S., (2023) Geological, Geochemical and Geospatial Investigations into the Geothermal Potential of the East Shore of Kootenay Lake – Summary Report, January 2023, Geoscience BC Report 2023-06, https://cdn.geosciencebc.com/project_data/GBCReport2023-06/GBC_Report_2023-06_Kootenay_Lake_Geothermal_Project_-_Phase%202.pdf

Majorowicz & Grasby, (2010) High Potential Regions for Enhanced Geothermal Systems in Canada, Natural Resources Research, Vol. 19, No. 3, September 2010.

Moeck, Inga, S., (2014) Catalog of geothermal play types based on geologic controls, Renewable and Sustainable Energy Reviews, Volume 37, 2014, Pages 867-882, <https://doi.org/10.1016/j.rser.2014.05.032>

Monger, J. W. H., Price, R. A., & Tempelman-Kluit, D. J. (1982). Tectonic accretion and the origin of the two major metamorphic and plutonic belts in the Canadian Cordillera. *Geology*, 10(2), 70-75.

Moyie #1 Well Report, Duncan Oil Properties Inc., Moyie d-8-C 82-G-5 well file, 1987, BC Ministry of Energy, Mines and Petroleum Resources

Moynihan, D. & Pattison, D.R.M., (2008). Origin of the Kootenay Lake Metamorphic High, Southeastern British Columbia. *British Columbia Geological Survey Geological Fieldwork, 2008-1*, 147–158.

Moynihan, D.P., and Pattison D.R.M., (2011) The Origin of Mineralized Fractures at the Bluebell Mine Site, Riondel British Columbia, Society of Economic Geologists, Inc., *Economic Geology*, v. 106, pp. 1043–1058.

Moynihan, D.P., and Pattison D.R.M., (2013) Barrovian Metamorphism in the Central Kootenay Arc, British Columbia: Petrology and Isograd Geometry, *Canadian Journal of Earth Science* 50: 769–794. Nightingale, M., (2023) Brief Field

Sampling Procedures for Groundwaters, Surface Waters and Oil Field Waters, Applied Geochemistry group, University of Calgary.

Nightingale, M., (2023) Brief Field Sampling Procedures for Groundwaters, Surface Waters and Oil Field Waters, Applied Geochemistry group, University of Calgary

Palacky, G. J. (1988). Resistivity Characteristics of Geologic Targets. In Electromagnetic Methods in Applied Geophysics (Vol. 1, pp. 53-129). Tulsa, OK: Society of Exploration Geophysicists.
<https://doi.org/10.1190/1.9781560802631.ch3>

Pattison, D.R.M., Moynihan, D.P., McFarlane, C.R.M., Simony, P.S. & Cubley, J.F. (2020) Field guide to the geology, metamorphism and tectonics of the Foreland and Omineca belts of SW Alberta and SE British Columbia. Geological Association of Canada Field Guide Series 2020-A, 257 pages.

Peters, J. (2012) Late Pleistocene Evolution of Glacial Lake Purcell: A Potential Floodwater Source to the Channeled Scabland, MSc Thesis Simon Fraser University Vancouver BC.

Rioseco, N.A. and Pattison, D.R.M. (2018): Preliminary investigations of the metamorphic and thermochronological interface between the Purcell Anticlinorium and the Kootenay Arc, southeastern British Columbia (NTS 082F, G); in Geoscience BC Summary of Activities 2017: Minerals and Mining, Geoscience BC, Report 2018-1, p. 47–56.

Robins, J., Kolker, A., Flores-Espino, F., Pettitt, W., Beckers, K. Pauling, H. and Anderson, B. (2021) 2021 U.S. Geothermal Power Production and District Heating Market Report, National Renewable Energy Laboratory (NREL).

Rosas-Carbajal, (2014) Time-lapse and probabilistic inversion strategies for plane-wave electromagnetic methods, Institut de Physique du Globe de Paris, Paris France.

Smith, Jerome, (2015) Geothermal Development for Colorado, Economics of Heat vs. Power Only, Advances in Geothermal Direct-Use Workshop. NREL 2015
https://www.energy.gov/sites/prod/files/2015/07/f24/03-The-Importance-of-Shifting-Exploration-Models---Jerry--Smith_0.pdf

Smith, M.T. and Gehrels, G.E., (1992) Structural Geology of the Lardeau Group Near Trout Lake, British Columbia: Implications for the structural evolution of the Kootenay Arc, Department of Geosciences, University of Arizona, Tuscon Az.

SRK Consulting (Canada) Inc., (2023) Results and Interpretation of the Phase 3 Water Quality Sampling Program. DRAFT V2. Prepared for South Kootenay Lake Community Service Society. Crawford Bay, BC. Project number: CAPR002883. Issued November. 2023.

Statistics Canada (2022), Population growth in Canada's rural areas, 2016-2021 – Census of Population 2021, released Feb 9 2022 www.statcan.gc.ca

Turner, R.J.W., Anderson, R.G., Franklin, R., Anderton, L., and Fowler, F. (2009) Geotour Guide for the West Kootenay's BC, Geological Survey of Canada Open File 6135.

Tuya Terra Geo Corp., (2016) Direct-use Geothermal Resources in British Columbia Report 2016-07 (Section A), Burnaby, BC.

Webster, E.M., (2016) Tectonothermal Evolution of the Southern Omineca Belt, Southeastern British Columbia (Unpublished doctoral thesis). University of Calgary, Calgary, AB.

Webster, E.R. and Pattison, D.R.M., (2013) Metamorphism and Structure of the Southern Kootenay Arc and Purcell Anticlinorium, Southeastern British Columbia (Parts of NTS 082F/02, /03, /06, /07); in Geoscience BC Summary of Activities 2012, Geoscience BC, Report 2013-1, p. 103–118.

Webster, E.R. and Pattison, D. R. M., University of Calgary, (2018) Spatially Overlapping Episodes of Deformation, Metamorphism, and Magmatism in the Southern Omineca Belt, Southeastern British Columbia, Canadian Journal of Earth Science 55: 84–110.

Webster, E.R., Archibald, D.A., Pattison, D.R.M., Pickett, J.A. and Jensen, J.C. (2020) Tectonic Domains and Exhumation History of the Omineca Belt in Southeastern British Columbia from $40\text{Ar}/39\text{Ar}$ Thermochronology, Canadian Journal of Earth Sciences 57: 918-946, 2020.

10) Appendix

- a. SRK Consulting - Results and Interpretation of the Phase 3 Water Quality Sampling Program, Leslie Harker, December 2023 (provided separately)

- b. Geotronics Consulting Inc. – Geophysical Report on a UAV Magnetometer Survey over the Kootenay Lake Geothermal Project Area, Crawford Bay BC, November 2023 (provided separately)
- c. University of Calgary - Geochemical Analyses, September 2023

UNIVERSITY OF CALGARY - LABORATORY ANALYSIS RESULTS Sept 2023

Sample Name	HCO3 (mg/L)	Br (mg/L)	Cl (mg/L)	F (mg/L)	NO3 (mg/L)	SO4 (mg/L)	Al (mg/L)	B (mg/L)	Ba (mg/L)	Ca (mg/L)	Fe (mg/L)	K (mg/L)	Li (mg/L)	Mg (mg/L)	Mn (mg/L)	Na (mg/L)	Si (mg/L)	Sr (mg/L)	TDS (mg/L)
CC-23-01	19.7	ND	0.07	0.06	0.23	12.9	0.02	0.10	0.02	4.63	0.01	1.38	0.00	2.79	0.00	2.21	11.1	0.04	55.25
CC-23-02	18.1	ND	0.07	0.03	0.29	7.1	0.01	0.00	0.01	4.41	0.00	0.91	0.00	1.85	0.00	1.57	6.9	0.03	41.26
CC-23-03	33.4	ND	0.07	0.06	0.22	13.2	0.01	0.00	0.01	7.33	0.00	1.36	0.00	3.79	0.00	2.81	11.7	0.06	74.02
CC-23-04	108.0	ND	0.07	0.03	0.05	10.8	0.02	0.00	0.02	31.19	0.01	2.42	0.00	3.66	0.00	2.40	6.2	0.06	164.86
CC-23-05	15.4	ND	0.07	0.05	0.16	8.3	0.00	0.00	0.02	3.37	0.01	1.08	0.00	2.05	0.00	2.01	9.0	0.04	41.54
CC-23-06	19.1	ND	0.44	0.05	0.18	9.5	0.00	0.00	0.02	4.00	0.00	1.22	0.00	2.37	0.00	2.40	9.4	0.04	48.78
GC-23-01	14.7	ND	0.07	0.02	0.00	1.6	0.01	0.00	0.02	3.12	0.00	0.33	0.00	1.02	0.00	0.73	3.3	0.01	24.96
GC-23-02	164.0	ND	0.10	0.09	0.03	14.2	0.02	0.00	0.02	49.37	0.01	2.02	0.00	6.69	0.00	2.03	9.2	0.09	247.90
CC-23-01B	19.8	ND	0.09	0.06	0.21	12.2	0.00	0.00	0.02	4.35	0.00	1.34	0.00	2.84	0.00	2.16	7.3	0.04	50.37
CC-23-02B	18.0	ND	0.09	0.05	0.04	7.0	0.00	0.00	0.01	4.17	0.00	0.96	0.00	1.87	0.00	1.73	4.5	0.03	38.44
CC-23-03B	33.1	ND	0.07	0.06	0.00	12.6	0.00	0.00	0.01	6.87	0.00	1.42	0.00	3.85	0.00	2.85	7.7	0.06	68.59
CC-23-04B	106.0	ND	0.08	0.03	0.02	10.2	0.00	0.02	0.02	31.33	0.00	2.40	0.00	3.81	0.00	2.34	4.0	0.06	160.39
CC-23-05B	15.5	ND	0.08	0.05	0.00	8.0	0.00	0.00	0.01	3.13	0.00	1.17	0.00	2.06	0.00	2.10	5.9	0.04	38.04
CC-23-07	69.9	ND	0.07	0.05	0.02	8.4	0.00	0.01	0.01	18.53	0.00	1.15	0.00	4.47	0.00	1.39	4.2	0.07	108.32
CC-23-08	8.2	ND	0.07	0.03	0.05	3.9	0.00	0.04	0.01	1.80	0.00	0.07	0.00	0.91	0.02	1.12	2.7	0.02	18.93
CC-23-09	8.6	ND	0.06	0.03	0.00	3.9	0.00	0.00	0.01	1.89	0.00	0.53	0.00	0.94	0.00	0.95	2.7	0.02	19.67
GC-23-03	21.0	ND	0.05	0.02	0.02	2.5	0.00	0.00	0.01	4.68	0.00	0.32	0.00	1.53	0.00	0.59	2.0	0.02	32.72
GC-23-04	9.4	ND	0.05	0.01	0.00	1.4	0.01	0.01	0.02	1.77	0.00	0.26	0.00	0.84	0.00	0.63	2.0	0.01	16.37
GC-23-05	9.4	ND	0.05	0.02	0.00	1.5	0.00	0.01	0.02	1.79	0.00	0.26	0.00	0.85	0.00	0.63	2.0	0.01	16.47
GC-23-06	9.4	ND	0.05	0.02	0.00	1.5	0.01	0.00	0.02	1.80	0.00	0.27	0.00	0.84	0.00	0.66	2.1	0.01	16.65
GC-23-07	190.0	ND	0.11	0.14	0.03	12.0	0.01	0.02	0.01	60.86	0.00	1.67	0.00	4.58	0.00	1.70	6.3	0.06	277.48
BC-23-01	57.8	ND	0.26	0.03	0.13	3.7	0.06	0.05	0.02	12.98	0.01	3.53	0.00	2.08	0.01	2.02	4.4	0.09	87.13
BC-23-02	93.1	ND	5.27	0.12	0.43	2.7	0.03	0.12	0.03	21.11	0.10	4.02	0.01	3.95	0.00	3.92	4.4	0.10	139.39
HC-23-01	33.0	ND	0.14	0.03	0.09	5.3	0.01	0.01	0.01	6.96	0.00	0.36	0.00	3.10	0.00	0.67	1.6	0.02	51.28
US-23-01	525.0	ND	1.61	0.13	0.00	20.5	0.05	0.05	0.16	148.90	0.00	2.79	0.02	13.03	0.03	19.01	4.0	1.53	736.75

ND = Not Detected

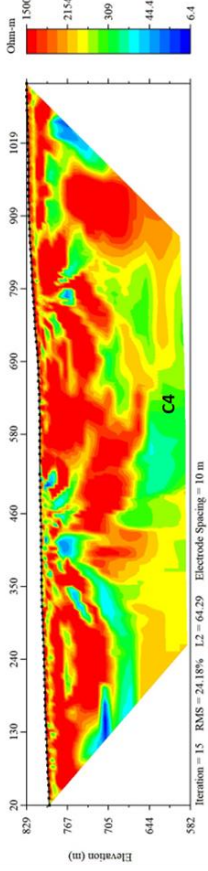
- d. Laboratory analysis summary – CARO Labs, Kelowna (provided separately)
- e. Multiparameter Testing 2023 Results Summary (provided separately)
- f. Temperature Data Logger Deployment Locations

Location_ID	Probe_ID	Date	Ground_Comments	Exposure_Comments	Elevation_m_
1	20900794	19-Jul	Rocky/sandy soil	shaded, near 16.2 temp stream	754
2	20900817	19-Jul	rocky clay rich soil on side of slope	partial sun	797
3	20880772	19-Jul	flat elevated rocky	shaded	778
4	20880769	19-Jul	rocky slope, organic rich soil	shaded	780
5	20894577	19-Jul	thick organic rich layer with rocky soil on slope	shaded	767
6	20880766	19-Jul	clay rich with organics	shaded	774
7	20900789	20-Jul	very clay rich and moist on slope by warm spring	exposed to sun	764
8	20900829	20-Jul	sandy clay by warm stream	shaded	792
9	20900670	20-Jul	sandy clay some rocks	shaded	820
10	20900675	20-Jul	sandy clay with some rocks	sun exposed	751
11	20900782	20-Jul	clay rich with sand red soil, dry	shady	776
12	20880774	20-Jul	sandy clay on lower shelf close to creek	shaded	780
13	20900795	20-Jul	lots vegetation, gravely, moist bottom hole filled w water	exposed to sun until vegetation regrows back over	799
14	20900805	20-Jul	very clay rich little rocks	shaded	797
15	20900820		Air Temperature data logger	in tree	837
16	20900822	21-Jul	Rocky soil, road construction soil	South exposure, partially shaded	808
17	20880776	21-Jul	rocky soil, road construction soil	southwest exposure partial sun	853
18	20900832	21-Jul	rocky reddish soil partially clay rich, more of natural forest soil	south exposure, partially shaded	856
19	20900827	21-Jul	reddish brown	shaded	839
20	20894579	21-Jul	reddish brown rocky	shaded	816
21	20880775	21-Jul	red forest soil	shaded	786
22	20900787	25-Jul	light brown gravel rich	shaded	809
23	20880777	25-Jul	light reddish brown, rocky	shaded	819
24	20900830	25-Jul	Air Temperature data logger	tree by creek	761

- g. Electrical Resistivity Tomography (ERT) Profiles, B. Worsnop, School of Earth and Ocean Science, University of Victoria

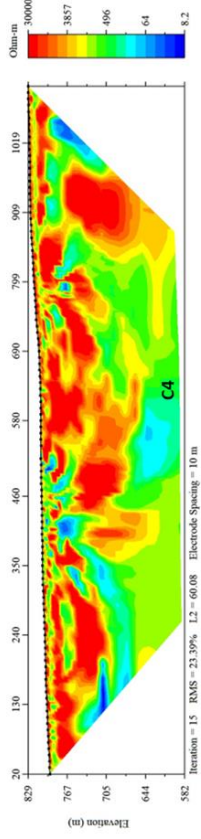
FSR PROFILE

Inverted Resistivity Section



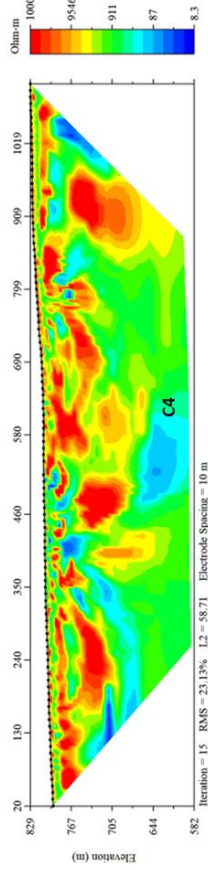
Smooth Inversion
 Max Resistivity: 15000
 Minimum Resistivity:1
 C4=171

Inverted Resistivity Section



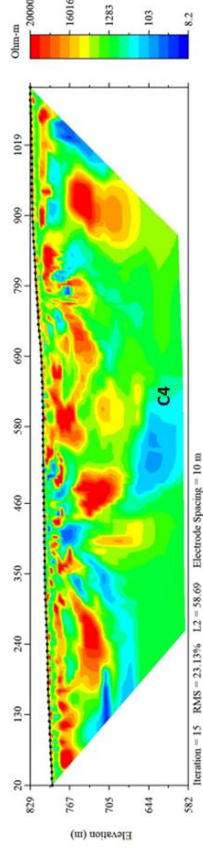
Smooth Inversion
 Max Resistivity: 30000
 Minimum Resistivity:1
 C4=83

Inverted Resistivity Section



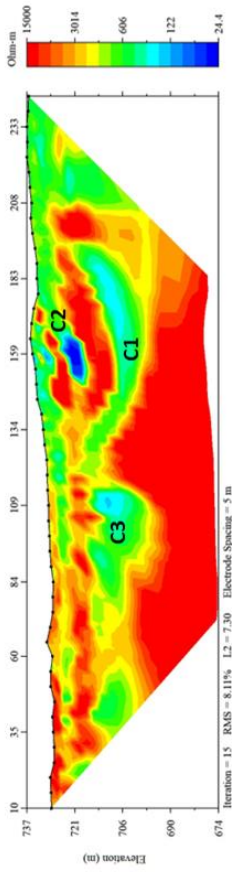
Smooth Inversion
 Max Resistivity: 100000
 Minimum Resistivity:1
 C4=70

Inverted Resistivity Section



Smooth Inversion
 Max Resistivity: 200000
 Minimum Resistivity:1
 C4=70

Inverted Resistivity Section



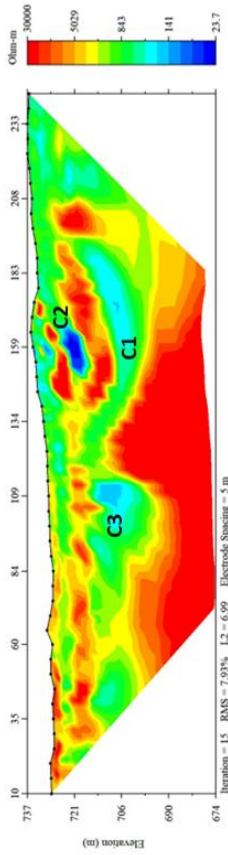
Smooth Inversion
 Max Resistivity: 15000
 Minimum Resistivity: 1
 C1=200
 C2=24
 C3=200

CC BANK PROFILE

Some Misfits removed after 33%

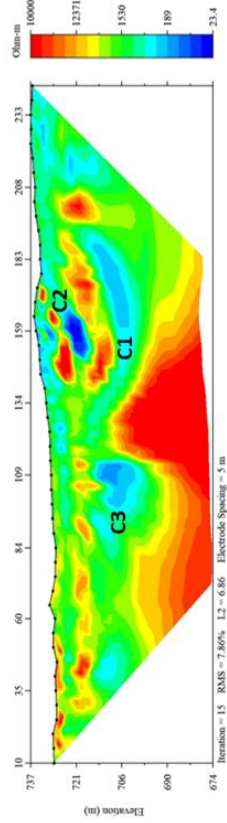
C1 is around 706m

Inverted Resistivity Section



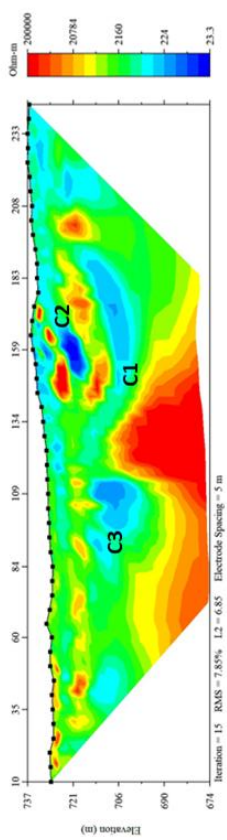
Smooth Inversion
 Max Resistivity: 30000
 Minimum Resistivity: 1
 C1=190
 C2=24
 C3=180

Inverted Resistivity Section



Smooth Inversion
 Max Resistivity: 100000
 Minimum Resistivity: 1
 C1=250
 C2=20
 C3=145

Inverted Resistivity Section



Smooth Inversion
 Max Resistivity: 200000
 Minimum Resistivity: 1
 C1=220
 C2=20
 C3=140

CC - FSR PROFILE

